IMPERIAL COLLEGE OF SCIENCE, TECHNOLOGY

AND MEDICINE

University of London

FORCED VIBRATION OF ROTATING DISCS AND INTERACTION WITH NON-ROTATING STRUCTURES

by

Hamid Mehdigholi

A thesis submitted to the University of London for
the degree of Doctor of Philosophy.

Dynamics Section
Department of Mechanical Engineering
Imperial College of Science, Technology and Medicine
London SW7 2BX

April 1991

IMPERIAL COLLEGE OF SCIENCE, TECHNOLOGY

AND MEDICINE

University of London

FORCED VIBRATION OF ROTATING DISCS AND INTERACTION WITH NON-ROTATING STRUCTURES

by

Hamid Mehdigholi

A thesis submitted to the University of London for
the degree of Doctor of Philosophy.

Dynamics Section
Department of Mechanical Engineering
Imperial College of Science, Technology and Medicine
London SW7 2BX

April 1991

ABSTRACT

This thesis is concerned with the flexural vibration of rotating discs and bladed discs. The preliminary part explores and unifies the definitions of different terms which have been used by previous workers in this subject. For harmonic excitation of a rotating disc, the general response of double modes is investigated. It is shown that there is more than one frequency component in the response. Also, the relationship are obtained between the frequencies of response and resonances, the disc rotation speed and the number of nodal diameters due to a given excitation.

A major part of the thesis reports the development of a practical simulation of vibration in a disc rotating past a static force. This kind of excitation occurs in practice due to non-uniformity of the pressure distribution on either side of a rotating disc but it is difficult to reproduce under laboratory conditions. It is shown that each mode of vibration can be excited in a stationary disc using two harmonic forces having certain spatial and temporal phase angles. For this simulation, a dual-sine excitation technique has been developed which may also be used for modal analysis of a disc or any axi-symmetric structure. There are close modes and even coincidences of natural frequencies of the modes in axi-symmetric structures which are often difficult to distinguish in normal experimental methods. These modes can be isolated and identified using the dual-sine excitation method.

The dual-sine excitation technique has been examined for different systems and excitation sets in terms of complex modes, mistuned systems and also different spatial and temporal phase angles for the exciters to see how widely the procedure can be applied in real

situations. A discrete mass model of a disc has been considered and different cases have been simulated using this model. On the experimental side, a phase and amplitude shifter has been developed for use in the dual-sine excitation method. Its input is a sinusoidal signal from the generator and its output is two sinusoidal signals with controlled relative amplitudes and phase angles.

A method is presented for displaying and interpreting the response in the vibrating disc. The response of an axi-symmetric structure is a combination of travelling waves and fixed vibration and the resulting complexity makes it difficult to visualise. A suitable format is devised for presentation of the response of a such structure to help understand what is going on at different points of the circumference when the disc is excited.

The final part of the thesis examines the vibration interaction between a rotating disc and an adjacent stator. There are two cases of interest which are likely to occur in practice. First, when the excitation initiated on the rotating disc due to an engine order excitation. Second, there is a possibility of vibration interaction of the stator with a disc when the stator is excited by a cyclic force input from an external source. In both of these vibration interactions, the critical speeds and conditions should be identified and examined in order to take them into consideration in practice.

In conclusion, this thesis provides a clear analytical and visual picture of the vibrational response of a rotating disc and a technique for displaying the response. The dual-controlled sine excitation method and its extension for more than two exciters is studied which may be used to simulate vibration response of a disc rotating past a static force (which is a travelling wave). A general formula for the simulation, a relationship between the excitation forces, spatial and temporal phase angles is presented. In the study of vibration interaction, it is shown that there is possibility of the transmission of disc vibration to the stator or vice versa. In the former case, the stator response is a travelling wave with frequency twice of the vibration frequency in the disc and in the latter case the vibration of the disc is a combination of ‘fixed vibration’ and ‘travelling waves’.

To My Family

ACKNOWLEDGEMENTS

I would like to express my gratitude to Prof. D.J. Ewins and Mr. D.A. Robb for their supervision and advice which have been essential to carry out this research.

I would like to thank all the members of Dynamics Section, specially to Dr. R.M. Lin and Mr. A. Nobari for discussions and comments on issues encountered in the work. Also Mr. B. Dale and Mr. P. Woodward are acknowledged for their assistance in the experimental part of the work.

I would also like to thank Dr. M. Movahedi from the Department of Electrical Engineering and Mr. M. Aref for their help and efforts in the design and making the controller 'PHASH'.

The assistance of the Department librarian Miss E. Archer and her assistant Miss A. Sage is appreciated, who are always ready to help students.

Finally, I am grateful to the sponsors of this research, The Ministry of Higher Education and Sharif University of Technology (in Iran), for the scholarship, financial support and encouragement which were given for this work.

NOTATIONS

A		A complex number, frequency dependent
A_1, A_2	-	Coefficients have been defined in equation (7.9)
A_{Fn}		Amplitude of forward travelling wave
A_{Bn}		Amplitude of backward travelling wave
$_rA_{jk}$	-	Modal constant of mode r from response measured at point j excited at point k
a_n, b_n	-	Amplitudes of sine and cosine components of the response
a, b		Two real constants are defined with the temporal phase angle in chapter 4
f(t), F(t)	-	Harmonic excitation forces
F_o		Amplitude of the sinusoidal force or - non-rotating static excitation force
F_n		Amplitude of the nth engine order excitation
$F_{i1}(\theta_o,t)$	-	A part of forcing function generated due to the vibration interaction
k		Stiffness of each spring in a tuned model in chapter 5
k_1, k_2, k_3, k_4	-	Functions of excitation parameters (in chapter 3)
k_m, k_n	-	Arbitrary integer coefficients
K		Stiffness of the interface between rotor and an adjacent stator
$M_,$, M_2 , etc.	-	Mass elements in discrete-mass model in chapter 5
m		Number of nodal diameters of an undesired mode to be excited or - in chapter 5, mass of every element in the tuned discrete mass model
n		Number of nodal diameters
N		Number of wave orders
p, q		Two constants
q(t)		Normal coordinate
Q(t)	-	Generalised force

R20		Control word for phase
R21		Control word for amplitude in channel 1
R22		Control word for amplitude in channel 2
s		Number of nodal circles
t		Time
V_g		Voltage on the command signal from generator
V_{f1}		Voltage towards shaker 1
V_{f2}		Voltage towards shaker 2
W_1, W_{12}, etc.	-	Amplitudes of different terms in the response
$x(\theta,t)$, X	-	Response and its amplitude
X_1, X_2	-	Amplitudes of travelling wave and fixed vibration terms in the response expression equation (3.33)
Y	-	Amplitude of response
[A]	-	System matrix=$[M]^{-1}[K]$
[H]	-	FRF matrix
[M]	-	Mass man-ix
[K]	-	Complex stiffness matrix
u	-	An eigenvector = $\{\psi\}$
u'	-	An eigenvector = $\{\psi'\}$
$\|\mathbf{u}\|$	-	Norm of the vector **u**
$[T_n]$	-	A matrix for wave order n defined in section 3.8
[T]	-	An expansion of [T,] containing all the 1 to N wave orders
a	-	Spatial phase angle between the excitation force and the origin of the stationary coordinate
α_1, α_2	-	Phase angle between travelling wave term and fixed vibration term in the response equation (3.33)
α_{Fn}, α_{Bn}	-	Phase angle of the forward and backward travelling wave terms
β	-	An angle as defined in equation (3.21)
β_n	-	Speed coefficient

Δ_1, Δ_2	-	Increments for R21 and R22 respectively
ϕ_s, ϕ_t	-	Spatial and temporal phase angles between excitation forces
$\phi(\theta)$	-	Eigenfunction of a diametral mode
γ	-	An angle as defined in equation (3.21), also it is the spatial angle between applied force and the origin in chapter 7
η	-	Damping loss factor
λ	-	A complex value which is a function of the eigenvalue
θ, θ_o	-	Coordinate systems, rotating with disc and stationary respectively
θ_p	-	Position of 'pseudo-nodal point' on the rim
$\{\psi\}$	-	An eigenvector
$\{\psi'\}$	-	Revised eigenvector of repeated eigenvalue to fulfil the uniqueness conditions
${}_n\{\psi'\}$	-	Normalised eigenvector of $\{\psi'\}$
$[\Psi]$	-	Matrix of eigenvectors
ω	-	Excitation frequency
ω_n	-	Natural frequency of n diameual mode of the disc
ω_a^-, ω_a^+	-	Backward and forward apparent resonance frequencies

Abbreviations

BBD	Bucket brigade delay
DAC	Digital to analogue converter
DCS	The dual-controlled sine technique
EM	Experimental method in simulation of navelling wave
E o	Engine order
FRF	Frequency response function
HM	Hybrid method in simulation of travelling waves
NAG	A collection of library routines for computing
ND	Nodal diameter
PHASH	- Phase and amplitude shifter

VPI	Vibration pattern imager, (a laser device)
VCO	Voltage controlled oscillator

Sub- and super-scriptions

a	Apparent resonance frequency
d	Disc
1, 2	First and second modes of a pair diametral mode, also refer to measurement points 1 and 2 on the structure
s	Stator (in chapters 6 and 7) and also for spatial phase angle ϕ_s
o	Stationary
c	Critical speed of the disc
n	The n nodal diametral mode
t	Temporal phase angle between excitations

Operators

II	-	Absolute value
II II	-	Norm of a vector or of a matrix
[ ]	-	Matrix
{ }	-	Vector
$\{\ \}^T$, $[\ ]^T$	-	Transpose of a vector or of a matrix
$[\ ]^{-1}$	-	Inverse of a square matrix
$[\ ]^+$	-	Pseudo-inverse of a matrix
..		Second time derivatives
$\angle$		Angle

CONTENTS LIST

CONTENTS LIST

2 FORCED RESPONSE OF A ROTATING DISC

3 EXPERIMENTAL SIMULATION OF A DISC ROTATING PAST A STATIC FORCE

6 VIBRATION INTERACTION OF A ROTATING DISC AND AN ADJACENT STATOR - Part I Excitation Applied to the disc

7 VIBRATION INTERACTION OF A ROTATING DISC AND AN ADJACENT STATOR - Part II Excitation Applied to the Stator

8 CONCLUSIONS AND RECOMMENDATIONS

APPENDICES

REFERENCES

LIST OF TABLES

LIST OF FIGURES

Chapter 1

GENERAL CONSIDERATIONS

1.1 INTRODUCTION

Vibration in structures and machines is normally an unwanted phenomenon behaviour which may cause fatigue failure, unreliability and noise pollution. In order to cope with this problem and to make sure that vibration levels are low enough to prevent damage and losses, methods and theories have been developed and practiced, e.g. references [1] and [2]. In recent decades, aided by development of computing and experimental facilities, there has been abundant research, both experimentally and analytically, in the identification of the dynamic properties of the structures. Modal testing - the experimental techniques in vibration analysis - has been established and publicised [3,33], which has significantly expanded the capability of the investigation and solving of structural vibration problems. On the theoretical side also there has been a lot of effort to predict the dynamic characteristics of a structure. However, neither theoretical nor experimental methods always give a precise estimate and each has certain deficiencies. In recent years, there have been many attempts to use experimental results in the theoretical model to make a representative dynamic model for the structure.

Among engineering structures, rotating machines have a specific place and are very important from the viewpoint of vibration analysis. For example, jet engines are in this category and it is needless to stress how important is the safety of these engines in an aeroplane or how costly it would be if just one blade fails in a steam turbine.

Vibration analysis concerned with rotating structures has several different aspects. Many researchers have worked on rotor dynamics and dealt with the vibration in rotating shafts [30,31]. Much work has been done on disc vibration and a lot of studies on the vibration analysis of the blades. Of course, these results have to be combined to present the vibration characteristics of the complete rotating machines. Blades are more sensitive to vibration and more failures have been reported in these components than in the others due to the high stresses developed.

In gas and steam turbines, blades have a very important role. Often the failure of one blade can be responsible for large economic, social and sometimes human losses. Fatigue failure has been diagnosed for many of these accidents. Since the beginning of this century, many researchers have tried to understand the real dynamic behaviour of the blades in a bladed disc assembly under operating conditions. Blades have been modeled as cantilevered beams, however in a bladed disc the flexibility of the disc and its significant effect on the dynamic properties of the blades have also been included in the considerations by some researchers [5,8].

The transverse or out-of-plane flexural vibration modes of a disc are characterised by nodal diameters and nodal circles [5]. The modes which consist of nodal diameters are encountered more in practice and their response can be excited as stationary waves [4]. The stationary wave has been recognised as a wave which caused severe vibration in the bladed disc. While this wave is stationary relative to a coordinate in space, it is rotating in the opposite direction relative to the disc with a speed equal to the disc speed (Ω). The stationary and travelling waves and their relationships have been discussed in references [3,6] and are described in more detail in section 1.3.

Analyses and experimental techniques needed to explore the vibration behaviour in rotating structures are not as simple as in the ordinary stationary ones. This is not only because some of the dynamic properties (such as the natural frequencies) change with rotation speed, but also the property of axi-symmetry or periodicity within most of the rotating components causes the problem to be more complex. The rotating disc used in gas and steam turbines or in other applications has been studied by many researchers. Since the invention and application of steam turbines in the early years of this century, research on blade properties started because many failures had occurred. In the early 1920s, Campbell [4] carried out his valuable work on the problem of failure of bladed discs in steam turbines. For the first time, comprehensive experiments were carried out on steam turbine bladed discs and different modes in the rotating discs were examined. Campbell found that both disc and buckets vibrate together as a continuous disc and must be treated as a unit in the study of vibrational behaviour. He also discovered the travelling and standing waves in vibrating discs and in his observations, he found that the standing wave - caused by a disc rotating past a static force - was the cause of most failures in bladed discs. One of the consequences of his research was that discs then had to be so designed that they did not operate at any of their critical speeds as always there is a possibility of such small excitation forces present in turbines.

Ewins [8,12] found analytically and experimentally that a bladed disc has many more natural frequencies than those predicted for one individual cantilevered blade. Figure 1.1, which is taken from reference [8], shows the families of modes of a bladed disc, and also those for the disc alone, compared with the cantilevered blade frequencies.

The general vibration behaviour of a bladed disc is similar to a solid disc and has nodal diameters and nodal circles in its mode shapes. Considering the lower bladed disc curve in figure 1.1 (which corresponds to the zero nodal circle family of modes), it is seen that by increasing the number of nodal diameters, the natural frequencies do not change very much and approach the first flexural cantilevered mode of the blade.

Analyses and experimental techniques needed to explore the vibration behaviour in rotating structures are not as simple as in the ordinary stationary ones. This is not only because some of the dynamic properties (such as the natural frequencies) change with rotation speed, but also the property of axi-symmetry or periodicity within most of the rotating components causes the problem to be more complex. The rotating disc used in gas and steam turbines or in other applications has been studied by many researchers. Since the invention and application of steam turbines in the early years of this century, research on blade properties started because many failures had occurred. In the early 1920s, Campbell [4] carried out his valuable work on the problem of failure of bladed discs in steam turbines. For the first time, comprehensive experiments were carried out on steam turbine bladed discs and different modes in the rotating discs were examined. Campbell found that both disc and buckets vibrate together as a continuous disc and must be treated as a unit in the study of vibrational behaviour. He also discovered the travelling and standing waves in vibrating discs and in his observations, he found that the standing wave - caused by a disc rotating past a static force - was the cause of most failures in bladed discs. One of the consequences of his research was that discs then had to be so designed that they did not operate at any of their critical speeds as always there is a possibility of such small excitation forces present in turbines.

Ewins [8,12] found analytically and experimentally that a bladed disc has many more natural frequencies than those predicted for one individual cantilevered blade. Figure 1.1, which is taken from reference [8], shows the families of modes of a bladed disc, and also those for the disc alone, compared with the cantilevered blade frequencies.

The general vibration behaviour of a bladed disc is similar to a solid disc and has nodal diameters and nodal circles in its mode shapes. Considering the lower bladed disc curve in figure 1.1 (which corresponds to the zero nodal circle family of modes), it is seen that by increasing the number of nodal diameters, the natural frequencies do not change very much and approach the first flexural cantilevered mode of the blade.

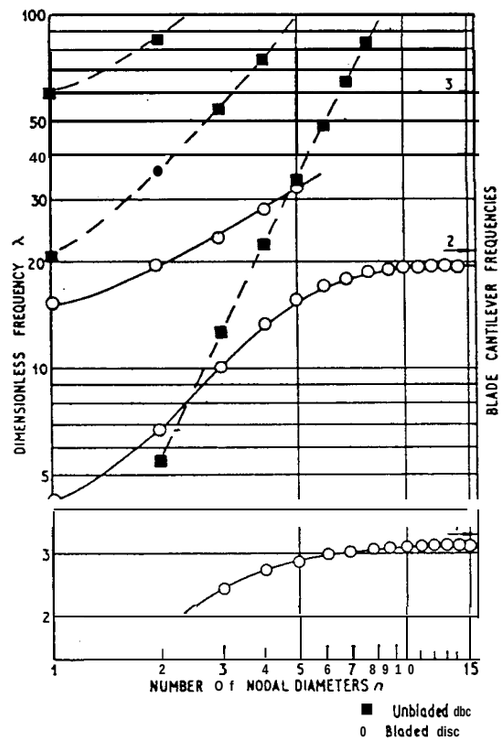

Figure 1.1 Natural frequencies of a uniform bladed disc

The basic theory for the vibration modes of a disc has been understood for many years by considering a circular plate [2]. However, research is still needed on how to predict the maximum response level in the bladed disc if it is not ideally axi-symmetric. Also, a problem still exists of how to estimate the modal properties of a mode close to the adjacent modes, which is usually the case for higher diametral modes due to the closeness of the frequencies, shown in figure 1.1. This figure is for a perfect and ideal axi-symmetric case but in real terms, the bladed discs are slightly imperfect and so there are more modal frequencies than seen in figure 1.1.

Ewins et al [7, 8, 10,131 have worked on the effect of imperfections on forced response levels as well as on the modal characteristics. It has been shown in [13] that the maximum

level could increase in some blades by up to 163 percent of the tuned case while at some other points the response level becomes less than in the tuned system so that the mean level is almost constant. Whitehead, in his theoretical investigation [28], explored an approximate formula to predict the maximum level of mistuned response relative to the tuned case. His formula is related to the number of blades and it has been deduced in this work that an odd number of blades has been selected in many designs to avoid vibration of the mode with number of nodal diameters equal to half of the number of blades. Due to mistuning, a rogue blade vibration can occur in a bladed disc [24]. This provides severe response levels in one or two blades while the others are at much lower levels. Susceptibility of a blade becoming a rogue is not only a function of mistuning but also of the excitation pattern. A significant degree of mistuning can be introduced to the bladed disc assembly by packeting the blades [25,26,27,32]. This is done in shrouded bladed discs and it has been shown that for certain patterns of packeted assemblies we can minimize the extent of blade vibration response levels to specific excitation orders.

Excitation sources originated from different mechanisms in the compressor and turbines, but the most common has been modeled as a static force applied in the axial direction to the bladed disc. This excitation could be from any non-uniformity in pressure distribution of the gas flow through stationary vanes, struts or nozzles and can cause a serious problem if the disc runs at one of the critical speeds. In reference [7], it is proposed that any diametral mode in a disc rotating past a static force can be simulated by a stationary disc with two harmonic forces. These forces are applied at the certain positions on the disc and have 90^{o} phase difference in time. This could be very important in the experimental investigation of vibration in the rotating discs. First, doing experiments on a stationary structure is more convenient than on a rotating one. Second, it is possible that any diametral mode may be chosen and excited while the other modes are not excited or their effects are very small, which can be a good procedure to identify modal characteristics. Developing this idea has been a major objective on this thesis. Staples [23] has simulated experimentally the travelling waves on a casing by using two

shakers . He showed that by increasing mistuning, the amplitude of the (with respect to the disc) decreased and so there was less possibility of ı the stator and the rotor by comparison with the tuned case.

esearch into the vibration of bladed discs assemblies, e.g. as reviewed in there are few works on the investigation of travelling wave responses. In : two studies mentioned - i.e. [7 and 23], Macke [22] has explored :s in vibrational shells and rotating cylinders. In his work, the similarities s between the frequency - speed diagrams of a cylinder and a disc are

nore familiar with the basic terms which are frequently used in this thesis modes, mistuning, Campbell diagram, engine order excitation and muli- ı, these are explained in the following sections.

L VIBRATIONAL MODES IN DISCS

ttems in a disc are comprised of nodal lines and nodal circles [5], as shown ples in figure 1.2. For a free-free disc, the first mode is a two nodal diameter , but if the boundary conditions are different, as it is in many applications, r vibrational modes for a disc with natural frequencies lower than the 2 ND ency [21].

ıal pattern of a disc with clamped-free boundaries, the amplitude changes in on on every non-nodal radius so that the maximum amplitude will be at the ce of the disc for the diametral modes. This is why, in most analyses, the f the disc is used to characterise the disc vibration.

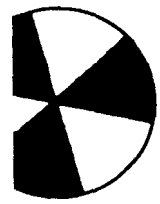

ı=3, s=0

isc;
nodal circles

like a disc. This has been
cs although in 1899 it had
ımenon of double modes
lamping and similar nodal
:c. This orientation means
es of the other mode.

epends on the position of
nti-nodal point no matter
However, double modes
in practice, any disc is to
ines is fixed in mistuned
arger mass is ***on the*** anti-
with the nodal diameters
very important factor in
n mass or stiffness in the
l within the tolerances in
the double modes and
Arnold [6] advised that
ibration and this can be

beneficial, (standing waves and fixed vibration are explained in the next section). In reference [17], it was shown experimentally that a pair of diametral modes with a split factor of 0.056 behaves like a double mode (or a tuned system) while another pair with a split factor equal to 0.25 percent acts as a mistuned system, (split factor has been defined as the ratio of frequency split to the average of the two frequencies). Mistuning also causes the number of resonance frequencies to be more than in the tuned case so that the mistuned disc is more susceptible to resonances than the tuned case [9]. According to reference [7], there is a correlation between the mistuning pattern and modes splitting; the n nodal diameter modes will split if there is a $2n\theta$ component in the mistuning distribution of mass or stiffness around the disc. In a tuned disc, the mode shapes are defined patterns each with a certain number of nodal diameters but in a mistuned case each mode shape does not consist of one single diametral order but is contaminated by other orders [25,26]. The contribution of other diametral orders depends on the patterns of mistuning. This results in mistuned systems being more susceptible to vibration at certain engine order excitations than are tuned assemblies.

1.3 'WAVES' IN VIBRATING ROTATING DISCS

In the literature describing vibration in rotating discs, we come across phrases like "travelling wave, standing wave and fixed vibration". It is found that some of these phrases are not used in a unified way by different groups. The definitions used and explained here are identical to those used by Tobias et al [6].

When a single-point excitation is applied to a stationary disc, vibration occurs in an ordinary manner as for any other simple structures. If the frequency of the excitation is close to just one of the nodal diameter modes of the disc, the response on the rim will be similar to that shown in figure 1.3 and is called a **fixed vibration.** In this figure, in fact, the unwrapped rim has been shown as a straight line scaled from 0^o to 360^o and this

display format will be used through out this thesis. The distorted mode shape is shown at 6 (or 7 in some cases) frames - equal increments of time during one cycle. For this case, the response is a fixed vibration since the nodal points - or nodal lines - are fixed on the disc. The amplitude of response changes from zero at nodal points to its maximum value at anti-nodal points. The response on the rim can be described as

$x(\theta_o,t) = A \sin n\theta_o \cos \omega t$, where n is the number of nodal diameters and it is equal to 2 in figure 1.3.

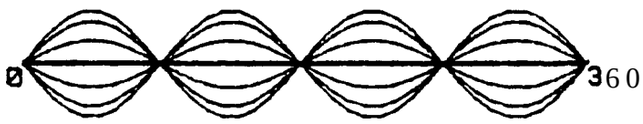

Figure 1.3 Fixed vibration response in a stationary disc (2 ND mode)

In a rotating disc, the excitation effect is normally complex since there is also relative motion between the excitation point(s) and the structure. In the study of vibration in rotating discs, either of two coordinates can be chosen; one stationary in space $\theta_o(t)$, and another one rotating with the disc 0(t). In a vibrating rotating disc, we can have a travelling wave and fixed vibration simultaneously. A **Travelling wave** in a coordinate is a deformed shape moving in or opposite to the direction of that coordinate. Figure 1.4 shows the response of a 3 diametral mode of a disc at three points in time which is travelling in the stationary coordinate θ_o to the right. For this case, the response can be expressed as:

$$x(\theta_o,t)=A \sin 3(\theta_o - \Omega_w t) \qquad (1.1)$$

where Ω_w is the angular speed of the wave. In this type of response, every stationary point

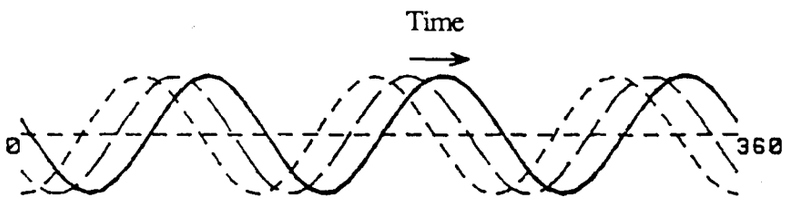

Figure 1.4 Schematic display of a travelling wave

experiences the same vibrational signal with frequency '$3\Omega_w$' but at a different phase to its neighbours and, clearly, when the response is a travelling wave, there are no longer any fixed nodal points. A travelling wave could also be obtained relative to rotating coordinates. In figure 1.5, it is assumed that the disc is rotating so that its circumference is moving to the left with speed Ω and it is vibrating such that its response is a travelling wave moving to the right with speed Ω_w relative to the disc. This motion can be expressed by:

$$x(\theta,t)=A \sin 3(\theta-\Omega_w t) \qquad (1.2)$$

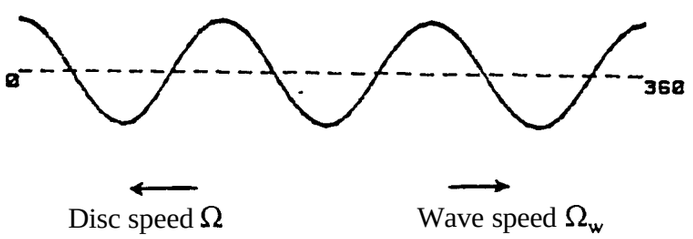

Figure 1.5 A standing wave (if $\Omega_w=\Omega$)

From a stationary viewpoint , the wave is moving with speed of 'Ω_w-Ω' to the right (Ω_w>Ω). Now assuming a case that Ω_w=Ω then, a stationary observer see the wave stationary in the space which is called a standing wave. From the mathematics , substituting 'θ_o' by 'θ+Ωt' in equation 1.2 gives $x(\theta_o,t)$=A sin θ_o, which represents a stationary shape - a standing wave. When the response is a standing wave, a stationary pick up or vibration sensor does not measure any vibratory movement.

Here, the terminological aspects of the waves have been explained without talking about the conditions in which they will be excited in vibrating discs. However, those conditions will be studied in the other sections.

1.4 FREQUENCY - SPEED DIAGRAM AND RESONANCES IN ROTATING DISCS

It is convenient to express the vibration characteristics of a rotating bladed disc in the diagrams introduced first by Campbell [4]. There are four main factors involved in considering vibration in rotating bladed discs: rotational speed, vibration frequency, number of nodal lines and the response level. A plot of frequencies against rotating speed is known as a Campbell diagram and in the following, a figure is used to explain the diagram. In figure 1.6, a Campbell diagram for the n - nodal diameter mode(s) of a disc has been illustrated where the n - diameter natural frequency has been named as curve ‘A’. The natural frequency increases with rotational speed due to stiffening of the disc and the following governing relationship applies.

$$\omega_n^2 = \omega_0^2 + \beta_n \Omega^2 \qquad (1.3)$$

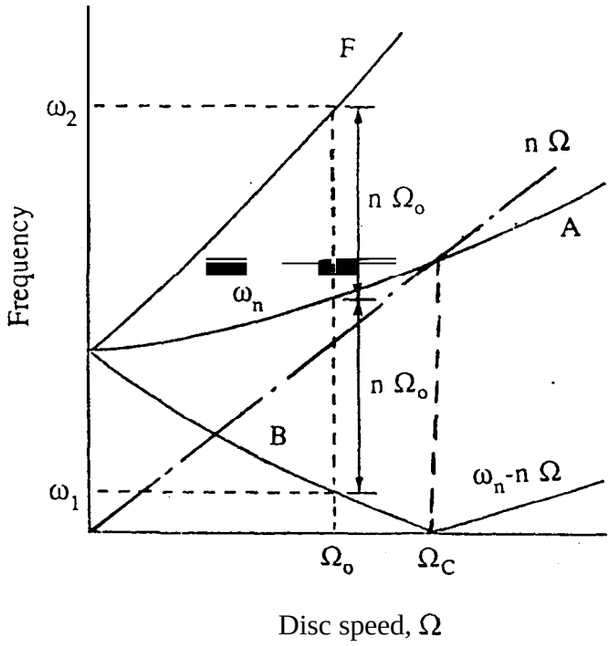

Figure 1.6 Frequency - speed diagram for the n ND mode

where ω_0 is natural frequency of the mode in the stationary state and β_n is a stiffening factor (**or** speed coefficient) which depends on the mode shape and also geometry and material of the disc.

There are two other curves in the diagram in figure 1.6: curves 'B' and 'F' which are offset '$n\Omega$' from the n diameter natural frequency curve 'A' and are the frequencies of the backward and forward travelling waves. Assume the disc is rotating at speed Ω_o, and that a stationary harmonic excitation with frequency ω_1 is applied to the disc so that $\omega_1=\omega_n-n\ \Omega_o$, i.e. the excitation frequency intersects the curve 'B' due to the influence of rotating speed. In this case, the disc will be at resonance with a frequency equal to ω_n and the response is a backward travelling wave. With the excitation frequency equal to ω_2 in figure 1.6, a similar situation will happen but the response is a forward travelling wave. In practice, this type of resonance - which can occur with some multiple of the rotational speed (h Ω) - is called a **minor resonance** [4,15]. Ewins [48] has investigated the possibility of coincidence of two resonances in a mistuned disc at one rotating speed

which causes certain blades to vibrate with amplitudes of up to 130 per cent above those under normal conditions. This was reported to be mainly due to mistuning or even small modification in design of the bladed disc.

French, in his experimental investigation on rotating compressor discs [16], explored minor resonances which can be generated by a defective anti-friction bearing. Kushner [15] and Jay et al [17] independently showed that in some turbine discs with certain differences in numbers of vanes and blades can cause minor resonances in the bladed disc.

Therefore, it can be stated that when a 'per-revolution' or multi-rotational excitation frequency is equal to the frequency of backward or forward curve of a diametral mode in the Campbell diagram, a minor resonance occurs. However, the 'major' resonances occur when the rotational speed is equal to Ω_C (shown in figure 1.6) which is called a critical speed. At this condition, if the excitation is a static force (i.e. $\omega=0$), a resonance occurs and the response of a double mode will be a standing wave. This excitation seems to be inevitable in practice since any non-uniformity in pressure distribution on either side of the disc, upstream of the stationary vanes to a bladed disc in a compressor (or gas flow from n nozzles in a turbine disc) can produce this kind of excitation.

These critical speeds were first found by Campbell [4]. He also introduced the term "standing waves" which have been found to be the cause of many failures in engine bladed discs. At this condition, the natural frequency is equal to the number of nodal diameters multiplied by the rotation speed,. $\omega_C=n\Omega_C$. It is concluded that the critical speeds in the Campbell diagram are found by intersections of line '$n\Omega$' with the curve of the n nodal diameter natural frequency line, figure 1.6. The radial lines, such as '$n\Omega$' ($n=1, 2, \ldots$), represent the excitation from n struts, vanes, nozzles or any obstacle in the flow towards the bladed disc which represents n engine order excitation,.as it has become known.

In reference [4], it has been shown that the one - diameter natural frequency line does not cross the 'Ω' line and so there is no critical speed for this mode. This is always true since the speed coefficient, β_n, is normally between 2 and 3 according to reference [4] and it can be shown that for n=l in the Campbell diagram line (ω_n-nΩ) does not cross the horizontal axis ω=0.

1.5 MODAL TESTING METHODS

Modal testing, or experimental modal analysis, is a technique for the identification of dynamic properties - natural frequencies, mode shapes and damping values - of a structure on the basis of a test on the real structure or on its model. There are other techniques which solve the problem mathematically, such as finite element (FE) methods. Both mathematical techniques and modal testing methods have been developed in the past two decades and have their own capability and advantages.

In order to test a structure for dynamic identification, it is usually excited by an external force. A simple test is using an instrumented hammer to apply an impulsive force to the test structure. Other methods of excitation are applied using an electro-dynamic shaker which is normally connected to the test piece by a push rod. Different signals can be applied to a shaker: sinusoidal, impulsive, random and periodic, and hence, different force functions may be applied to the structure.

Input (force) and output (response) signals are measured and analysed to get information about the dynamic properties of the structure. The technique was first introduced by Kennedy and Pancu [36] and then developed by others. For more practical aspects and details of modal testing, reference [3] may be used.

There are two principal methods of excitation in modal testing: Single-point excitation and multi-point excitation techniques which are introduced in the following.

1.5.1 Single-point excitation

Single-point excitation techniques are very common in modal testing and are simple as just one exciter is used in each test. A single point excitation method has some advantages and disadvantages compared with multi-point excitation techniques. The instrumentation is simple as there is just one exciter and there is no need to control the input signals, unlike in multi-excitation methods where relative phase control is necessary. However, problems can arise when the test structure is big or the modal density is high. In the former case, the input excitation energy may not be spread evenly over all parts of the test structure. Also, using one excitation, most of the modes of vibration are excited except ones whose nodal points coincide with the excitation point. By increasing the number of excitation points, the possibility increases that modes are preferentially excited and even a particular mode can be isolated and enhanced for better identification. In reference [35], the problem of cross-axis motion and fragile test articles are also mentioned as limitations of single point excitation. Despite these limitations, single point excitation techniques are widely used in most modal tests on ordinary structures.

1.5.2 Multi-Point Excitation

The application of multiple excitation began more than forty years ago when Kennedy and Pancu [36] introduced a method using two vibrators for the identification of symmetric structures such as aeroplanes. At that time, the applied mathematical techniques for determination of modal characteristics in a complex structure involved some approximation and experimental verification of the analytical results were needed. This led to the employment of multi-point excitation to excite **normal modes** by adjusting the

different excitation forces.The idea of excitation of a normal mode is also important when there are close-frequency modes where the single-point excitation method may not be able to generate accurate modal properties.

The theory of the normal mode excitation technique has been established strictly for an undamped - or a lightly-damped - lumped mass system [37], but the technique can also be applied to continuous systems by considering a limited number of coordinates. The general procedure of normal mode excitation is that the vibrators are located at proper points for excitation. Then, arbitrary excitation forces at the desired frequency are applied to the structure. This is done by checking on the oscilloscope the phase of the response relative to the input force. At a resonance frequency, the phase angle is 90° for an individual normal mode and, hence, we have to adjust the in-phase forces (except for polarity) to achieve this phase angle at all the stations. This adjustment will be very difficult for complex structures using many shakers. Asher [38] estimated the natural frequencies and the force ratios needed to excite a normal mode theoretically. It has been shown that the modal vectors are equivalent to those of the undamped or proportionally-damped system and that the desired force vector can be calculated and predicted for excitation. Craig et al [39] developed Asher's method for more applications. In the case studied, a nine lumped mass system with proportional damping, they examined different combinations of shakers and close natural frequencies. They also explored the case of addition of another shaker and suggested best locations. In reference [40] the limitations on the modal testing with single-excitation as well as multi-excitation have been discussed. The basis of the analysis of in-phase excitation using multi-point excitation is applicable for a finite, discrete mass model and undamped or proportionally damped systems. In a proportionally-damped system, once the forces are adjusted at a natural frequency, they excite the normal mode; if the frequency is changed, the force pattern remains unchanged and the shape of the response is still the normal mode. However, if the system is non-proportional damped, it has been explained in reference [40] that by varying frequency, we have to re-adjust the forces to maintain the normal mode shape in

the response. Moreover, application of classical in-phase excitation technique for non-proportionally damped systems may lead to incorrect estimates. The non-proportional damping (general case) has been explored further in reference [40] and proposed that for excitation of a complex mode, a mode of a non-proportionally damped system , a complex excitation frequency should be applied. That is, excitation should be in the form of a damped sinusoid to concentrate the energy in the vicinity of the desired complex response frequency. Another requirement which has been added to the modal testing system in reference [40] is the generalisation of the control the shakers. It has employed phase and amplitude control of shakers instead of polarity (0 or 180° phase) and amplitude control of the input forces.

Hallauer et al [41] also considered a coupled-damping (non-proportionally damped) system in two numerical examples and showed that for these systems perfect mode tuning is achieved only at the natural frequency with response quadrature phase relative to excitation, even though all degrees of freedom are excited. They used multiple shaker sinusoidal excitation and developed Asher's method for real continuous structures where finite coordinates or incomplete excitation are applied and they showed the strengths and weakness of the technique.

Sinusoidal excitation is the earliest technique applied for the identification of dynamic characteristics and is still widely used. This is because of some properties of this type of excitation. It is simple to apply and to measure the input - output signals. This factor was very important a few decades ago regarding the experimental equipment at that time. The most important factor of sinusoidal excitation is the possibility to reveal any non-linearity present in the system. In the past decade, with more improvement in signal processing and digital control systems, random excitation is applied widely in modal analysis even in multiple input methods. Allemang et al [42] used a two random input excitations procedure and developed a formula to estimate the frequency response functions. They have given some experimental example for their method. In reference [43], multiple input random (MPR) and multi-phase sine sweep (MISS) methods have been introduced and

discussed. In these techniques, uncorrelated inputs are used and so FRFs can be computed between every response location and each of the inputs. They also have proposed a method using multiple input FRF acquired via MPR or MPSS to determine frequencies, repeated or closely spaced modes and the force associated with each mode. The FRFs are employed in an eigenvalue solution to determine at which frequencies the in-phase response is a minimum compared to the total response. This automated procedure produces the force appropriation required to perform isolation and excitation of real normal modes. In reference [44] another technique called 'Spatial Sine Testing' (SST) has been introduced in which the test structure is excited with an arbitrary force vector at a particular frequency. The force vector and the forced mode (response) are measured, then the parameter estimation algorithm extracts the modal parameters using an eigensolution technique. More experimental results using SST method have been presented in reference [45] which show the capability of this method.

In a single-point excitation technique, cross-axis motions may cause to fail the test results. One way to deal directly with such undesired response is to actively suppress the cross-axis motion, Stroud et al [35] introduced the multi-exciter single axis (MESA) technique and have employed phase control as well as cross coupling compensation. With coordinated exciters, out-of-phase drive signals can be used to suppress unwanted motion reducing cross-axis response and undesired coupling effect.

In the modal testing of axi-symmetric structures, we often deal with repeated natural frequencies and high modal density. As mentioned before, one of the objectives of using multi-point excitation is to enhance a mode which is difficult to identify and to analyse with an ordinary single-point excitation test. On the other hand, simulation of a travelling wave in a rotating disc is of the interest of this work. Here, special dual sine excitation must be developed which enables preferential excitation of a double mode or two close diametral modes with the same order (number of nodal diameters). The input force amplitudes and phase have to be controlled in order to fulfil the corresponding conditions.

1.6 SCOPE AND OBJECTIVES OF THIS THESIS

One of the main objective of the research reported in this thesis is to develop a procedure for simulating, displaying and interpreting vibration in a disc rotating past a static force. In order to do that the basic understanding of forced vibration of a rotating disc is investigated in chapter 2. A simple model is assumed in this stage since the qualitative understanding of the response - in terms of frequencies and components - is of interest in this work. The response is obtained in both stationary coordinates and rotating coordinates to show the resonance frequencies and the nature of the response in respect of travelling waves or fixed vibration. Some of the analytical results are checked on a rotating disc with the prediction and the assumed model results.

In chapter 3, the theoretical aspects of the simulation are described. First, the basic concept of the simulation of a disc rotating past a static force is studied and it is shown how the vibration can be simulated by exciting the stationary disc with two harmonic forces. Then, the generalisation of the simulation is discussed which leads to a formula presents the relationship between number of nodal diameters, spatial and temporal angles between two excitation forces. In another part of this chapter, the application of more than two excitations in the simulation is examined and a technique is proposed to improve the simulation by increasing the number of exciters. In order to present the response of the disc in an animated shape - which is very helpful for appreciating the complexity of response- a decomposition procedure is introduced. In this method, we can estimate the contributions of different wave orders in the response by carrying out a form of Fourier transform of the response function of the rim with respect to the wave order.

In chapter 4, the application and the experimental aspects of the simulation are described. Two methods are suggested which are basically the same. The first is a hybrid method in which after obtaining the FRF matrix from experimental data, the response to the

simulation condition are calculated. In the second method, the vibrational response of a rotating disc is simulated experimentally on a stationary disc. Both methods are tested on a real bladed disc and there is some discussion of the results. For controlling the magnitude and relative phase of two forces, a phase and amplitude shifter is developed and corresponding software is introduced. It is worth mentioning that to control the two excitation forces is not easy in practice. Because there is non-proportionality between the voltage input to a shaker and the out put force of the shaker around resonance, we have to adjust relative phase and amplitudes of forces by a trial - and - error procedure.

In the next part of the thesis, a discrete-mass model of the disc is considered to examine the simulation procedure in a model having more than one or two pairs diametral modes assumed in the earlier simple model. Also, the simulation can be tried for the system with complex modes and mistuned systems. These investigations are achieved by introducing different data in the lumped mass model.

Another related subject concerned with the vibration in rotating bladed discs is the possibility of vibration interaction between a rotating disc and an adjacent stator, and this is the subject of chapters 6 and 7. It is shown that the vibration from one substructure can transfer to the other through the medium in between. Regarding the vibration in the disc discussed earlier, its interaction in the stator is obtained. Also, assuming that the stator vibrates by a harmonic excitation, which is quite possible, the vibration induced on the rotating disc is explored. The possibility of coincidence of resonances in the both cases is examined by some numerical examples.

The conclusions from this work are drawn in chapter 8 where also suggestions for further development are presented.

Chapter 2

FORCED RESPONSE OF A ROTATING DISC

2.1 INTRODUCTION

A clear understanding of the steady-state response of rotating discs to harmonic excitation is essential in most investigations of the vibration of structures having these components. Although many workers have explored the response of the rotating disc, a comprehensive theory of forced response of rotating discs has not been presented. Frequency components of response, natural frequencies and the critical speed concepts are usually used in most of the corresponding literature.

Nodal diameter modes are particularly important in the vibration analysis of a rotating disc. These modes are the origins of the travelling and standing waves which have been identified as the cause of many failures in turbine discs. The response of a disc due to the excitation of a diametral mode is normally represented by the response on a concentric circle on the disc such as rim of the disc, This consideration is simple and accurate since the travelling waves are created in the circumferential direction and the maximum response is on the rim.

Other assumptions have also been made here to simplify and to make the analysis possible. A disc is treated as a lightly-damped structure. The stiffening effects due to

rotation and centrifugal forces are not considered; these assumptions do not change the generality of the conclusions.

In this chapter, steady-state response of a rotating disc under stationary harmonic excitation is investigated in tuned and mistuned discs.

2.2 RESPONSE OF THE *SINE* MODE TO HARMONIC EXCITATION

2.2.1 Analysis Using Rotating Coordinates

2.2.1.1 Analysis

Let us consider a single mode of the pair of n ND mode of a disc rotating at speed Ω. The mode shape is assumed to be $\phi(\theta) = \sin n\theta$ and the natural frequency ω_{n1}. The coordinate θ is assumed to be on the disc and the excitation is a harmonic stationary point force applied initially at a spatial angle a as shown in figure 2.1. The direction of coordinate θ is assumed in the opposite direction to the disc rotation.

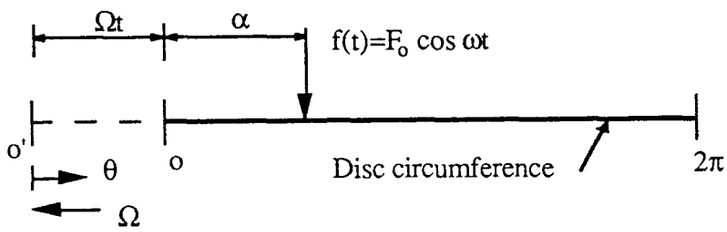

Figure 2.1 Coordinate on the rotating disc

The forcing function for such a system is [51]:

$$F(\theta,t) = (F_0 \cos \omega t)\ \delta[\theta-(\Omega t+\alpha)] \qquad (2.1)$$

where $\delta[\theta-(\Omega t+\alpha)]$ is a delta function and defined as:

$$\left.\begin{aligned} &\delta[\theta-(\Omega t+\alpha)] = 0 \qquad \text{for } \theta \neq (\Omega\ t+a) \\ \text{and} \qquad &\int_{-\infty}^{+\infty} \delta\,[\theta-(\Omega\ t+a)]\ d\theta = 1 \end{aligned}\right\}$$

The generalized force for the assumed mode is :

$$Q(t)= \int_0^{2\pi} F(\theta,t)\ \phi(\theta)\ d\theta$$

or :

$$Q(t)= \int_0^{2\pi} (F_0 \cos\ \omega t)\ \delta[\theta-(\Omega t+\alpha)]\ \sin\ n\theta\ d\theta$$

After integration, this becomes:

$$Q(t)= F_0 \cos\ (\omega t) \sin\ n(\Omega t+\alpha) \qquad (2.2)$$

Equation (2.2) represents the generalized force for the n ND mode. Having obtained the generalized force, the normal response is calculated by using the convolution integral for a very lightly-damped system [55]:

$$q(t) = \frac{1}{m_{n1}\,\omega_{n1}} \int_0^t Q(\tau)\ \sin\ \omega_{n1}(t-\tau)d\tau \qquad (2.3)$$

W h e r e : m_{n1} is the modal mass or generalized mass of the mode;

ω_{n1} is the natural frequency of the mode;

Substituting from equation (2.2) in (2.3) and integrating will give:

$$q(t) \quad \frac{F_0}{4m_{n1}\,\omega_{n1}} \left\{ \frac{\sin\,[(\omega+n\Omega)t+n\alpha] - \sin(-\omega_{n1}t+n\alpha)}{\omega+n\Omega+\omega_{n1}} \right.$$

$$\frac{\sin\,[(\omega+n\Omega)t+n\alpha] - \sin(\,\omega_{n1}t+n\alpha)}{\omega+n\Omega\,-\,\omega_{n1}} \qquad \frac{\sin\,[(\omega-n\Omega)t-n\alpha] - \sin(-\omega_{n1}t-n\alpha)}{\omega-n\Omega\,+\,\omega_{n1}}$$

$$\left. i\frac{\sin\,[(\omega-n\Omega)t-n\alpha] - \sin(\omega_{n1}t\,-na)}{\omega-n\Omega-\omega_{n1}} \right\} \qquad (2.4)$$

This equation contains the transient response where the terms of natural frequency ω_{n1} exist. The investigation is concerned with the steady-state problem, that is considering only the terms which are relevant to the excitation frequency. After simplification of equation (2.4) we will have:

$$q(t) = \frac{F_0}{2m_{d1}} \left\{ \frac{-1}{(\omega+n\Omega)^2 - \omega_{n1}{}^2} \sin\,[(\omega+n\Omega)t+n\alpha] + \frac{+1}{(\omega-n\Omega)^2 - \omega_{n1}{}^2} \sin\,[(w-nQ)t-na] \right\}$$

This equation gives the normal coordinate of the n ND mode and by using it , the response is calculated :

$$X_{n1}(\theta,t) = q(t)\ \phi(\theta)$$

or

$$X_{n1}(\theta,t) = -W_1 \sin\,[(\omega+n\Omega)t+n\alpha] \sin n\theta + W_2 \sin\,[(\omega-n\Omega)t-n\alpha] \sin n\theta \qquad (2.5)$$

where :

$$\left.\begin{aligned} W_1 &= \frac{+F_0}{2\,m_{n1}[(\omega+n\Omega)^2 - \omega_{n1}{}^2]} \\ \text{and} \qquad W_2 &= \frac{+F_0}{2\,m_{n1}[(\omega-n\Omega)^2 - \omega_{n1}{}^2]} \end{aligned}\right\} \qquad (2.6)$$

Equation (2.5) presents the response of a single ND mode of a rotating disc excited by a stationary harmonic force. It consists of two 'fixed vibration' components with frequencies of $(\omega \pm n\Omega)$. The response frequencies at different speeds are shown in figure 2.2 for a defined excitation frequency ω.

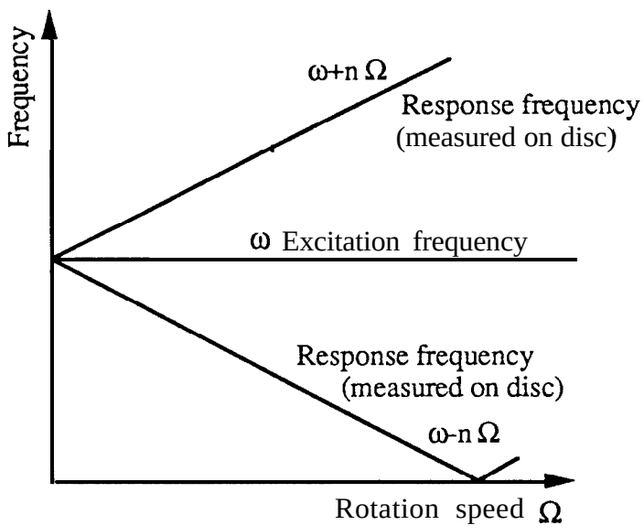

Figure 2.2 Excitation and response frequencies of single n ND mode in a rotating disc; (Stationary harmonic excitation; and response coordinate on the disc)

Equations (2.5) and (2.6) show that there are two frequencies for the system at which the denominators are zero: $(\omega \pm n\Omega)^2 - \omega_{n1}^2 = 0$. It follows that there are two 'apparent resonant frequencies' at each spinning speed Ω:

$$\left.\begin{aligned} \omega_a^+ &= \omega_{n1} + n\Omega \\ \text{and} \quad \omega_a^- &= \omega_{n1} - n\Omega \end{aligned}\right\} \qquad \textbf{(2.7)}$$

where ω_a^+ and ω_a^- are apparent resonant frequencies and are shown in figure 2.3 for different speeds. Note that the analysis has been based on the coordinate fixed on the disc. In the next section, the analysis is carried out in terms of a stationary coordinate.

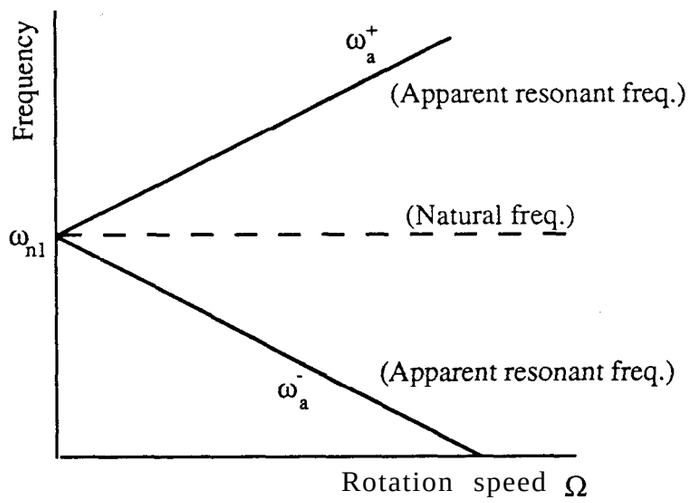

Figure 2.3 Apparent resonance frequencies for a rotating disc vs rotation speed (In the stationary harmonic excitation)

2.2.1.2 Resonance frequencies in rotating discs

Response frequencies and resonant frequencies are shown schematically in figure 2.4. It has been assumed that the excitation frequency ω is less than ω_{n1}. The crossing points of A and B in this figure are in a vertical line since for example, the lines ω_a^+ and $(\omega+n\Omega)$ are parallel. These two points in figure 2.4 correspond to the rotating speed Ω_r and at this speed coincidence of resonance occurs. This resonance can be interpreted either by the intersection of the horizontal line ω with the apparent resonant line ω_a^- - point A, or by point B which is the intersection point of the response line $(\omega+n\Omega)$ with horizontal line ω_{n1}. The former interpretation is in fact in the stationary coordinate while the second one

refers to the coordinate rotating with the disc. Both points A and B in figure 2.4 have $\omega = \omega_{n1} - n\Omega$ which is equal to the apparent resonant frequency introduced in equation (2.7).

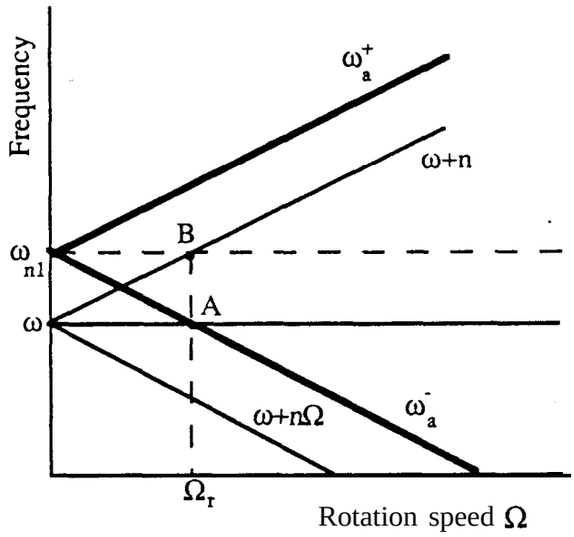

Figure 2.4 Resonance frequencies in a rotating disc at speed Ω_r (Excited by a stationary excitation with frequency ω)

An interesting case is when the excitation frequency is equal to the disc's actual natural frequency and the disc is spinning, that is $\omega = \omega_{n1}$ and $\Omega > 0$. For this case, there will be no coincidence of resonance; because we can not find any point which satisfies equation (2.7).

A similar analysis could be done for the case $\omega > \omega_{n1}$. In this case we will find that there are two points like A and B in figure 2.4 where the equation $\omega = \omega_{n1} + n\Omega$ is applied and resonance occurs.

It is concluded that in the forced excitation of a single ND mode of a rotating disc, for any excitation frequency ω, there is a rotation speed at which resonance occurs. We can state this in another way, at each rotation speed there will be two apparent resonance frequencies, one below and one above the actual natural frequency.

2.2.2 Analysis using Stationary Coordinate

Next, a stationary coordinate θ_0 is used in the analysis of harmonic excitation of the sine n ND mode, as shown in figure 2.5. In this coordinate the forcing function is:

$F(\theta_0,t) = (F_0 \cos ot)\ \delta[\theta_0-\alpha]$ and the eigenfunction will be sin $n(\theta_0+\Omega t)$.

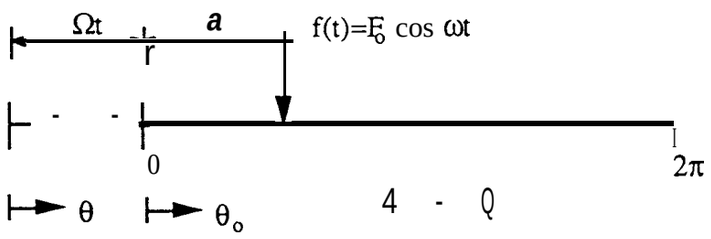

Figure 2.5 Stationary coordinate θ_o for the rotating disc

We can either (a) conduct a similar analysis to that carried out for the coordinate located on the disc θ; or (b) replace θ by $(\theta_0+\Omega t)$ in equation (2.5) to obtain the response of the disc in terms of the stationary coordinate. If we substitute θ by $(\theta_0+\Omega t)$ in equation (2.5), we will have:

$$X_{n1}(\theta_0,t) = -W_1 \sin[(\omega+n\Omega)t+n\alpha] \sin n(\theta_0+\Omega t) + W_2 \sin[(o-nR)t-na] \sin n(\theta_0+\Omega t)$$

If the terms of this equation are multiplied and simplified, it becomes:

$$X_{n1}(\theta_0,t) = -\frac{W_1}{2}\cos[n\theta_0-\omega t-n\alpha] + \frac{W_1}{2}\cos[n\theta_0+(\omega+2n\Omega)t+n\alpha]$$

$$+\frac{W_2}{2}\cos[n\theta_0-(\omega-2n\Omega)t+n\alpha] - \frac{W_2}{2}\cos[n\theta_0+\omega t-n\alpha] \qquad (2.8)$$

Equation (2.8) represents the response of the rotating disc in terms of the stationary coordinate θ_0 and shows that the response frequencies measured with a stationary sensor are ω and $(\omega \pm 2n\Omega)$. These three frequencies are shown in figure 2.6. Note that the apparent resonant frequencies are the same as those presented in equation (2.7) and figure 2.3. Thus they are independent of the chosen coordinate.

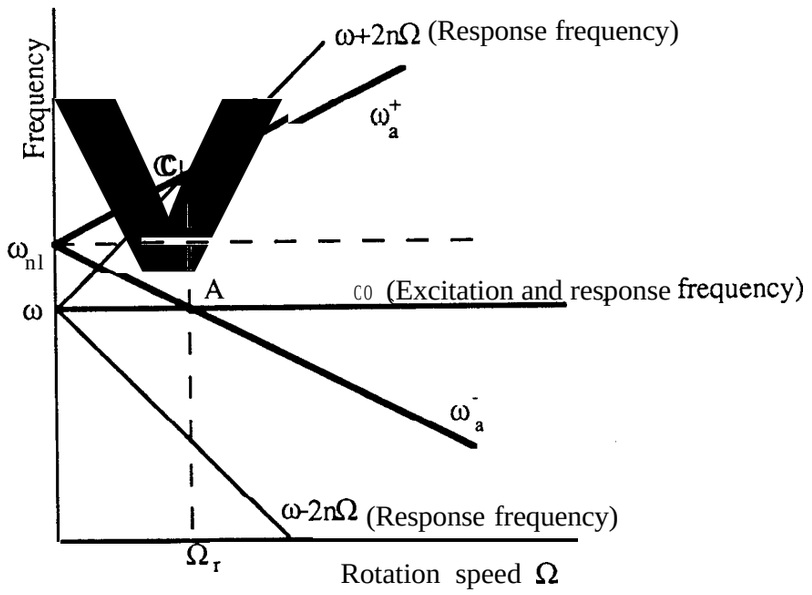

Figure 2.6 Excitation and response frequencies in a rotating disc; Coincidence of resonance at speed Ω_r (As detected in the stationary coordinate)

In figure 2.6 the apparent resonant frequencies ω_a^+ and ω_a^- have also been plotted. It is seen that at points A and C the coincidence of resonance occurs since at these points $\omega = \omega_{n1} - n\Omega$ and W_1 becomes infinity which is same as obtained in rotating coordinate in section 2.2.1.2.

2.3 RESPONSE OF THE COSINE MODE TO HARMONIC EXCITATION

In section 2.2 the response of a single diametral mode has been obtained. In this section similar analysis is used for the other n ND mode of the pair (cosine mode). Again, the analysis is carried out in two parts. First, the response is analysed in terms of a coordinate on the disc, then it is extended to a stationary coordinate.

2.3.1 Analysis Using Rotating Coordinates

The mode shape in this coordinate is described by $\phi(\theta) = \cos n\theta$ and the forcing function is the same as that introduced in section 2.2.1, that is:

$$F(\theta,t) = (F_0 \cos \omega t)\, \delta[\theta-(\Omega t+\alpha)]$$

The generalized force for the assumed mode is:

$$Q(t)= \int_0^{2x} (F_0 \cos ot)\, \delta[\theta-(\Omega t+\alpha)] \cos n\theta \, d\theta$$

After integration, this becomes:

$$Q(t)= F_0 \cos(\omega t) \cos n(\Omega t+\alpha) \qquad (2.9)$$

Equation **(2.9)** represents the generalized force for the cosine conjugate of the n ND mode pair. Having obtained the generalized force, the normal response is calculated by using the convolution integral; similar to that mentioned in section 2.2.1.1.

$$q(t) = \frac{F_0}{4\, m_{n2}\, \omega_{n2}}$$

$$\left\{ \frac{\cos[(\omega+n\Omega)t+n\alpha] + \cos(\omega_{n2}t+n\alpha) + \cos[(\omega+n\Omega)t+n\alpha] - \cos(-\omega_{n2}t+n\alpha)}{\omega+n\Omega-\omega_{n2} \qquad\qquad \omega+n\Omega+\omega_{n2}} \right.$$

$$\left. \frac{\cos[(\omega-n\Omega)t-n\alpha] + \cos(\omega_{n2}t-n\alpha) + \cos[(\omega-n\Omega)t-n\alpha] - \cos(-\omega_{n2}t-n\alpha)}{\omega-n\Omega-\omega_{n2} \qquad\qquad \omega-n\Omega+\omega_{n2}} \right\}$$

(2.10)

Where ω_{n2} and m_{n2} are natural frequency and modal mass of the cosine mode. The terms containing the natural frequency ω_{n2} are transient and are not considered in the steady-state study. Thus, the steady state response is:

$$q(t) = \frac{F_0}{2m_{n2}} \left\{ \frac{-1}{(\omega+n\Omega)^2 - \omega_{n2}^2} \cos[(\omega+n\Omega)t+n\alpha] - \frac{+1}{(\omega-n\Omega)^2 - \omega_{n2}^2} \cos[(\omega-n\Omega)t-n\alpha] \right\} \quad (2.11)$$

This equation gives the normal coordinate of the n ND mode and by using it , the response of this mode is obtained:

$$X_{n2}(\theta,t) = q(t)\ \phi(\theta)$$

or:

$$X_{n2}(\theta,t) = -W_3 \cos[(\omega+n\Omega)t+n\alpha] \cos n\theta - W_4 \cos[(o-nQ)t-na] \cos n\theta \quad (2.12)$$

where :

$$\left.\begin{aligned} W_3 &= \frac{+F_0}{2m_{n2}[(\omega+n\Omega)^2 - \omega_{n2}^2]} \\ \text{and} \quad W_4 &= \frac{+F_0}{2m_{n2}[(\omega-n\Omega)^2 - \omega_{n2}^2]} \end{aligned}\right\} \quad (2.13)$$

Equation (2.12) represents the response of the cosine mode of the diametral pair excited by a non-rotating harmonic force. It consists of two 'fixed vibration' components with frequencies of $(\omega \pm n\Omega)$. Figure 2.2 which shows the response frequencies for different speeds in the rotating coordinate, is also applicable for this mode.

Equations (2.12) and (2.13) show that there are two resonance frequencies for the system, when the denominators are zero $(\omega \pm n\Omega)^2 - \omega_{n2}^2 = 0$. It follows that there are two

'apparent resonant frequencies' at each spinning speed Ω, and these are similar to the apparent natural frequencies of the other mode, equation (2.7):

$$\omega_a^+ = \omega_{n2}+n\Omega \quad , \text{and} \quad \omega_a^- = \omega_{n2}-n\Omega$$

2.3.2 Analysis in the Stationary Coordinate

In the previous section the response of the cosine pair of n ND mode to the stationary harmonic excitation was obtained. Next, that response is obtained in a stationary coordinate, θ_0, as shown in figure 2.4. In this coordinate the forcing function is $F(\theta_0,t) = (F_0 \cos ot)\ \delta[\theta_0-\alpha]$ and the eigenfunction will be $\cos n(\theta_0+\Omega t)$. We can replace θ by $(\theta_0+\Omega t)$ in equation (2.12) to obtain the response of the disc expressed in terms of the stationary coordinate.

$$X_{n2}(\theta_0,t) = -W_3 \cos[(\omega+n\Omega)t+n\alpha] \cos n(\theta_0+\Omega t) - W4 \cos[(\omega-n\Omega)t-n\alpha] \cos n(\theta_0+\Omega t) \tag{2.14}$$

where W3 and W_4 have been defined in equation (2.13).

If the terms of equation (2.14) are multiplied and simplified, it will give:

$$X_d(\theta_0,t) = -\frac{W_3}{2}\cos[n\theta_0-\omega t-n\alpha] - \frac{W_3}{2}\cos[n\theta_0+(\omega+2n\Omega)t+n\alpha]$$

$$-\frac{W_4}{2}\cos[n\theta_0-(\omega-2n\Omega)t+n\alpha] - \frac{W_4}{2}\cos[n\theta_0+\omega t-n\alpha] \tag{2.15}$$

Equation (2.15) represents the response the cosine pair of n ND mode of the rotating disc in the stationary coordinate and shows that the response frequencies are ω and $(\omega\pm2n\Omega)$ the same as have been obtained for the other pair and shown in figure 2.5. Note that the

apparent natural frequencies are the same as those presented in equation (2.7) and shown in figure 2.3 and they are independent of the chosen coordinate.

2.4 RESPONSE OF THE n ND MODE PAIR TO HARMONIC EXCITATION

2.4.1 Analysis of the response

In the previous two sections 2.2 and 2.3 we obtained the responses of each of the pair of n ND modes in a rotating disc to a stationary harmonic force. These have been presented in equations (2.5) and (2.12) in terms of rotating coordinates and in equations (2.8) and (2.15) relative to the stationary coordinates. In order to obtain the combined response of both n ND modes to the stationary harmonic excitation, we can just add equation (2.8) and (2.15), that is:

$$X_n(\theta_0,t) = -\frac{W_1+W_3}{2}\cos[n\theta_0-\omega t-n\alpha] + \frac{W_1-W_3}{2}\cos[n\theta_0+(\omega+2n\Omega)t+n\alpha]$$

$$+\frac{W_2-W_4}{2}\cos[n\theta_0-(\omega-2n\Omega)t+n\alpha] - \frac{W_2+W_4}{2}\cos[n\theta_0+\omega t-n\alpha] \qquad (2.16)$$

where W_1, W_2, W_3 and W_4 are defined in equations (2.6) and (2.13).

2.4.2 Discussion

Equation (2.16) represents the response of the pair of n ND modes of a rotating disc to the harmonic excitation in the stationary coordinates. It is seen that the coincidence of

resonance occurs at the same conditions as for the pairs of the n ND modes presented in equation (2.7). In a tuned disc the natural frequencies and modal masses of a pair diametral modes are identical but usually the disc is slightly mistuned and so $m_{n1} \neq m_{n2}$ and $\omega_{n1} \neq \omega_{n2}$. For a tuned case, equation (2.16) is simplified to the following formula which represents two travelling waves:

$$X_n(\theta_0,t) = - W_{13} \cos [n\theta_0-\omega t-n\alpha] - W_{24} \cos [n\theta_0+\omega t-n\alpha] \qquad (2.17)$$

where: $W_{13}=W_1=W_3$ and $W_{24}=W_2=W_4$

Figure (2.7) shows an example for a tuned case where the response frequency is just a single frequency equal to ω. The apparent resonant frequencies are $(\omega_n \pm n\Omega)$ where $\omega_n=\omega_{n1}=\omega_{n2}$ and therefore at point R there is the possibility of coincidence of resonance since at this point $\omega=(\omega_n-n\Omega)$. This makes W_{13} tend towards infinity and means that the first term in equation (2.17), which is a backwards travelling wave, dominates in the response. Recall the reason that the term presenting a travelling wave: The wave moves in θ_0 direction (due to negative sign of 'ωt') and on the other hand the disc is rotating opposite to θ_0. Thus, the wave travels opposite to the disc's rotation and is called a backward uavelling wave.

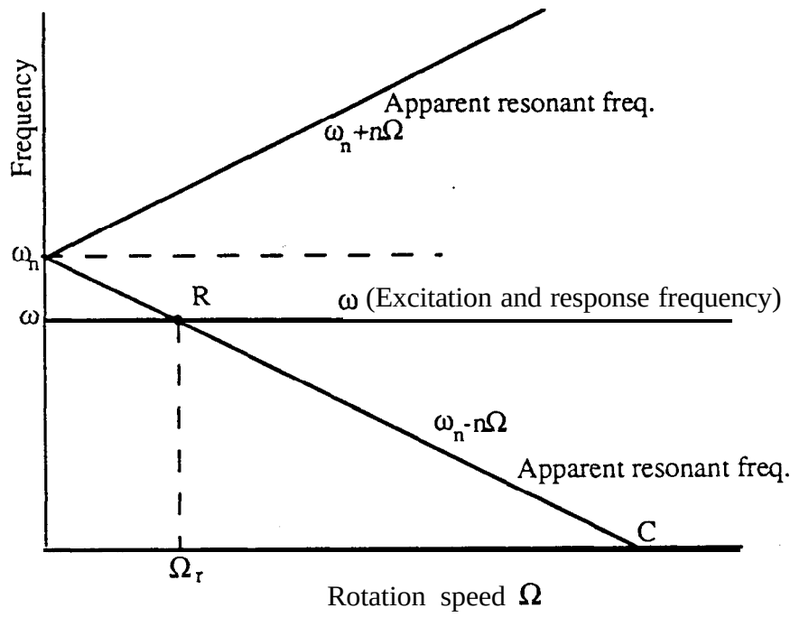

Figure 2.7 Harmonic excitation the n diametral pair modes in a tuned disc.
Point R : Coincidence of resonance which presents a backward travelling wa
Point C : **Critical** speed where a standing wave is formed

(Detected in the stationary coordinate, θ_o)

It is worth mentioning a special case here which is the case of static force excitation i.e. when $\omega=0$. Point C in figure (2.7) represents this situation. For this case $W_{13}=W_{24}=W$ and equation (2.17) becomes:

$$X_d(\theta_0,t) = - 2W \cos [n\theta_0-n\alpha] \qquad (2.18)$$

which represents a 'standing wave', since the response is time-independent and the disc rim takes up a cosine deformed shape stationary in space while the disc is rotating.

In a mistuned disc there are two different natural frequencies for n ND modes, ω_{n1} and ω_{n2}. This general case is illustrated in figure (2.8):

2.5 CASE STUDY

It has been shown in sections 2.2.2 and 2.3.2 that for a rotating disc excited by a stationary harmonic force, a stationary pickup at a point should detect three frequency components $-(\omega_n-2n\Omega), \omega$ and $(\omega+2n\Omega)$. The initial analysis has been carried out for a single mode and then the response of the pair has been obtained. Although according to equation (2.16) the response of n diametral modes pair has three frequency components, this part of the case study is going to examine and check the three frequency components of a single diametral mode as the basis of the analysis results. Therefore, in a real situation, we have to examine the response frequencies at an excitation frequency near to a natural frequency which is well separated from any adjacent modes. To achieve this, we have to make the disc mistuned in order to have separated modes, since in practice there are close ND modes in pairs. This investigation concentrates on the 2 ND modes, that is $n=2$, and can be applied to the other diametral modes.

2.5.1 Description of the rig and equipment

2.5.1.1 Test rig

The test rig and measuring equipment are shown schematically in figure 2.9. The disc which has been tested is a simple steel disc with diameter of 34 c.m.made of a plate 5m.m. thick. It is mounted on a shaft of a electric-motor with adjustable and controlled speed. There are four identical steel masses which can be bolted to the disc to make it significantly mistuned for the 2 ND modes.

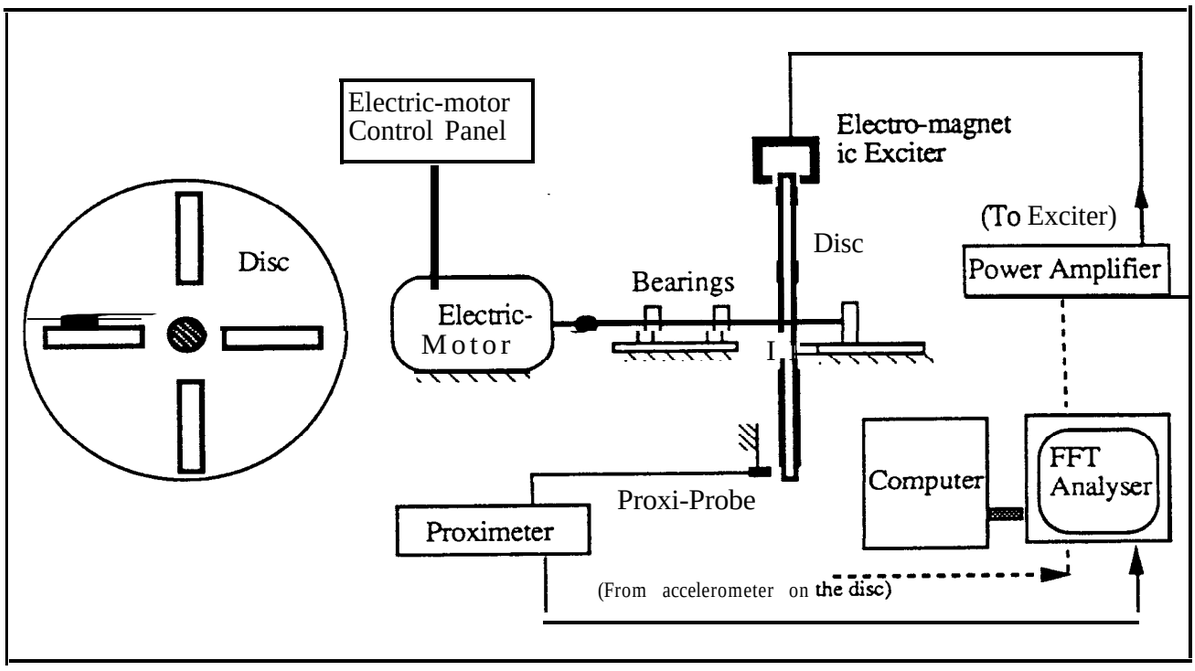

Figure 2.9 Test rig and measuring equipment in the forced excitation test on a rotating disc (- - - - - is in case of the hammer tests)

2.5.1.2 Excitation

In the experiments on the rotating disc, the excitation device is an electro-magnet made from a coil on a **C** shape core. One problem with this type of exciter is that it produces harmonics of the excitation frequency rather than a single frequency, as shown in figure A.1 in Appendix A. In our case, the second harmonic is stronger and is used as the main excitation frequency. The input signal for the magnet exciter is generated from a power amplifier LOS TPO300. By using this exciter and command signal from B&K 2032 FFT Analyser, experiments with random excitation also have been done to find the general wide band response of the rotating disc.

Initial hammer tests also have been carried out to find out the natural frequencies and modes of the stationary disc stationary disc. From the FRFs, we can easily find the desired ND modes.

251.3 Response Measurement

In this work the response of the rotating disc is measured at a stationary coordinate by using a proximity probe. This is a non-contacting device used to measure displacement and is assembled on a support of the test rig such that it is positioned close to the rim. At the beginning, the gap between the probe and the disc should be about 1 m.m. which produces 7 to 8 volts on the oscilloscope.

The VPI sensor [58] is another non-contacting device which is based on the laser Doppler phenomenon, measuring velocity at a point on the structure. These non-contacting sensors have the advantage that they do not affect the mass and dynamic characteristics of the structure whose vibration they are measuring.

One problem with using the proximity probe is that there is the possibility of transmission of excitation from the shaker to the probe through the support. This effect was examined by using the VPI sensor and proximity probe simultaneously in the same measurements. Figures 2.16 to 2.18 will be explained in the following sections; however, they can be referred here to see that in each figure, three major frequencies have appeared exactly in both measurements. Therefore, the excitation frequency which appears in the response spectrum is from the vibration in the disc and we shall assume that we can trust the frequencies measured by the proximity probe mounted on the test rig support.

2.5.2 Experimental results

The experimental work has been carried out in three parts and using three different methods: hammer tests on a stationary disc, single frequency excitation on the rotating disc and random excitation on the rotating disc.

2.5.2.1 Hammer tests

The results of the hammer tests on the disc when this is not rotating are shown in figures 2.10 to 2.15. The first three figures are for the disc without added masses and the others are for the disc with added masses (mistuned). The positions of the measurement and excitation points, which are identical in each test so called 'point measurement', are also shown alongside the main FRFs. From figure 2.10, we understand that the natural frequencies of the 2 ND modes are 150.0 Hz and 158.0 Hz. This has been confirmed by changing the measurement point to two special points in sides of the first measurement point, figures 2.11 and 2.12. Each of these two points is, in fact, on a nodal line of one of the pair of 2 ND modes so that in figure 2.11 only lower frequency mode and in figure 2.12 only the higher 2 ND mode has been excited .When the masses are attached they are at 153 Hz and 200.5 Hz according to figure 2.13. It is seen that even when the pieces are not bolted to the disc, the disc is mistuned for the 2 ND mode by about 8 Hz. This is because of the existence of four holes on the disc and other non-uniformities in the structure. By bolting pieces to the disc, the two 2 ND natural frequencies are about 48 Hz apart, making two well-separated modes.

For comparison, the accelerometer and the proximity probe have been used simultaneously in one test and the results are shown in Appendix A figure A.2. Good agreement is found from this comparison.

2.5.2.2 Single frequency excitation of rotating disc

For the case where the natural frequencies of the 2 ND modes are well separated (by bolting four identical pieces on four perpendicular radii), we can examine the response of a single 2 ND mode to a harmonic excitation. An excitation frequency is chosen on the generator near to the natural frequency of one of the 2 ND modes. For this excitation the response spectrum has been measured to find the frequency components in the response. The results of different excitation frequencies are presented.

a) Excitation frequency below a natural frequency

The rotation speed of the disc was set to 120 rev/min, which is equivalent to 2 Hz, and excitation frequency was chosen to ω=196.0 Hz which is below the higher 2ND mode shown by letter D in figure 2.13. The auto spectrum of the response was obtained using the proximity probe and at the same time using the laser facility for comparison. The result is shown in figure 2.16. It is seen that in the region of the excitation frequency there are three peaks at :

188 Hz, **196** Hz and **204** Hz.

These frequencies are equivalent to the theoretical response frequencies ω and $(\omega \pm 2n\Omega)$ which have been predicted in the analysis of response of a rotating disc in a stationary coordinate.

b) Excitation frequency above a natural frequency

The excitation frequency was set at ω=204.0 Hz while the disc was spinning at the same speed of 120 rev/min. This excitation frequency has shown by letter E in figure 2.13. **The**

auto spectrum of the response is shown in figure 2.17 as a zoom measurement from 150 to 250 Hz. We can recognise the three dominant frequencies at 196.0 Hz, 204.1 Hz and 212.2 Hz. These frequencies are also in good agreement with theory which predicts that the response of a single ND mode of rotating disc to harmonic stationary excitation in a stationary coordinate consists of three frequency components, $(\omega-2n\Omega)$, ω and $(\omega+2n\Omega)$.

c) Excitation frequency near to the first 2ND mode .

Similar tests to those in parts a) and b) have been carried out around the lower 2 ND natural frequency, 153 Hz. The excitation frequencies are 156.5 and 145.6 and corresponding auto spectrums are shown in figures 2.18 and 2.19 respectively. Again we can simply check that the response contains three frequency components which correspond to $(\omega-2n\Omega)$, ω and $(\omega+2n\Omega)$.

2.5.2.3 Random excitation of the rotating disc

A random noise signal can be generated by the FFT analyzer and applied to the (non-contacting) shaker to excite the rotating disc. In this test the disc has been used without adding the auxiliary pieces. Figure 2.20 shows the auto spectrum of the response when the speed of rotation is equal to 180.0 rev/min (3.0 Hz). The apparent resonant frequencies which have been defined in earlier sections are shown. Remembering that in a rotating disc the apparent resonant frequencies and the actual (non-rotating state) natural frequency ω_n have the relationship of

$$\omega_a = \omega_n \pm n\Omega$$

In figure 2.20 the frequencies corresponding to 2ND are 143, 151, 155, and 163 Hz. On the other hand for this case $n\Omega=2(3)=6$ Hz, $\omega_{n1}\cong149$ Hz, $\omega_{n2}\cong157$ Hz. We see that resonant frequencies 143 and 155 correspond to ω_{n1} and resonant frequencies 151 and 163 come from ω_{n2}.

The apparent resonant frequencies of the 3 ND mode have been obtained 301, 319 Hz and shown in figure 2.20. For this case $n\Omega=3(3)=9$ Hz, and $\omega_{n1}\cong\omega_{n2}=310$ Hz.(see figures 2.9 and 2.10). It is seen that the apparent resonant frequencies are identical to the theoretical values $\omega_n\pm n\Omega$.

2.6 CONCLUSION

In the harmonic excitation of a single diametral mode of a rotating disc, the response has three frequency components ω and$(\omega\pm2n\Omega)$ while in rotating coordinates there are two frequency components, $(\omega\pm n\Omega)$.

In a rotating disc the value of natural frequency ω_n no longer indicates the resonance frequency directly but each single ND mode represents two apparent resonant frequencies $(\omega_n\pm n\Omega)$. Of course, this does not depend on which coordinate is used. It is further concluded that if the excitation frequency is exactly equal to a diametral natural frequency, as long as the disc is rotating there is no coincidence of resonance for that mode at any speed Ω.

For a mistuned disc, the harmonic excitation response of a pair of ND modes is a combination of four travelling waves. In the tuned case the total response comprises two

travelling waves forward and backward with effective vibration frequencies equal to the excitation frequency.

In the case of static excitation, $\omega=0$, and a tuned disc, the response is stationary in space and is referred to as a ‘standing wave’. This situation is for any rotation speed. However, it will be at resonance at a particular speed called the critical speed which is equal to the natural frequency divided by the number of nodal diameters.

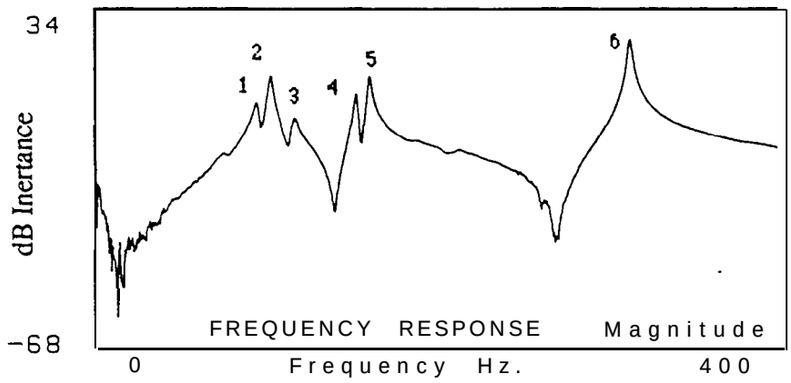

No.	Freq.
1	
2	100.5 93.5
3	114.5
5	150.0
6	310.5 158.0

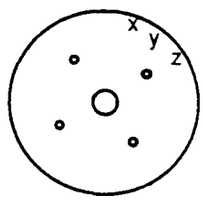

Position of measurement point 'y' on the disc

Figure 2.10 FRF of the stationary disc from hammer test (Excitation point at 'y')

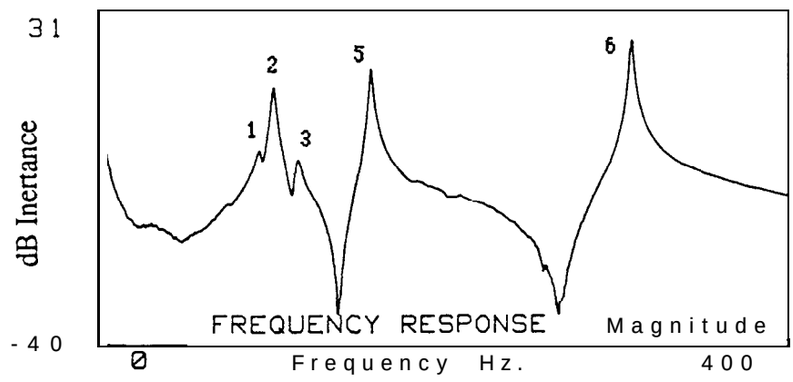

No.	Freq.
1	93.0
2	
3	101.5 115.0
4	
5	158.0
6	311.0

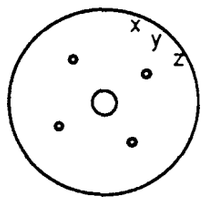

Position of measurement point 'x' on the disc

Figure 2.11 **FRF** of the stationary disc from hammer test (Excitation point at 'x')

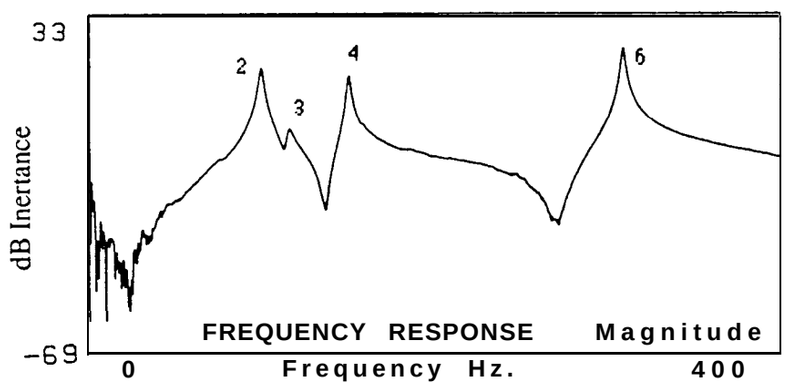

No.	Freq.
1	
2	99.0
3	115.5
4	150.0
5	
6	310.5

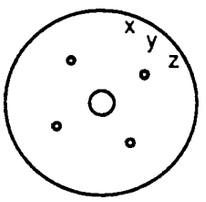

Position of measurement point 'z' on the disc

Figure 2.12 FRF of the stationary disc from hammer test (Excitation point at 'z')

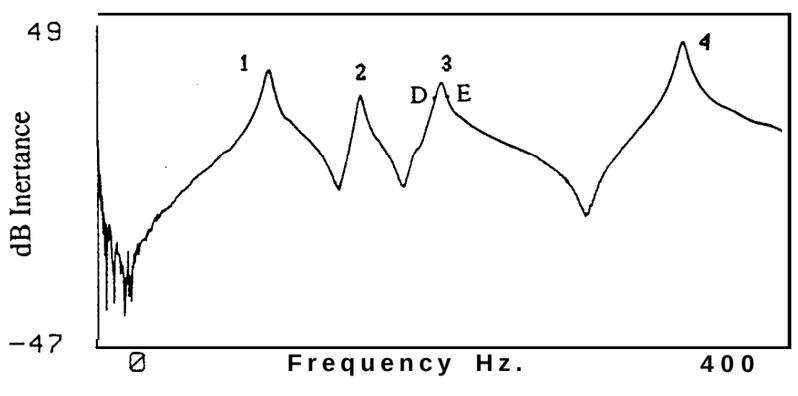

No.	Freq.
1	loo.5
2	153.0
3	200.5
4	339.5

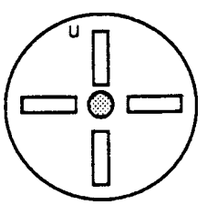

Position of measurement point 'u' on the disc

Figure 2.13 **FRF** of the **mistuned** stationary disc from hammer test (Excitation point at 'u')

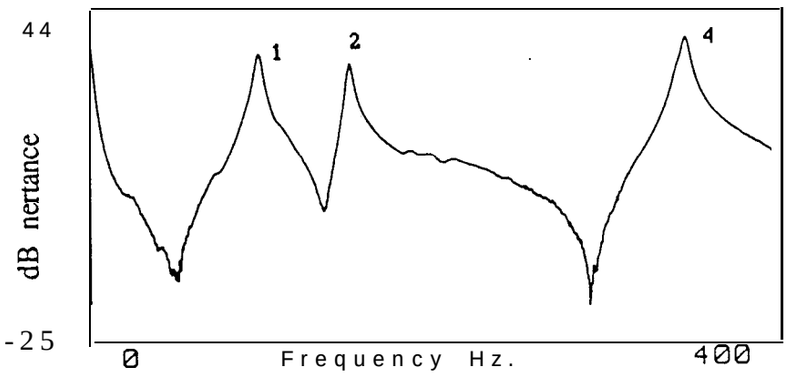

No.	Freq.
1	100.0
2	153.0
3	
4	345.0

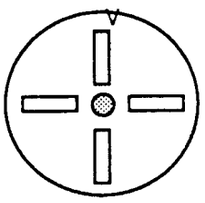

Position of measurement point 'V' on the disc

Figure 2.14 FRF of the stationary disc with added masses from hammer test (Excitation point at 'V')

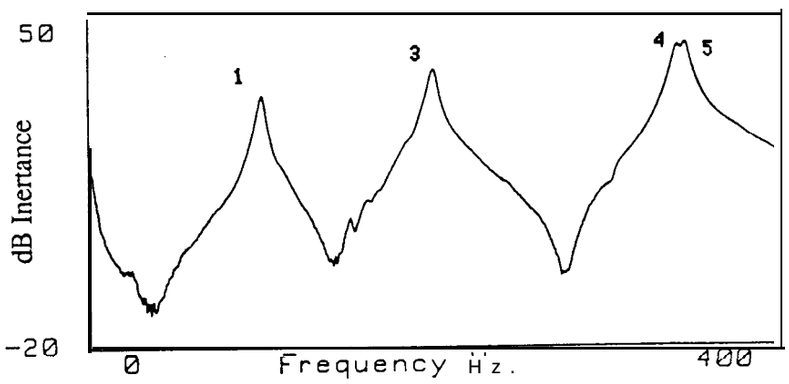

No.	Freq.
1	101.0
2	
3	200.5
4	339.5
5	344.5

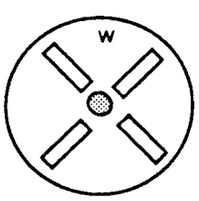

Position of measurement point 'W' on the disc

Figure 2.15 FRF of the stationary disc with added masses from hammer test (Excitation point at 'W')

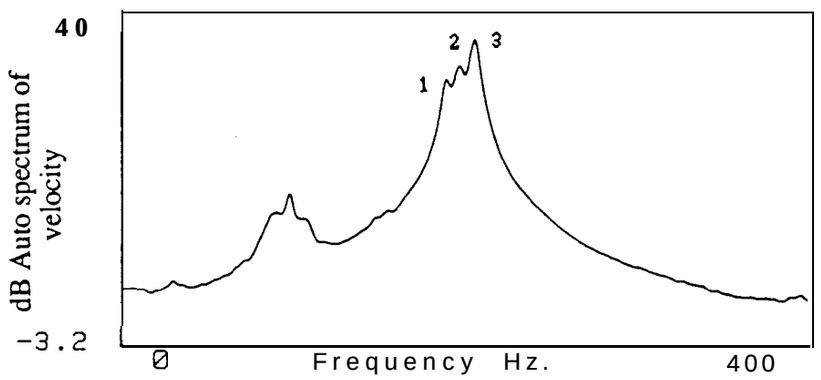

No.	Freq.
1	188.0
2	196.0
3	204.0

a) Using Laser (Velocity has been measured)

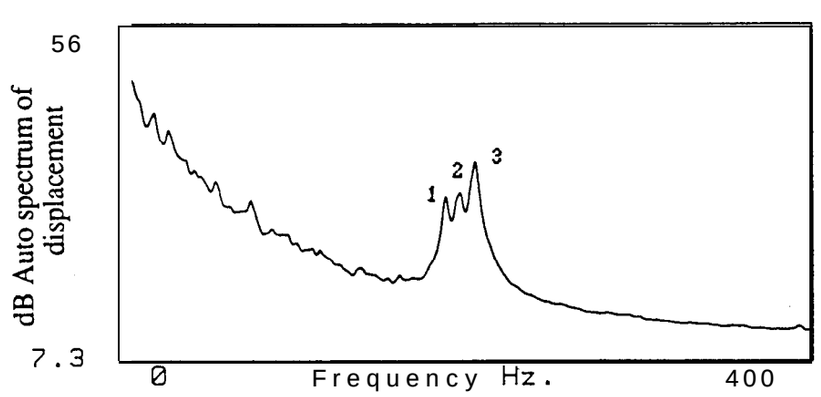

No.	Freq.
1	188.0
2	196.0
3	204.0

b) Using Proximeter (Displacement has been measured)

Figure 2.16 Response of rotating disc
(Excitation frequency=196 Hz)
(Rotating speed= 120 rev/min.)

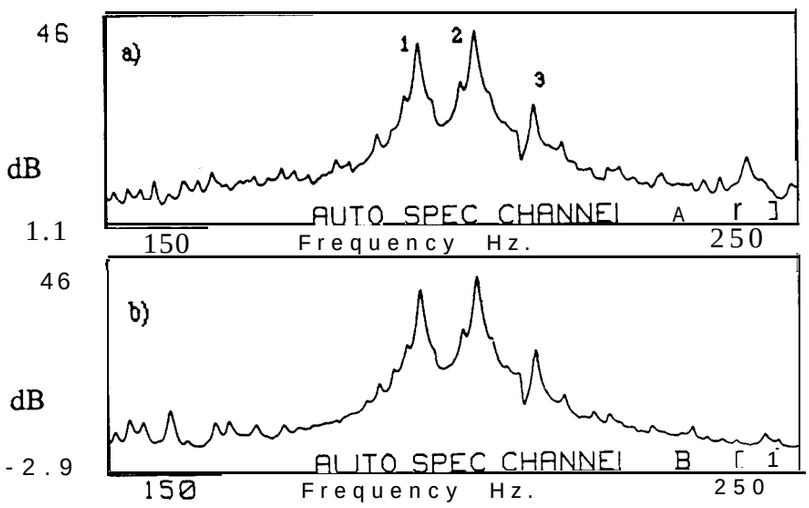

No.	Freq.
1	196.0
2	204.1
3	212.2

Figure 2.17 Response of rotating disc; a) using Laser (VPI sensor) b) using Proximeter
(Excitation frequency=204.1 Hz)
(Rotating speed= 120 rev/min)

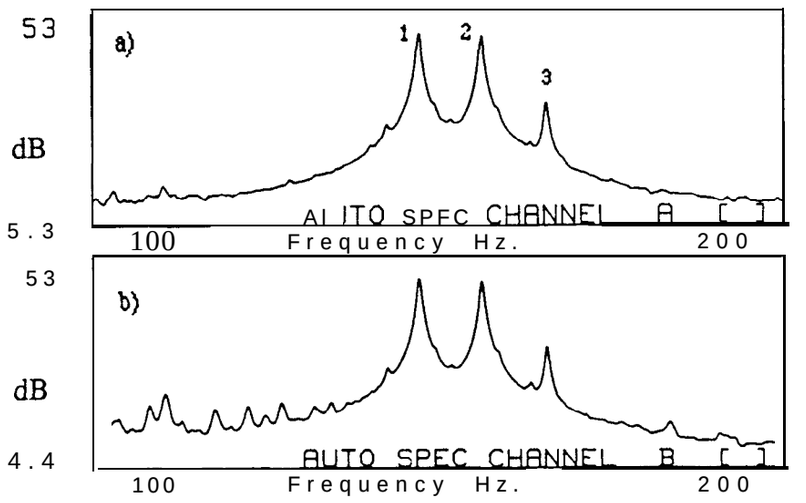

No.	Freq.
1	147.1
2	156.6
3	163.6

Figure 2.18 Response of rotating disc; a) using Laser (VPI sensor) b) using Proximeter
(Excitation frequency=156.6 Hz)
(Rotating speed=140 rev/min)

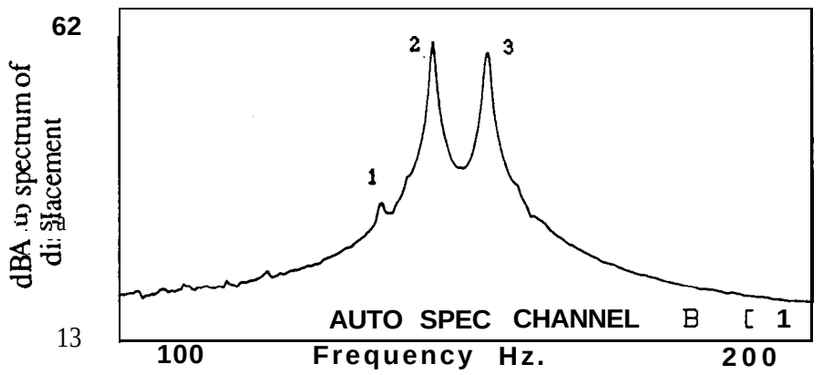

No.	Freq.
1	137.7
2	145.6
3	153.6

Figure 2.19 Response of rotating disc
(Excitation frequency=145.6 Hz)
(Rotating speed=120 rev/min = 2 Hz)

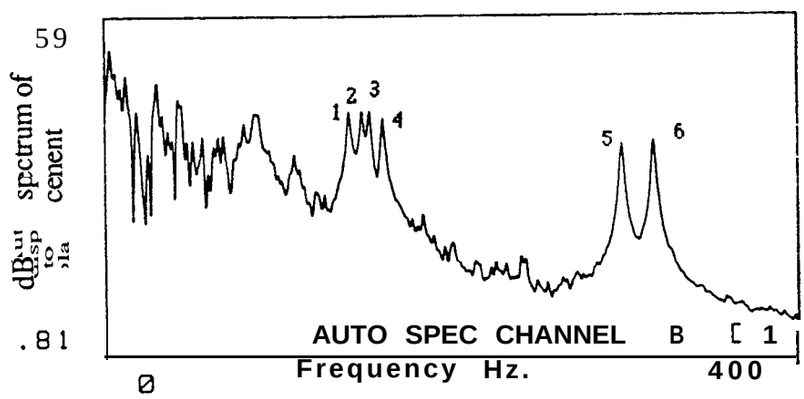

No.	Freq.
1	
2	143.0
	151.0
3	155.0
4	163.0
5	301.0
6	319.0

Figure 2.20 Response of rotating disc to random excitation. Frequencies at points 1, 2, 3 and 4 are resonant frequencies of 2 ND modes and frequencies at points 5 and 6 are resonant frequencies of 3 ND modes.
(Rotating speed=180 rev/min = 3 Hz)

Chapter 3

THEORY OF VIBRATION FOR A DISC ROTATING PAST A STATIC FORCE

3.1 INTRODUCTION

In the previous chapter, the response of the rotating disc to a non-rotating harmonic excitation was analysed. A special case of this analysis is when the excitation frequency is zero i.e. the static forced excitation of the rotating disc. In practice there are many cases where this kind of excitation occurs, such as nonuniformity in the pressure distribution on either side of the discs in gas and steam turbines. The response of a rotating disc to a static force excitation can generate standing waves, as mentioned in chapter 2 as a special case of zero excitation frequency.

It is possible to simulate the response of a specific nodal diameter (ND) mode in a rotating disc with harmonic forces applied on the disc in a stationary state [7]. This is very important since it changes the test on a rotating structure to a stationary one which is more practical. This simulation technique can be developed for more general cases to obtain the relation between forces and their spatial position and temporal phase angle. In fact, this

technique can be considered as a special form of multi-excitation method which is useful for the modal identification of axisymmetric structures.

Normally, the response of a disc to a non-rotating excitation comprises travelling waves and on the other hand the well-known “standing wave” in a rotating disc is simulated by a backward travelling wave in the stationary disc. A uavelling wave response is generated by the excitation of the diametral modes in a disc and they are complex, for which the normal methods of presentation are not applicable. A proper technique for demonstration of the response is needed.

In the simulation, the response of a tuned disc is a pure backward travelling wave with the same order as the order of the desired diametral mode. However, in a mistuned disc or any real case, the response to the same excitation is contaminated by other wave orders. Mathematically, we can obtain the contribution of the other wave orders in the response and display the spectrum of different waves in the response.

In this chapter, the response of a rotating disc to the non-rotating and static excitation is analysed and then the theory of the simulation of travelling waves is developed. Also, a method is presented to estimate the contribution of different wave orders in the response.

3.2 RESPONSE OF A ROTATING DISC PAST A STATIC FORCE

In chapter 2, the general case of harmonic forced excitation of a rotating disc has been presented. A special case for that analysis is the static force excitation of a rotating disc which can be obtained by substituting a zero excitation frequency ($\omega=0$) in the response expressions. Also, it can be achieved similarly by direct analysis, as follows.

Let us consider a pair of n ND modes of a disc rotating at speed Ω. The orthogonal mode shapes on the rim are assumed to be $\phi^{(1)}(\theta) = \cos n\theta$ and $\phi^{(2)}(\theta) = \sin n\theta$. The

coordinate θ is assumed to rotate with the disc and the direction of coordinate θ is assumed to be in the opposite direction to the disc rotation Ω. The disc is passing a static stationary force F_0 applied initially at a spatial angle α as shown in figure 3.1.

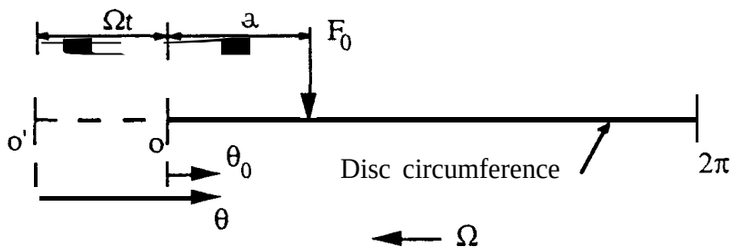

Figure 3.1 Coordinates on the rotating disc past a static force

The forcing function for such a system is:

$$F(\theta,t) = F_0\,\delta[\theta-(\Omega t+\alpha)] \qquad (3.1)$$

It can be shown that the generalized forces for the assumed modes are:

$$\left.\begin{aligned} Q_n^{(1)}(t) &= F_0 \cos n(\Omega t+\alpha) \\ Q_n^{(2)}(t) &= F_0 \sin n(\Omega t+\alpha) \end{aligned}\right\} \qquad (3.2)$$

Equations (3.2) represents the generalised forces for the n ND modes. The normal responses are calculated by using the convolution integral and then the response can be obtained using the mode summation formula, in the same way that has been applied in the previous chapter. Having done this, we will get the steady-state response as:

$$X_n(\theta,t) = -Y_1 \cos[n\Omega t+n\alpha] \cos n\theta - Y_2 \sin[n\Omega t+n\alpha] \sin n\theta \qquad (3.3)$$

where :

$$\left.\begin{aligned} Y_1 &= \frac{F_0}{m_{n1}\left[(n\Omega)^2 - \omega_{n1}^2\right]} \\ Y_2 &= \frac{F_0}{m_{n2}\left[(n\Omega)^2 - \omega_{n2}^2\right]} \end{aligned}\right\} \qquad (3.4)$$

Equation (3.3) represents the response of an n ND mode of a rotating disc excited by a static force. It is a complex vibration at frequency ($n\Omega$) and consists of two 'fixed vibration' terms. For a tuned disc, it can be shown that $Y_1=Y_2=Y$ and so the response is a pure backward travelling wave:

$$X_n(\theta,t) = -\,Y\cos[n\theta - n\Omega t - n\alpha] \qquad (3.5)$$

The analysis can be transformed to the stationary coordinate θ_0 by substituting θ by $(\theta_0+\Omega t)$ in the response equation (3.3). After substituting and simplification, we will have:

$$X_n(\theta_0,t) = -\left(\frac{Y_1-Y_2}{2}\right)\cos[2n\Omega t + n\theta_0 + n\alpha] + \left(\frac{Y_1+Y_2}{2}\right)\cos[n\theta_0 - n\alpha] \qquad (3.6)$$

The response of a tuned rotating disc to a static force in the stationary coordinate is obtained by just considering $Y_1=Y_2=Y$ in equation (3.6):

$$X_n(\theta_0,t) = Y\cos[n\theta_0 - n\alpha] \qquad (3.7)$$

This represents a standing wave and it means that the disc rim looks deformed with a cosine shape, static in the view of a stationary observer. Also, equation (3.7) shows that the configuration of the 'standing wave' is independent of Ω and hence it forms at any rotational speed.

3.3 SIMULATION OF TRAVELLING WAVES

In section 3.2 the general formulae for the n ND modes of a disc rotating past a static force have been obtained. Recalling equation (3.3) for the generalized forces;

$$Q_{n}^{(1)}(t) = F_0 \cos n(\Omega t+\alpha)$$
$$Q_{n}^{(2)}(t) = F_0 \sin n(\Omega t+\alpha)$$

we see that each expression is a harmonic force with frequency ($n\Omega$) and presents the forcing function for a normal mode. It seems that it is possible to simulate the response of an n ND mode by applying two harmonic forces equivalent to the generalised forces and positioned at nodal points of the ND modes. This means that, the spatial phase angle $\phi_s = \frac{360^o}{4n}$ and the temporal phase angle is -90^o, equal to the phase angle between $Q_n^{(2)}$ and $Q_n^{(1)}$. This excitation results in a travelling wave in the non-rotating disc just as in the disc rotating past a static force. In this way, the response of each ND mode of a disc rotating past a static force is simulated in a stationary disc with two harmonic excitations. This idea was first proposed by Ewins [7] and it can now be developed for a more general case.

When the generalised forces of a particular ND mode are applied to the main structure, rather than applying to the modal mass in a SDOF (normal mode) system, there is no guarantee that the response level will be the correct value since two generalised forces do not necessarily have the same effect as the real forcing function. However, from the quality point of view, the two harmonic forces create the same shape of response.

In the simulation, the excitation frequency should be equal to the number of nodal diameters of the mode to be excited, multiplied by the rotating speed of the disc, i.e. $\omega=n\Omega$. Therefore, each time just one wave order can be simulated for a certain rotating speed.

3.4 GENERALISED SIMULATION FOR PRESCRIBED SPATIAL PHASE ANGLE

3.4.1 Analysis

As the result of the idea of the simulation of a rotating disc, a stationary disc is considered vibrating at a frequency ω near to the natural frequency of its n nodal diameter mode. The excitation source consists of two harmonic forces f_1 and f_2 acting at points 1 and 2 on the rim, (Fig.3.2). In the general case, f_1 and f_2 have a temporal phase difference (ϕ_t), and the excitation points are positioned at an angle ϕ_s apart (the spatial phase angle). The angle between point 1 and the nearest nodal diameter is called a . The origin of coordinate θ is assumed to be at point I and point 3 is considered at position θ on the rim.

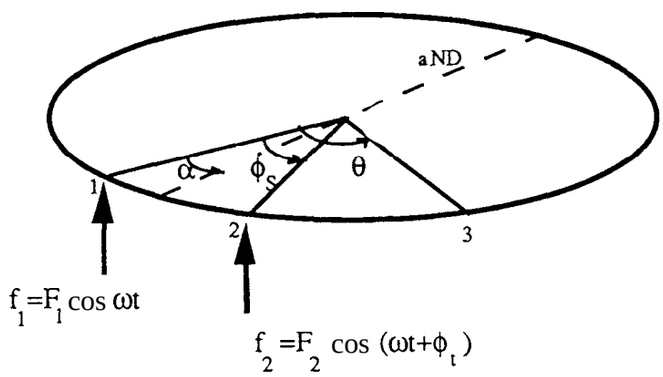

Figure 3.2 Two excitations on a stationary disc

The harmonic response can be calculated by using the general equation:

$$\{x\} = [H]\{f\} \tag{3.8}$$

where $\{x\}$ is the response vector, $[H]$ is FRF matrix and (f) is the excitation vector. From equation (3.8), the following equation can be written for point 3:

$$x_3 = H_{31}.f_1 + H_{32}.f_2 \tag{3.9}$$

where :

$$\left.\begin{aligned} f_1 &= F_1 \cos \omega t \\ f_2 &= F_2 \cos(\omega t + \phi_t) \end{aligned}\right\} \tag{3.10}$$

H_{31} and H_{32} can be obtained from the general FRF formula:

$$H_{jk} = \sum_{r=1}^{\infty} \frac{{}_r\phi_j \, {}_r\phi_k}{\omega_r^2 - \omega^2 + i\eta_r\omega_r^2} \tag{3.11}$$

where ${}_r\phi_j$ and ${}_r\phi_k$ are the mass normalised eigenvector elements for points j and k when vibrating in mode r .

At the disc rim, the eigenfunctions are known for any nodal diameter mode. Also, it is well known that most of the modes are dual modes. In the case of an n ND mode, by assuming that modal masses are equal to one, the mass-normalised eigenfunctions are:

$$\left.\begin{aligned} \phi_n^{(1)} &= \cos n(\theta - \alpha) \\ \phi_n^{(2)} &= \sin n(\theta - \alpha) \end{aligned}\right\} \tag{3.12}$$

The natural frequencies of the dual modes which are close are assumed to be ω_1 and ω_2; and the damping loss factors, η_1 and η_2. Knowing that $\theta_1 = 0, \theta_2 = \phi_s$ and $\theta_3 = \theta$ (in figure 3.2), and substituting in equation (3.11) from (3.12), H_{31} and H_{32} can be obtained:

$$\left.\begin{aligned} H_{31} &= \frac{\cos n(\theta-\alpha)\cos(-n\alpha)}{\omega_1^2-\omega^2+i\eta_1\omega_1^2} + \frac{\sin n(\theta-\alpha)\sin(-na)}{\omega_2^2-\omega^2+i\eta_2\omega_2^2} \\ H_{32} &= \frac{\cos n(\theta-\alpha)\cos(\phi_s-\alpha)}{\omega_1^2-\omega^2+i\eta_1\omega_1^2} + \frac{\sin n(\theta-\alpha)\sin n(\phi_s-\alpha)}{\omega_2^2-\omega^2+i\eta_2\omega_2^2} \end{aligned}\right\} \quad (3.13)$$

Denoting $A_1=\frac{1}{\omega_1^2-\omega^2+i\eta_1\omega_1^2}$, $A_2=\frac{1}{\omega_2^2-\omega^2+i\eta_2\omega_2^2}$, and substituting H_{31} and H_{32} into equation (3.10) , we will have:

$$x_3=[A_1\cos n(\theta-\alpha).\cos na - A_2\sin(n\alpha).\sin n(\theta-\alpha)].F_1\cos\omega t$$

$$+[A_1\cos n(\theta-\alpha).\cos n(\phi_s-\alpha)+A_2\sin n(\theta-\alpha).\sin n(\phi_s-\alpha)].F_2\cos(\omega t+\phi_t) \quad (3.14)$$

In the general case when $A_1\neq A_2$, no further simplification can be made of equation (3.14). However, for a tuned disc, $\omega_1=\omega_2$ and $\eta_1=\eta_2$ and, consequently, $A_1=A_2=A$ so that equation (3.14) becomes:

$$x_3=AF_1\cos n\theta\,.\cos\omega t + AF_2\cos n(\theta-\phi_s).\cos(\omega t+\phi_t) \quad (3.15)$$

This equation shows that a has been cancelled out and so the response is independent of the position of the excitation set on the rim. In other words, location of the excitation points spaced around the disc is not important to the response of any particular n nodal diameter mode.

Equation (3.15) can be written in another form:

$$x_3=k_1\cos n\theta\,.\cos\omega t - k_2\cos n\theta.\sin\omega t$$

$$-k_3\sin n\theta.\sin\omega t + k_4\sin n\theta.\cos\omega t \quad (3.16)$$

where :

$$\left.\begin{aligned} k_1 &= AF_1 + AF_2 \cos n\phi_s . \cos \phi_t \\ k_2 &= AF_2 \cos n\phi_s . \sin \phi_t \\ k_3 &= AF_2 \sin n\phi_s . \sin \phi_t \\ k_4 &= AF_2 \sin n\phi_s . \cos \phi_t \end{aligned}\right\} \quad (3.17)$$

In fact, point 3 can be any point on the rim and so x_3 can be replaced by $x(\theta,t)$ to present the general case. Rearranging equation (3.16) will give :

$$x(\theta,t) = k_3 \cos(n\theta+\omega t) + (k_1-k_3) \cos n\theta . \cos \omega t$$

$$+ k_4 \sin(n\theta+\omega t) - (k_2+k_4) \cos n\theta . \sin \omega t \quad (3.18)$$

This formulation has been rearranged to form the forward travelling wave, $(n\theta+\omega t)$. It can be also written on the base of the backward travelling wave (i.e. the term of $(n\theta-\omega t)$), which is more useful, since we are expecting a backward travelling wave from the simulation:

$$x(\theta,t) = k_1 \cos(n\theta-\omega t) - (k_1+k_3) \sin n\theta . \sin \omega t$$

$$+ k_4 \sin(n\theta-\omega t) - (k_2-k_4) \cos n\theta . \sin \omega t \quad (3.19)$$

From this equation, for the cases that $k_1 \neq 0$ and $(k_1+k_3) \neq 0$, we can write:

$$x(\theta,t) = k_1[\cos(n\theta-\omega t) + \frac{k_4}{k_1} \sin(n\theta-\omega t)]$$

$$- (k1+k3)[\sin n\theta + \frac{k_2-k_4}{k_1+k_3} \cdot \cos n\theta] \sin \omega t. \quad (3.20)$$

By letting :

$$\left.\begin{aligned} \tan \beta &= \frac{k_1}{k_4} \\ \text{and} \qquad \tan y &= \frac{k_2-k_4}{k_1+k_3} \end{aligned}\right\} \quad (3.21)$$

the final formula for the response of the rim excited by two harmonic forces will be obtained:

$$x(\theta,t) = \frac{k_1}{\sin \beta} \sin(n\theta-\omega t+\beta) - \frac{k_1+k_3}{\cos y} \sin(n\theta+\gamma) \sin \omega t. \qquad (3.22)$$

The first term represents a backward travelling wave and the second term implies a fixed vibration component.

Before discussing the applications of equation (3.22) in the following sections, the usual conditions in the simulation are examined. Assuming that the two equal harmonic forces with spatial phase angle $\phi_s = \frac{360"}{4n}$ and temporal phase angle ϕ_t=-90° are applied to a tuned disc. If these conditions are applied to equations (3.17), we will have:

$$k_1 = A\ F$$

$$k_2 = 0$$

$$k_3 = -A\ F$$

$$k_4 = 0$$

Substituting in equation (3.20), the response is obtained:

$$x(\theta,t) = A\ F \cos(n\theta-\omega t)$$

which represents a backward travelling wave, as expected.

In the following sections, some concluding remarks from the above analysis are presented.

3.4.2 General formula in simulation

In practice, sometime, there is a restriction on the choice of spatial angle for the exciters' positions, or a certain value for this angle is applied for simplicity. This value may not be equal to its normal value for the mode of interest, i.e. $(\frac{360^o}{4n})$. In this section, we seek conditions which result in the n nodal diameter modes being excited as a backward travelling wave.

From equation (3.19), in order for only a backward travelling wave to exist, the following relations should be satisfied:

$$\begin{cases} k_1 + k_3 = 0 \\ k_2 - k_4 = 0 \end{cases}$$

Substituting from (3.17) :

$$\begin{cases} AF_1 + AF_2 \cos n\phi_s . \cos\phi_t + AF_2 \sin \phi_t \sin n\phi_s = 0 \\ AF_2 \cos n\phi_s . \sin \phi_t - AF_2 \sin n\phi_s \cos \phi_t = 0 \end{cases}$$

or :

$$\left.\begin{aligned} 1+\frac{F_2}{F_1}\cos(n\phi_s - \phi_t) &= 0 \\ \sin(n\phi_s - \phi_t) &= 0 \end{aligned}\right\} \qquad (3.23)$$

From the latter equation:

$$n\phi_s - \phi_t = k\pi \quad , \quad (k=...-2,-1,0,1,2,3,...)$$

If $\frac{F_2}{F_1} > 0$, $\cos(n\phi_s - \phi_t)$ will be negative, so that only k=.. .-1,1,3,... are acceptable values.

Thus, for exciting the n nodal diameter modes in the form of a backward travelling wave only, the following conditions should be satisfied:

$$\left.\begin{aligned} n\phi_s - \phi_t &= k\pi \qquad (k=...-1,1,3,...) \\ \frac{F_2}{F_1} &= 1 \end{aligned}\right\} \qquad (3.24)$$

The analysis can be repeated on equation (3.18) to obtain the conditions to have a uavelling wave in the other direction i.e. a forward travelling wave. According to equation (3.18), in order for only a forward travelling wave to exist, the following relation should be satisfied:

$$\begin{cases} k_1 - k_3 = 0 \\ k_2 + k_4 = 0 \end{cases}$$

Substituting from (3.17) and rearranging in the similar forementioned way, finally the following conditions are obtained in order to excite the n ND modes in the form of a uavelling wave only:

$$\left.\begin{array}{l} n\phi_s + \phi_t = k\pi \qquad (k = \ldots -1, 1, 3, \ldots) \\ \dfrac{F_2}{F_1} = 1 \end{array}\right\} \tag{3.25}$$

In a disc rotating past a static force, the n ND mode is excited as a backward travelling wave i.e. opposite to the direction of rotation of the disc. In the simulation, we can change the direction of the wave by just imposing the conditions indicated in equation (3.25) rather than those in equation (3.24). However, we should remember that in fact, equation (3.24) represents the condition of simulation of the vibration of n ND mode in the rotating disc excited by a static force and that using $+\phi_t$ (i.e.appIying equation (3.25)) produces the same travelling wave but in the other direction. This is like to assume the other direction for rotation of the disc. Also note that k_1 is bigger than the other coefficients, which confirms that the backward travelling wave is the dominant component in the response of such a disc.

3.4.3 **Excluding a diametral mode in the simulation**

In the previous section, two necessary conditions were found to excite the n nodal diameter modes in the form of a travelling wave. Now, further conditions are being sought in order that another mode, (say the m nodal diameter modes), is **not** excited :

From equation (3.19), the following relations should be satisfied in order to prevent excitation on m ND mode as a backward travelling wave:

$$k_1 = 0, \text{ and } k_4 = 0$$

Substituting from equation (3.17), these can be written as:

$$\left.\begin{aligned} 1+\frac{F_2}{F_1}\cos\phi_t.\ \cos\ m\phi_s &= 0 \\ \sin\ m\phi_s.\cos\phi_t &= 0 \end{aligned}\right\} \qquad (3.26)$$

It is assumed that the n ND modes are the target of the excitation set and have been excited in the form of a backward travelling wave so that equations (3.24) are satisfied; therefore from (3.24) :

$$\cos\phi_t = -\cos n\phi_s \qquad (3.27)$$

By substituting into equation (3.26) , we will have:

$$\left.\begin{aligned} \text{Cos}\ n\phi_s\ \cos\ m\phi_s &= 1 \\ \sin\ m\phi_s\ (-\cos\ n\phi_s) &= 0 \end{aligned}\right| \qquad (3.28)$$

The solutions for the first equation are:

$$\cos n\phi_s = \pm 1 \qquad \text{and} \qquad \cos m\phi_s = \pm 1$$

or:

$$\left.\begin{aligned} m\ \phi_s &= k_m \pi \\ n\ \phi_s &= k_n \pi \end{aligned}\right\} \qquad (3.29)$$

where k_m and $k_n = 1, 3, 5, \ldots$ or: k_m and $k_n = 2, 4, 6, \ldots$

If n and m are considered as two successive numbers i.e. In-ml=l, there is no solution for ϕ_s from these equations except $\phi_s = 360^o$, which makes no sense. However, for the other cases where In-ml>1, a solution can exist.

If the second equation of (3.28) is considered : $\sin m\phi_s = 0$ and/or $\cos n\phi_s = 0$. Their solutions will be :

$$\left.\begin{aligned} m\,\phi_s &= k_m \pi \qquad k_m = 1\ 2\ 3\ldots \\ \text{and/or}\ :\ n\phi_s &= k_n \frac{\pi}{2} \qquad k_n = 1\ 3\ 5\ldots \end{aligned}\right\} \qquad \textbf{(3.30)}$$

The first equation in (3.30) is equivalent to the first equation in (3.29). Therefore, if the spatial angle and the modes are such that equations (3.29) are satisfied, k_1 and k_4 become zero and the m ND mode will not be excited.

From the second equation in (3.30), we have :

$$\phi_s = \frac{k_n}{n}\frac{\pi}{2} \qquad k_n = 1,\ 3,\ 5,\ldots$$

This means that if ϕ_s is chosen such that the above relation is satisfied, then the effects of other modes are decreased but, of course, cannot be removed completely.

3.4.4 **'Pseudo-nodal point' for m ND mode**

It is possible to find a particular point on the rim ($\theta = \theta_p$) at which the fixed vibration component of the response for a particular m ND mode is zero. It is appropriate to call this a 'pseudo-nodal point' for the m ND modes. To establish this condition, it can be found from equation (3.22) that:

$$\sin(m\theta_p + \gamma) = 0 \qquad \textbf{(3.3 1)}$$

Using the definition in equation (3.21), $\tan y = \frac{k_2 - k_4}{k_1 + k_3}$, and substituting for parameters from equations (3.17), gives:

$$\tan y = \frac{\frac{F_2}{F_1}\sin(\phi_t - m\phi_s)}{1 + \frac{F_2}{F_1}\cos(\phi_t - m\phi_s)} \qquad \textbf{(3.32)}$$

From equation (3.31) :

$$m\theta_p + \gamma = 0, \pi, 2\pi, 3x, \ldots$$

or: $$\tan(m\theta_p) = -\tan\gamma$$

Substituting tan y from equation (3.32) and solving for θ_p, gives :

$$\tan\theta_p = \frac{1}{m}\,\text{atan}\left[-\frac{\frac{F_2}{F_1}\sin(\phi_t - m\phi_s)}{1+\frac{F_2}{F_1}\cos(\phi_t - m\phi_s)}\right]$$

Therefore, for a given excitation set, i.e. $(\frac{F_2}{F_1}\angle), \phi_s$ and ϕ_t, we can find a position θ_p at which there is a travelling wave component of m nodal diameter mode only and no other components such as fixed vibration. This position could be suitable to measure the response when the excitation of the n ND mode is the objective and it is close to an m ND mode.

3.4.5 **Representation of response as travelling waves**

According to equation (3.22), the general form for the two-excitation response of n ND modes on the rim can be represented as :

$$x(\theta,t) = X_1\cos(n\theta - \omega t + \alpha_1) - X_2\sin(n\theta + \alpha_2)\,.\,\sin\omega t \qquad (3.33)$$

where X_1 and X_2 vary with frequency. Equation (3.33) gives the response of vibration of the n ND modes with the assumption that two natural frequencies and damping factors are identical, i.e. the disc is tuned (or perfect). It can be shown that this equation is applicable for mistuned discs too, but the coefficients and constants in it do not have same relations as those which have been obtained for the tuned case.

In the more general case, equation **(3.33) can** be recast to a form containing two travelling waves, one backward and one forward, as follows:

$$x(\theta,t)=X_1 \cos(n\theta-\omega t+\alpha_1)-\frac{X_2}{2}[\cos(n\theta-\omega t+\alpha_2)-\cos(n\theta+\omega t+\alpha_2)]$$

$$=X_1\cos(n\theta-\omega t+\alpha_1)-\frac{X_2}{2}\cos(n\theta-\omega t+\alpha_2)+\frac{X_2}{2}\cos(n\theta+\omega t+\alpha_2)$$

$$=X_1[\cos(n\theta-\omega t)\cos\alpha_1-\sin(n\theta-\omega t)\sin\alpha_1]$$

$$-\frac{X_2}{2}[\cos(n\theta-\omega t)\cos\alpha_2-\sin(n\theta-\omega t)\sin\alpha_2+\frac{X_2}{2}\cos(n\theta+\omega t+\alpha_2)$$

$$x(\theta,t)=[X_1\cos al-\frac{X_2}{2}\cos\alpha_2]\cos(n\theta-\omega t)$$

$$-[X_1\sin\alpha_1+\frac{X_2}{2}\sin\alpha_2]\sin(n\theta-\omega t)+\frac{X_2}{2}\cos(n\theta+\omega t+\alpha_2)$$

Denoting:

$$\frac{X_1\sin al+\frac{X_2}{2}\sin\alpha_2}{X_1\cos al-\frac{X_2}{2}\cos\alpha_2}=\tan\alpha_{Bn}$$

then:

$$x(\theta,t)=\frac{X_1\cos al-\frac{X_2}{2}\cos a2}{\cos\alpha_{Bn}}\cos(n\theta-\omega t+\alpha_{Bn})+\frac{X_2}{2}\cos(n\theta+\omega t+\alpha_2)$$

By letting:

$$\frac{X_1\cos\alpha_1-\frac{X_2}{2}\cos\alpha_2}{\cos\alpha_B}=A_{Bn}\ ;$$

$$\frac{X_2}{2}=A_{Fn}\ ;$$

and $\alpha_2=\alpha_{Fn}$, the general formula for the response of the rim to the excitation of the n nodal diameter modes will be obtained:

$$x(\theta,t)=A_{Fn}\cos(n\theta+\omega t+\alpha_{Fn})+A_{Bn}\cos(n\theta-\omega t+\alpha_{Bn}) \qquad (3.34)$$

In section 3.8, this formula is used to decompose and display the response of the rim at any particular excitation frequency, ω.

3.5 COMPLEXITY OF RESPONSE

In the simulation using two excitation sources due to the existence of double modes the response is complex even if the mode shapes are real. A model with complex modes will be considered in chapter 5. The degree of complexity of the response can be obtained easily for the tuned disc. Recalling equation (3.15) for the response at a point on the rim , we have:

$$x(\theta,t) = A\ F_1 \cos n\theta \cdot \cos \omega t + A\ F_2 \cos n(\theta-\phi_s) \cdot \cos(\omega t+\phi_t)$$

This is the response to the excitation set shown in figure 3.2 and is independent of α.

In order to excite the n nodal diameter mode into a travelling wave, the force magnitudes should be equal, $F_1=F_2$, and the relationship between the temporal and spatial phase angles should be:

$$n\phi_s - \phi_t = \pi$$

Substituting for ϕ_t and F_2 in equation (3.15), and expanding, we have :

$$x(\theta,t) = A\ F_1\ [\cos n\theta \cos \omega t - \cos n\theta \cos^2 n\phi_s \cos \omega t + \cos n\theta \cos n\phi_s \sin n\phi_s \sin \omega t$$

$$- \sin n\theta \sin n\phi_s \cos n\phi_s \cos \omega t + \sin n\theta \sin 2 n\phi_s \sin \omega t\ ]$$

Noting that $\cos^2 n\phi_s = 1 - \sin^2 n\phi_s$ and factorising the corresponding terms, we will obtain:

$$x(\theta,t) = A\ F_1 \sin n\phi_s \sin (\omega t - n\theta + n\phi_s) \qquad (3.35)$$

which represents a backward travelling wave, as expected, since the appropriate simulation conditions have been applied to the disc.

In order to obtain the phase angle between x and excitation $f_1(t)=F_1 \cos \omega t$, equation (3.35) is written as:

$$x(\theta,t) = (A\, F_1 \sin n\phi_s) \cos (\omega t - n\theta + n\phi_s - 90^o)$$

Recalling that $A = \frac{1}{\omega_n^2 - \omega^2 + i\eta_n^2\omega_n^2}$, it can be shown that:

$$\frac{x}{f_1} = \left(\frac{\sin n\phi_s}{\omega_n^2 - \omega^2 + i\eta_n^2\omega_n^2}\right) e^{i\gamma}$$

where $\gamma = (-n\theta + n\phi_s - 90^o)$. For cases of low damping, the angle γ is the degree of apparent complexity of n nodal diameter mode which will appear in the modal analysis of this mode.

3.6 EXTENSION OF THE PROCEDURE TO MORE THAN TWO EXCITATIONS

Assume that three exciters have been applied on the disc rather than two and the n ND modes are to be excited in the form of a travelling wave. A similar analysis to that mentioned in sections 3.4.1 and 3.4.2 can be used to obtain the relations between parameters to produce a travelling wave in this case. Having obtained and simplified the equations, we will have:

$$\left.\begin{aligned} 1 + \left(\frac{F_2}{F_1}\right) \cos (n\phi_{s1} - \phi_{t1}) + \left(\frac{F_3}{F_1}\right) \cos (n\phi_{s2} - \phi_{t2}) &= 0 \\ \left(\frac{F_2}{F_1}\right) \sin (\phi_{t1} - n\phi_{s1}) + \left(\frac{F_3}{F_1}\right) \sin (\phi_{t2} - n\phi_{s2}) &= 0 \end{aligned}\right\} \qquad (3.36)$$

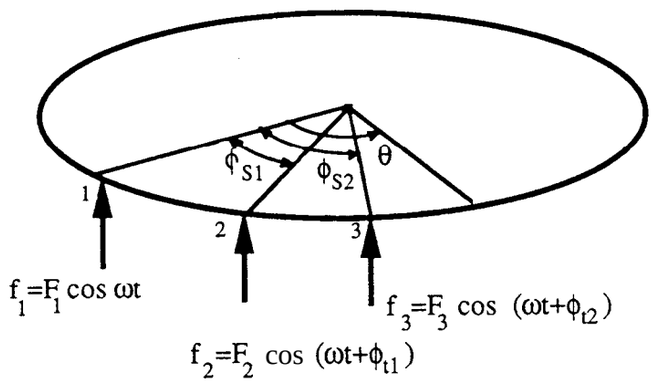

Figure 3.3 **Three** excitations on a stationary disc **-** General case

This is equivalent to equation (3.23) for the two-excitation method. In the general case, finding the relationship between forces ratios, spatial and temporal phase angles from equations (3.36) is not straightforward as it is in the two-excitation case. However, if we assume that the force amplitudes are identical $\frac{F_2}{F_1} = \frac{F_3}{F_1} = 1$, then the exact relation between spatial and temporal phase angles are obtained.

$$\left.\begin{aligned} \phi_{t1} - n\phi_{s1} &= k\,\pi \pm \frac{\pi}{3} \\ \phi_{t2} - n\phi_{s2} &= k\,\pi \pm \frac{\pi}{3} \end{aligned}\right\} \quad k=\ldots -1, 0, 1, 2,\ldots \qquad (3.37)$$

These equations show the relationship between spatial and temporal phase angles in the three-excitation technique to excite n ND mode as a travelling wave. The difference from the two-excitation case is that in that case, we had only one solution for $(\frac{F_2}{F_1})$ which is equal to 1, but here, we have assumed that $\frac{F_2}{F_1} = \frac{F_3}{F_1} = 1$. It can be concluded that using more than two exciters to simulate a travelling wave is difficult in general, even to find the required relation between parameters.

However, we can take advantage of the symmetry of ND modes and expand the two-exciter method to any even number of excitations: 4, 6,8, etc. The idea is originally based on the two-exciter technique but there are more than one pair of excitation sets and all of these pairs are identical to the main two excitations in amplitude and phase but at different and proper spatial positions.

In figure 3.4 four excitations are shown applied to a disc. Forces f_1 and f_2 are the original excitations with spatial and temporal angles ϕ_s and ϕ_t respectively, corresponding to n ND modes. The third excitation f_1' is chosen such that its magnitude and phase are exactly same as for f_1 and its spatial angle is $k'(\frac{360^o}{4n})$, where k' is any integer number. The force f_2' is exactly the same as f_2 and having a spatial angle ϕ_s with f_1'. It is obvious that when we are using more than two exciters, the response level on the disc is no longer the same as on the simulated rotating disc, unless proper levels for all forces are calculated and chosen.

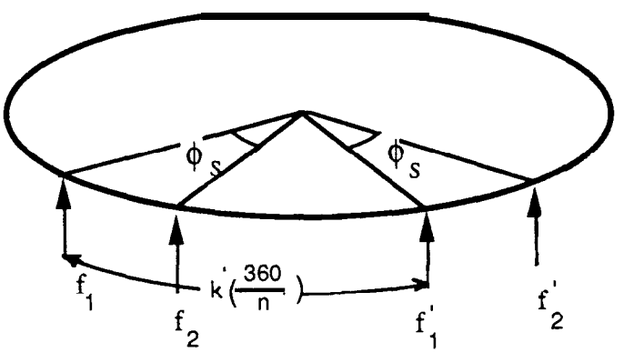

Figure 3.4 Four excitations on a stationary disc

3.7 ISOLATION OF A PARTICULAR DIAMETRAL MODE

Excitation of a structure at a frequency in order that one mode only dominates is called by different expressions such as 'normal mode tuning' and ' isolating of a mode'. There are different techniques to isolate a particular mode but here a method is proposed to isolate a pair of diametral modes in the form of travelling wave which can be detected as a normal vibration by a stationary sensor.

The simulation technique of vibration in a disc rotating past a static force has a secondary application which is the isolation of certain ND modes. Selected nodal diameter modes of a stationary disc can be excited and identified by using two (or more) excitations, as are used in the simulation. By using this method we can excite just the mode of interest. This is more important when the modes are very close and the response is strongly affected by the adjacent modes.

If the disc is heavily mistuned for that mode, each individual mode behaves as an ordinary single mode and the response will be a fixed vibration for dual-sine excitation method. However, for most cases the disc may be assumed to be nearly tuned so that the response is dominated by the travelling wave.

The technique for isolating a ND mode is to apply two shakers at spatial positions ϕ_s apart on the rim. The forces these shakers exert should be controlled to be equal in magnitude with a temporal phase difference (ϕ_t) which should satisfy equation (3.24), that is:

$$\phi_t = n\,\phi_s - k\,\pi \qquad (k=\cdots -1, 1, 3,\cdots)$$

By increasing the number of exciters, as mentioned in section 3.6, the isolation would be achieved more effectively. This method is a special type of tuned sine excitation in which some mono-phase excitations are used to excite or isolate a particular mode of a structure.

3.8 CONTRIBUTION OF DIFFERENT WAVE ORDERS IN THE RESPONSE

In section **3.4.5, the** general formula for the response of a disc's rim was obtained as a combination of forward and backward travelling waves:

$$x(\theta,t) = A_{Fn} \cos(n\theta+\omega t+\alpha_{Fn}) + A_{Bn} \cos(n\theta-\omega t+\alpha_{Bn}) \qquad \textbf{(3.38)}$$

Remembering that this formula represents the response of the n ND modes and is applicable for the general case of exciters' positions and also for the mistuned case as well as the tuned case.

At the frequency of excitation ω, the response x can be determined or measured at any position, 8. Knowing x, we can calculate the unknown parameters of equation (3.36), i.e. : A_{Fn}, α_{Fn}, B_{Fn} and α_{Bn}, then it is possible to display the response. In the following, it is shown how the foregoing parameters can be calculated from x.

The response 'x' at each point is a harmonic quantity which can be measured in magnitude and phase or in the form of real and imaginary components. Here, the real and imaginary components of x are used which are called $a^{(m)}$ and $b^{(m)}$, where 'm' implies to the measured values:

$$x = a^{(m)} \sin \omega t + b^{(m)} \cos \omega t \qquad (3.39)$$

Equation (3.38) can be expanded and re-written in the form of equation (3.39) :

$$x(\theta,t) = [-A_{Fn} \sin(n\theta+\alpha_{Fn}) + A_{Bn} \sin(n\theta+\alpha_{Bn})] \sin \omega t$$

$$+ [A_{Fn} \cos(n\theta+\alpha_{Fn}) + A_{Bn} \cos(n\theta+\alpha_{Bn})] \cos \omega t \qquad (3.40)$$

By letting :

$$\left.\begin{aligned}[-A_{Fn}\ \mathrm{Sin}\ (n\theta+\alpha_{Fn}) + A_{Bn}\sin(n\theta+\alpha_{Bn})] &= a_n \\ [A_{Fn}\ \cos\ (n\theta+\alpha_{Fn}) + A_{Bn}\ \cos\ (n\theta+\alpha_{Bn})] &= b_n\end{aligned}\right\} \qquad (3.41)$$

equation (3.40) becomes:

$$x(\theta,t)= a, \sin \omega t + b_n \cos \omega t \qquad (3.42)$$

which has same form as equation (3.39) so that a_n and b_n are equivalent to the measured values $a^{(m)}$ and $b^{(m)}$ respectively.

Equations (3.41) can be written in matrix form:

$$\begin{Bmatrix} a_n \\ b_n \end{Bmatrix} = \begin{bmatrix} -\sin n\theta & -\cos n\theta & +\sin n\theta & +\cos n\theta \\ +\cos n\theta & -\sin n\theta & +\cos n\theta & -\sin n\theta \end{bmatrix} \begin{Bmatrix} U_{Fn} \\ V_{Fn} \\ U_{Bn} \\ V_{Bn} \end{Bmatrix} \qquad (3.43)$$

where :

$$\left.\begin{aligned} U_{Fn} &= A_{Fn}\ \cos\ \alpha_{Fn} \\ V_{Fn} &= A_{Fn}\ \sin\ \alpha_{Fn} \\ U_{Bn} &= A_{Bn}\ \cos\ \alpha_{Bn} \\ V_{Bn} &= A_{Bn}\ \sin\ \alpha_{Bn} \end{aligned}\right\} \qquad (3.44)$$

Now, by letting :

$$[T_n] = \begin{bmatrix} -\sin n\theta & -\cos n\theta & +\sin n\theta & +\cos n\theta \\ +\cos n\theta & -\sin n\theta & +\cos n\theta & -\sin n\theta \end{bmatrix}$$

and $\{A_n\}^T = \{U_{Fn}\ V_{Fn}\ U_{Bn}\ V_{Bn}\}$, equation (3.43) will be:

$$\begin{Bmatrix} a_n \\ b_n \end{Bmatrix}_{2x1} = [T_n]_{2x4}\,\{A_n\}_{4x1} \qquad (3.45)$$

In this equation, a_n and b_n can be substituted for $a^{(m)}$ and $b^{(m)}$, and vector {An} calculated. However, there are four unknowns in this vector, so two sets of data or

response at two points θ_i and θ_j have to be measured. Thus, from equation (3.45), we will have:

$$\begin{Bmatrix} a_i^{(m)} \\ b_i^{(m)} \\ --- \\ a_j^{(m)} \\ b_j^{(m)} \end{Bmatrix}_{4x1} = \begin{bmatrix} T_{ni} \\ --- \\ T_{nj} \end{bmatrix}_{4x4} \{ A_n \}_{4x1} \qquad (3.46)$$

Knowing or measuring $a^{(m)}$ and $b^{(m)}$ for points i and j , the unknown parameters can be determined provided $\begin{bmatrix} T_{ni} \\ --- \\ T_{nj} \end{bmatrix}^{-1}$ exists:

$$\{A_n\} = \begin{bmatrix} T_{ni} \\ --- \\ T_{nj} \end{bmatrix}^{-1} \begin{Bmatrix} a_i^{(m)} \\ b_i^{(m)} \\ --- \\ a_j^{(m)} \\ b_j^{(m)} \end{Bmatrix}$$

In equation (3.38), it has been assumed that the response is comprised of just one wave order (order n). Now, the analysis can be extended for the general case by assuming that N wave orders have contributed in the response at the excitation frequency CO. In this case instead of equation (3.38), we have :

$$\begin{aligned} x(\theta,t) = {} & A_{F1} \cos(\theta+\omega t+\alpha_{F1}) + A_{B1} \cos(\theta-\omega t+\alpha_{B1}) \\ & + A_{F2} \cos(2\theta+\omega t+\alpha_{F2}) + A_{B2} \cos(2\theta-\omega t+\alpha_{B2}) \\ & + \ldots \\ & + A_{Fn} \cos(n\theta+\omega t+\alpha_{Fn}) + A_{Bn} \cos(n\theta-\omega t+\alpha_{Bn}) \\ & + \ldots \\ & + A_{FN} \cos(N\theta+\omega t+\alpha_{FN}) + A_{BN} \cos(N\theta-\omega t+\alpha_{BN}) \end{aligned} \qquad (3.47)$$

It should be noted that at a particular excitation frequency ω, different wave orders travel at different angular speed Ω around the disc. This angular speeds are such that :

$$n\,\Omega_n = \omega \quad , \quad (\text{for } n=1 \text{ to } N)$$

where: n = wave order or number of nodal diameter of the mode;

Ω_n = angular speed of wave order n around the disc, (rad/sec);

ω = Excitation frequency or vibration frequency, (rad/sec).

In equation (3.47), each wave order can be treated as shown for wave order n in equations (3.40) and (3.41). As a result, equation (3.47) can be written in another form:

$$\begin{aligned} x(\theta,t) = {} & a_1 \sin \omega t + b_1 \cos \omega t \\ & + a_2 \sin \omega t + b_2 \cos \omega t \\ & + \ldots \\ & + a_n \sin \omega t + b_n \cos \omega t \\ & + \ldots \\ & + a_N \sin \omega t + b_N \cos \omega t \end{aligned}$$

or :

$$x(\theta,t) = \left(\sum_{n=1}^{N} a_n\right) \sin \omega t + \left(\sum_{n=1}^{N} b_n\right) \cos \omega t$$

Now, if $a_i^{(m)}$ and $b_i^{(m)}$ are the real and imaginary parts of the response at point θ_i, then :

$$\begin{Bmatrix} a_i^{(m)} \\ b_i^{(m)} \end{Bmatrix} = \begin{Bmatrix} \left(\sum_{n=1}^{N} a_n\right) \\ \left(\sum_{n=1}^{N} b_n\right) \end{Bmatrix} \qquad (3.48)$$

Substituting for a, and b_n from equations (3.45), will give :

$$\begin{Bmatrix} a_i^{(m)} \\ b_i^{(m)} \end{Bmatrix} = [T_{1i} \quad T_{2j} \quad \dots \quad T_{ni} \quad \dots \quad T_{Ni}]_{2x4N} \begin{Bmatrix} A_1 \\ --- \\ \vdots \\ --- \\ A_n \\ --- \\ \vdots \\ --- \\ A_N \end{Bmatrix}_{4Nx1} \qquad (3.49)$$

This equation is for just one data set or one measured point. For p data points, we can write:

$$\{ab\}_{2px1} = [T]_{2px4N} \{A\}_{4Nx1} \qquad (3.50)$$

where :

$$\{ab\}^T = \{ a_1^{(m)} \; b_1^{(m)} \; \vdots \; a_2^{(m)} \; b_2^{(m)} \; \vdots \; \dots \; \vdots \; a_i^{(m)} \; b_i^{(m)} \; \vdots \; \dots \; \vdots \; a_p^{(m)} \; b_p^{(m)} \}_{1x2p} \; ;$$

$$[T] = \begin{bmatrix} T_{11} & T_{12} & \dots & T_{1n} & \dots & T_{1N} \\ T_{21} & T_{22} & \dots & T_{2n} & \dots & T_{2N} \\ \vdots & \vdots & & \vdots & & \vdots \\ T_{i1} & T_{i2} & \dots & T_{in} & \dots & T_{iN} \\ \vdots & \vdots & & \vdots & & \vdots \\ T_{p1} & T_{p2} & \dots & T_{pn} & \dots & T_{pN} \end{bmatrix}_{2px4N} \; ;$$

and $[A]^T = [A, A, \dots A_n \dots A_N]_{1x4N}$

For N wave orders, at least 2N points or data points are needed. In this case, matrix $[T]_{2px4N}$ is a square matrix and can be inverted to calculate waves parameters, (of course inversion of a matrix is valid only if its determinant $\neq 0$):

$$\{A\}_{4Nx1} = [T]^{-1}_{2px4N} \{ab\}_{2px1}$$

However, the elements of matrix [T] are such that its determinant is equal to zero for p=2N. Therefore, p should be greater than 2N. If p>2N then the matrix [T] is not square and cannot be inverted. In this case the pseudo-inverse of [T] is used, that is :

$$\{A\}_{4Nx1}=[T]^{+}\{ab\}_{2px1}$$

where $[T]^{+}$ has been called the 'pseudo-inverse' of [T] and it is defined as :

$$[T]^{+} = ([T]^{T}[T])^{-1}[T]^{T}$$

Therefore, at excitation frequency ω, by measuring response at different points, (p points where p>2N), wave parameters can be calculated from equation (3.50). Knowing the wave parameters and using equation (3.47), the response can be identified and displayed in an animated form.

Having obtained the wave parameters, the contribution of different wave orders are identified and the dominant mode in the response can be recognized.

If the excitation arrangement is such that a particular mode is to be excited in the form of a backward travelling wave, the contribution of this mode in the total response is determined. By repeating the measurement and analysis for different frequencies near the natural frequency, the frequency response for this mode can be obtained.

For the analysis mentioned in this section, programs 'HDISK4' and 'WAVE6' have been written in Basic for H.P. computers. They calculate the response and give wave parameters from measured data; then the response is displayed as explained in the next sec tion.

3.9 DISPLAYING RESPONSE AS A COMBINATION OF TRAVELLING WAVES AND FIXED VIBRATION

The response pattern in ND modes of a disc simulation is complex. If the response equation is known or enough points on the rim can be measured, we can display the response and in cases where we have a travelling wave, we can show the direction by an arrow.

Suppose $x(\theta,t)$ is known, as a formula or by some discrete values of the response. In the latter case they could be from measurements,we can use the method mentioned in section 3.9 to find the contribution of the different wave orders as well as a formula for the whole of the response

One period of response $\left(T=\frac{2\pi}{(n\Omega)}\right)$ is divided into equal intervals, say six. At each of these "frames", we can calculate the response at a number of, say 50, different positions on the rim. It will be clearer in demonstration if we use a straight line representing the circumference of the disc. The shape at each frame in the period is displayed in sequence. If the shape is a travelling wave, the direction of the wave is shown in the hard copy by using a small arrow. In the following section, there are examples of displaying the response of the disc under the different conditions.

3.10 NUMERICAL EXAMPLES

In order to show the concept of the simulation and also the isolation of a diametrical mode in a disc, four different systems are considered, as shown in table 3.1. All these systems have only

Table 3.1 Different systems in the numerical study

	Modes	Natural. frequencies. [Hz]		Damping loss factor		Excitation pts.	
		2ND	3ND	2 ND	3 ND	ϕ_s	ϕ_t
System I	2 & 3 ND	100, 100	130, 130	0.001. 0.001	0.001, 0.001	45	-90
System II	2 & 3 ND	100, 100	102, 102	0.001, 0.001	0.001, 0.001	30	-90
System III	2 & 3 ND	100, 101	130, 130	0.002, 0.001	0.001, 0.001	30	-120
System IV	2 & 3 ND	100, 100	102, 120	0.001. 0.001	0.001, 0.002	30	-90

two pairs of modes: the 2 ND and 3 ND modes. figure 3.5 shows the response of system I to the two harmonic excitations. This is a tuned system with well-separated 2ND and 3ND natural frequencies.The spatial phase for exciters is 45^o and temporal phase angle is selected so that the 2 ND mode to be excited as a backward travelling wave, ϕ_t=-90^o. Angle a, the offset between one excitation point and an adjacent antinode point, is assumed to be equal to zero since the modes are tuned.

Figure 3.5 shows that the dominant wave is a 2 ND backward travelling wave, and that it constitutes 83% of the total response. These calculations have been carried out on the basis of the analysis in sections 3.2 and 3.8 respectively. The response at each of 15 points around the disc has been calculated. Then, the contribution of the different waves has been obtained up to order 6 and are presented in table 3.2. The total response, dominant wave and other waves have been displayed separately in figure 3.5. Each display is constructed of six curves and each curve represents the response at one frame (a sixth fraction of a period); so that we can visualize the response of the rim in time. The direction of the dominant wave has been shown by a small arrow in the above.

In system II, the modes are assumed to be close and a 3 ND mode is excited by choosing the appropriate exciter positions. The excitation frequency is 95 Hz which is quite

different from the natural frequencies. Figure 3.6 shows the response for this case and it is seen that in spite of the fact that the 3 ND mode is the target of the excitation, the dominant backward travelling wave is 2 ND.This is because of the proximity of the 2 ND mode whose natural frequency is closer to the excitation frequency than that of the 3 ND mode.

Table 3.2 Waves parameters obtained for system I

Wave order n	Forward t. wave Ampl. A_{Fn}	Forward t. wave phase. α_{Fn}	Backward t. wave Ampl. A_{Bn}	Backward t. wave phase α_{Bn}
1	6.17E-22	329.0°	1.63E-21	166.8
2	4.19E-21	79.8	2.47E-05	269.4
3	1.64E-06	337.3	3.98E-06	67.6
4	7.28E-22	119.36	1.71E-21	80.6
5	6.69E-22	71.5	6.35E-22	0.0
6	9.76E-22	102.5	4.73E-22	153.4

The possibility of improving the situation is examined by using 4 exciters which are identical two by two and are positioned at $0^{\circ}, 30^{\circ}, 120^{\circ}$ and 150°. The result has been shown in figure 3.7 and it is seen that the dominant backward travelling wave is 3 ND and it is 54% of the total response. We can see here the significant effect of the number of excitors in the simulation and in the isolation of a mode.

In figure 3.8, the excitation frequency has been set exactly to the target mode (3 ND) natural frequency. It is seen that almost the entire response is a backward travelling wave of this mode. However, figure 3.9 shows that if the natural frequency of the target mode is not chosen correctly, then the response is far from a pure travelling wave and could even be dominated by an unexpected order.

The simulation has next been applied to a mistuned system in figure 3.10 (system III). The 2 ND mode is excited by two exciters with a spatial angle equal to 30^{o}, which is different from its normal value for this mode. The simulation formula $n\phi_s - \phi_t = \pi$ has been used to determine the temporal phase angle. It is seen that the total response is presenting essentially a 2 ND backward travelling wave, which is comparable with the corresponding tuned case in figure 3.5. By increasing the number of exciters, the response of the target ND mode can be improved significantly, which has been shown in figure 3.11 for four exciters.

The case of a ND mode which is heavily mistuned, and appears as a single mode, is presented in system IV and figure 3.12. The target mode is one of the 3 ND pair and the excitation frequency is assumed equal to the natural frequency of this mode (102 Hz). For such a case, the response is a fixed vibration which can be decomposed into one backward travelling wave and one forward travelling wave as shown in figure 3.12.

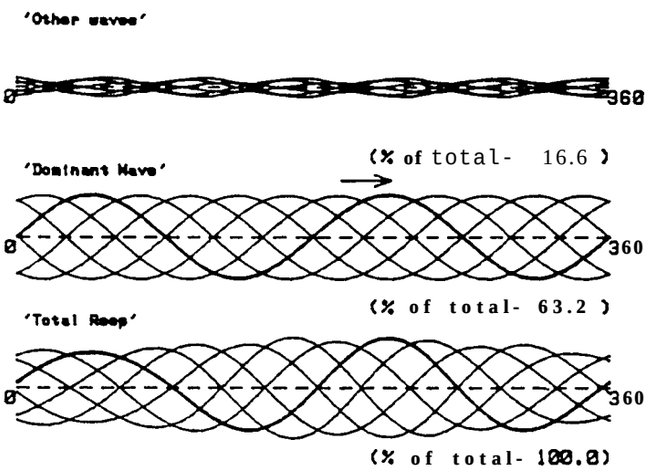

Data:

Natural frequencies		Damping		Excitation parameters				
2ND	3 ND	2 ND	3 N	D Exc. fred.		ϕ_s Mode to be exci ted	α , 2 NL	α , 3 ND
100, 100 Hz	130, 130 Hz	0.001 0.001	0.001, 0.001	105 Hz	45	2ND	0.0	0.0

Figure 3.5 Response of a tuned disc at a frequency different from natural frequencies, (System I)

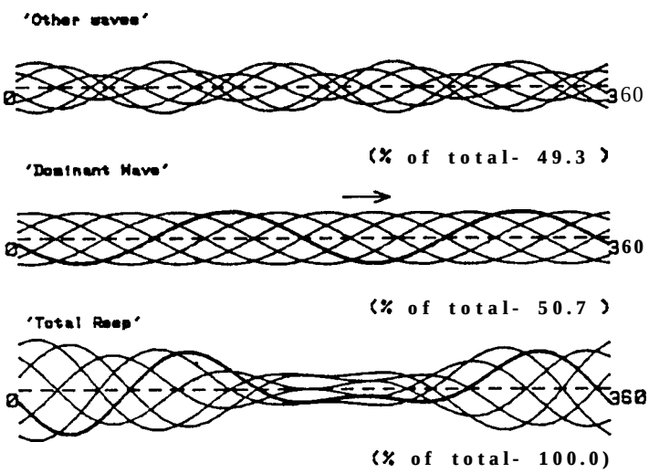

Data

Natural frequencies		Damping		Excitation parameters				
2 ND	3 ND	2 ND	3ND	Exc. freq	ϕ_s	Mode to be exci ted	α , 2 ND	α , 3 ND
100, 100 Hz	102, 102 Hz	0.001, 0.001	0.001, 0.001	95 Hz	30	3 ND	0.0	0.0

Figure 3.6 Response of a tuned disc with close modes, (system II)

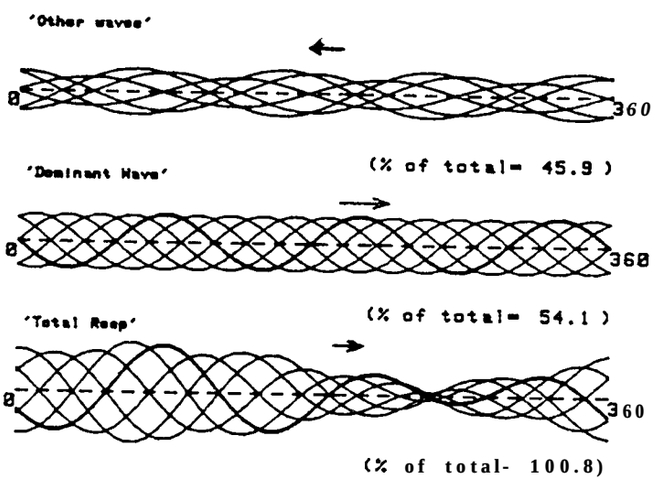

Data:

Natural frequencies		Dan-mine		Excitation parameters				
2ND	3ND	2 N D	3 N D	E x c . f r e q	ϕ_s	Mode to be exci ted	α , 2 ND	α , 3 ND
100, 100 Hi	102, 102 Hz	0.001, 0.001	0.001, 0.001	95 Hz	30	3ND	0.0	0.0

Figure 3.7 Response of a tuned disc using 4 excitations

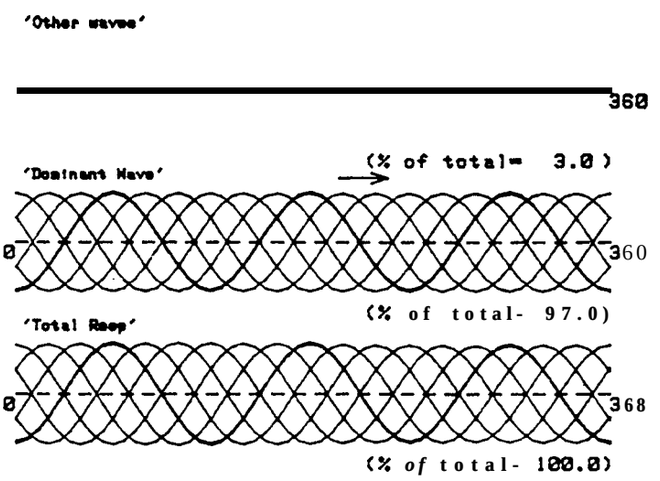

Data:

Natural frequencies		Damping		Excitation parameters				
2ND	3ND	2 N D	3 N D	Exc. freq	ϕ_s	Modetobeexcited	α , 2 ND	α , 3 ND
100, 100 Hz	102.102 Hz	0.001, 0.001	0.001, 0.001	102 Hz	30	3ND	0.0	0.0

Figure 3.8 Response of a tuned disc at frequency equal to the natural frequency

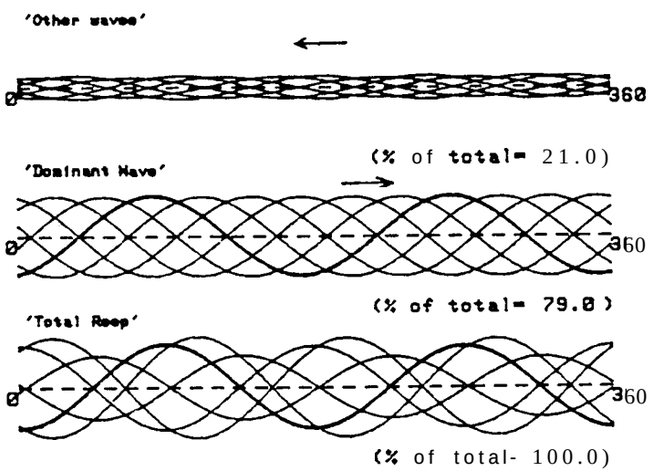

Data:

Natural frequencies		Damping		Excitation parameters				
2 ND	3 ND	2ND	3ND	Exc. freq	ϕ_s	Modetobeexcited	α, 2 ND	α, 3 ND
100, 100 Hz	102 102 Hz	0.001, 0.001	0.001, 0.001	100 Hz	30	3 ND	0.0	0.0

Figure 3.9 Response of a tuned disc at the natural frequecy of another mode

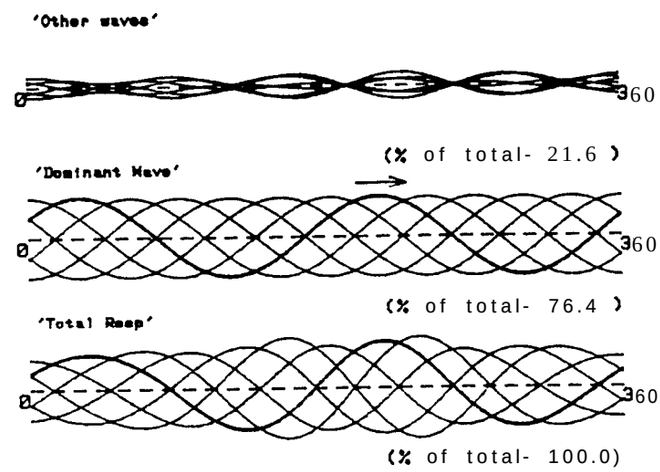

Data:

Natural frequencies		Damping		Excitation parameters				
2 ND	3 ND	2 ND	3ND	Exc. freq	ϕ_s	Mode to be exci ted	α, 2 ND	α, 3 ND
100, 101 Hz	130, 130 Hz	0.001, 0.002	0.001, 0.001	105 Hz	30	2 ND	10.0	0.0

Figure 3.10 Response of a mistuned disc at frequency different from the natural frequency (system III)

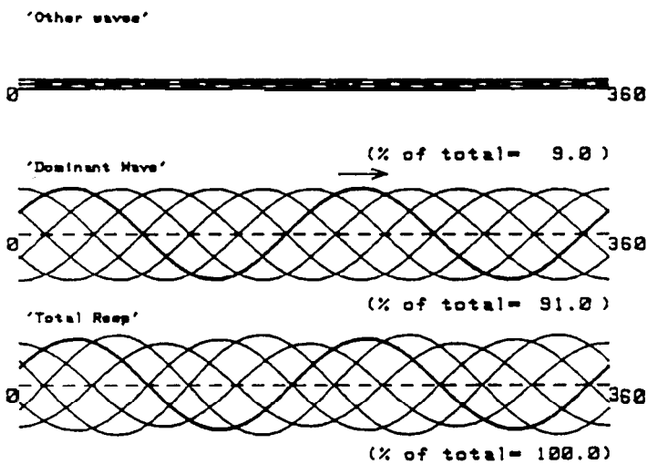

Data:

Natural frequencies		Damping		Excitation parameters				
2ND	3ND	2 ND	3ND	Exc. freq. ϕ_s	Mode tobeexci ted		α, 2ND	α, 3 ND
100, 101 Hz	130, 130 Hz	0.002 0.001	0.001 0.001	105 Hz	30	2ND	10.0	0.0

Figure 3.11 Response of a mistuned disc at frequency different from the natural frequency using 4 excitations

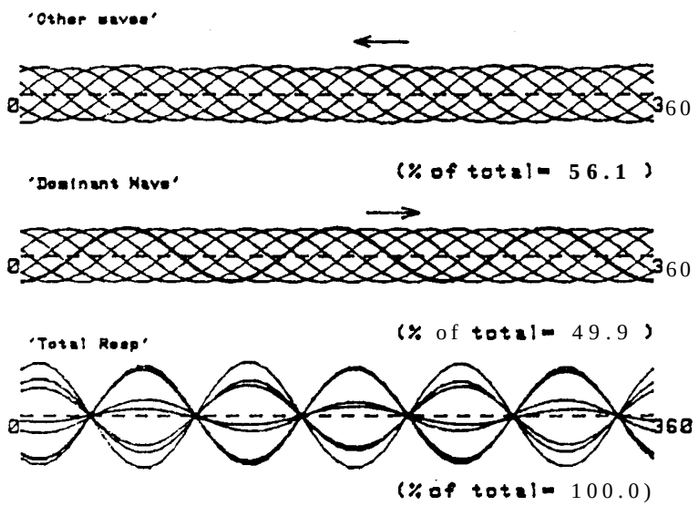

Data:

Natural frequencies		Damping		Excitation parameters				
2ND	3ND	2ND	3ND	Exc. freq. ϕ_s	Mode to be excited		α, 2 ND	α, 3 ND
100, 100 Hz	102, 120 Hz	0.001	0.001, 0.001	102 Hz	30	3ND	0.0	10.0

Figure 3.12 Response of a single ND mode to the simulation in system IV

3.11 CONCLUSIONS

For vibration of a disc rotating past a static force, a standing wave is generated which is seen by a stationary observer. It happens at any speed of rotation but there is a resonance if the rotating speed is equal to one of the wave frequencies, (Wave frequency = Natural frequency of ND mode divided by number of ND of that mode).

The response of each ND mode in a rotating disc excited by a static force may be simulated on a stationary disc using controlled multiple harmonic forces. In such a simulation, the standing wave response mentioned above appears as a backward travelling wave since the disc is stationary.

The simplest form of such simulation is for two forces which are orthogonal in time and spatial position. However, in the general case, there is a particular relation between spatial and temporal phase angles ($n\phi_s - \phi_t = \pi$) whilst the amplitudes of two forces should always be equal.

The dual sine-excitation technique can be used to isolate a particular ND mode to provide a secondary result from the simulation. For greater effectiveness, it is possible to apply more than two exciters, but it is preferable to use even numbers of exciters and identical pairs of exciters at the proper positions.

The contribution of different wave orders can be determined if there are more measurement points than twice of the maximum number of considered wave orders. An animated display of the response of a disc can be shown on a video screen and a hard copy of the travelling waves are presented.

Chapter 4

EXPERIMENTAL SIMULATION OF VIBRATION IN A DISC ROTATING PAST A STATIC FORCE

4.1 INTRODUCTION

In chapter 3 it was demonstrated that vibration in a disc rotating past a static force can establish a travelling wave on the disc and at a certain speed, called the critical speed, a resonance occurs. Also, it was explained that this system can be simulated for each diametral mode in a stationary disc when excited by at least two harmonic forces. These forces should be orthogonal in time and spatial position with regard to the diameual mode concerned. This is very useful, since rather than rotating the disc, we can test a stationary disc with simpler and better modal testing methods than are possible under spinning conditions. In addition to simulating the response for a pair of ND modes, there are other applications for this method of excitation. Isolation of a particular mode and modal testing can be the objectives of the dual-excitation of an axisymmetric structure.

In the previous chapter, the general relation has been obtained for the excitation set parameters when the magnitude of the forces is kept equal (n $\phi_s \pm \phi_t = 1$ SO"). In this

chapter, it is intended to show how this condition can be applied to a disc in practice. A bladed disc test piece has been chosen. First, a standard sine test with one shaker is carried out to find out the general FRF and natural frequencies. Then, the two-shaker test and simulation is carried out on the disc. Attention has been paid to the 2 ND modes as an example but a similar procedure can be followed for other diametral modes.

4.2 SINE-SWEEP TEST ON THE DISC

4.2.1 **The general description of the test**

One of the most accurate methods in modal testing is the sine-sweep test. A sinusoidal excitation is applied to the structure at each step and the steady-state response is measured at the same frequency as the excitation. The excitation frequency is shifted to the next value and the corresponding response is measured. By changing the frequency and measuring the response, it is possible to plot the frequency response function (FRF) which has been defined as:

$$H_{jk}(\omega)=\frac{x_j}{f_k}\Bigg|_{f_l=0,\ l=1,\infty \text{ but } l\neq k} = \sum_{r=1}^{\infty} \frac{{}_rA_{jk}}{\omega_r^2-\omega^2+i\eta_r\omega_r^2} \qquad (4.1)$$

According to this definition, the only force causing x_j should be f_k and this is an important point in this equation which is the foundation of the conventional modal testing.

One disadvantage of using the shaker excitation is that there is an interaction between the shaker and structure. The dynamic characteristics of the structure can change due to this interaction.

4.2.2 Frequency-dependency of the input force

In the sine- step excitation tests, the input voltage of the signal for the shaker is usually chosen to have a certain value and does not change during the test. However, the applied force to the structure may change with frequency due to the changing impedance of the shaker. The electrical impedance of the shaker depends on the displacement level and this, in turn, depends on the vibration characteristics of the structure. Therefore, around the resonance and anti-resonance, there will be more variation in the input force and less variation far from these points. In figure 4.1, we can see the varying force level as the exitation frequency pass two natural frequencies.

The variation of input force is not important in a standard modal test using single-point excitation as the ratio of acceleration per unit force is measured. But it makes it difficult to control and to adjust the forces which are required in some special tests for example, in the two-shaker method proposed here.

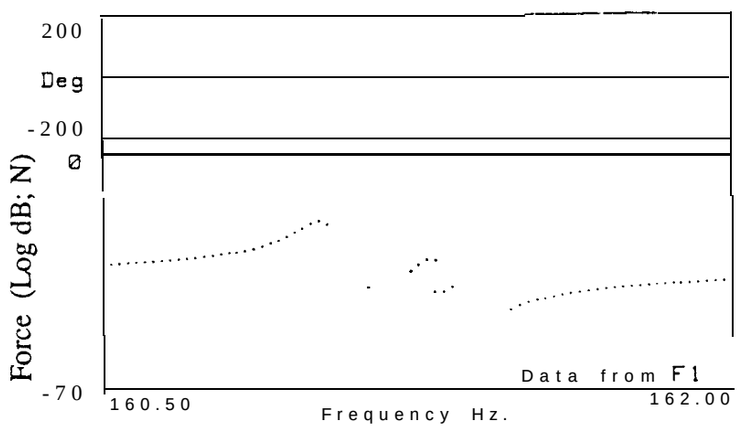

Figure 4.1 Variation of excitation force with excitation frequency
(There are two natural frequencies in this range.)

4.2.3 Results of single-excitation tests

A disc with 45 integral blades has been chosen for the tests. It is suspended in a vertical plane by flexible ropes as shown in figure 4.2.

In a preliminary test, the natural frequencies were found and are presented in figure 4.3. For the freely-supported disc, the first flexural mode is the 2 ND mode (n=2) at 264 Hz. This was confirmed by carrying out some hammer test on different points on the rim and observing the sign of the imaginary part of each FRFs in the vicinity of the resonance. Remembering that the sign of the imaginary part of the response shows whether that point vibrates in phase or out of phase with the force, this is a simple way to estimate the mode shape of a structure.

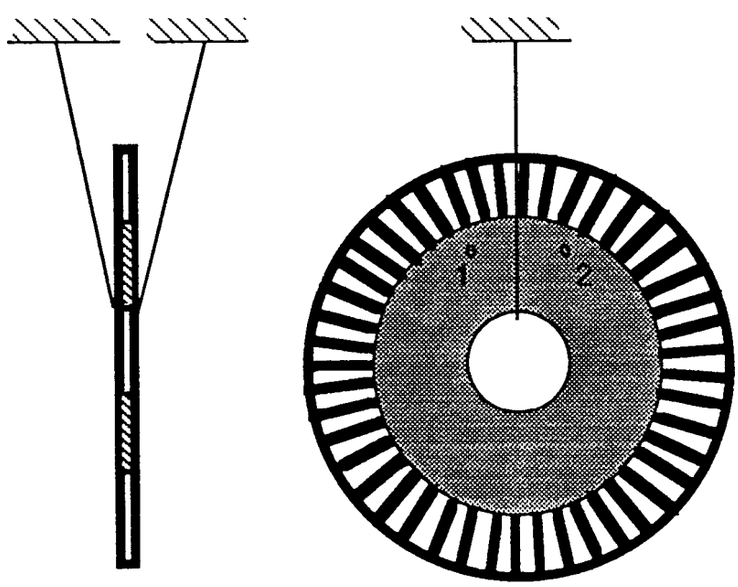

Figure 4.2 Schematic of the freely supported disc in the tests and measurment points 1 and 2

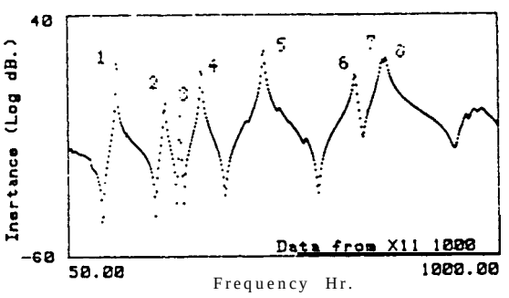

Ref No.	Freq [Hz]
1	158
2	264
3	296
4	344
5	482
6	682
7	746
8	752

Figure 4.3 First natural frequencies of the disc

Having recognised the 2 ND mode natural frequencies, we can perform a zoom measurement around these frequencies to obtain more information about the 2 ND modes. Figure 4.4 shows the FRFs from a point measurement and a transfer measurement respectively. The modal data from these FRFs have been obtained by using 'MODENT and are presented in table 4.1.

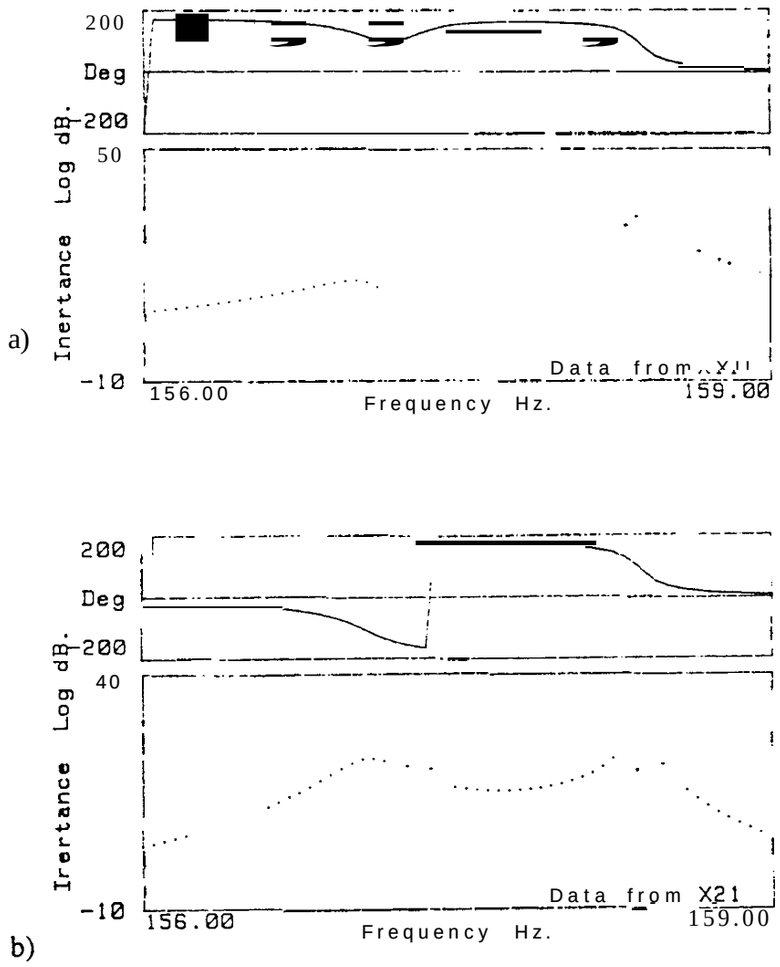

Figure 4.4 Single-excitation test on the 2 ND modes of the disc
a) Point measurement; b) Transfer measurement

Table 4.1 Modal properties from measurements at points 1 and 2

	2NDmode No.	Natural frequency [Hz]	Modal constant [1/Kg]	Phase [Deg.]	Damping loss factor; η
Data from point 1 (Point meas.)	1	157.05	0.0113	-6.6	0.00235
	2	158.38	0.0513	-4.3	0.00118
Data from point 2 (Transfer meas.)	1	157.06	0.0298	+172.8	0.00234
	2	158.38	0.025 1	-7.0	0.00118

4.3 EXPERIMENTAL SIMULATION OF A TRAVELLING WAVE

In order to simulate a travelling wave, at least two sinusoidal excitations should be applied at specific positions around the disc (or any other axisymmetric structure). The two forces should be equal in magnitude and have ϕ_t phase difference in time so that the general simulation equation ($n\phi_s \pm \phi_t = 1$ SO") is satisfied. This set of excitation conditions is hereafter called "dual controlled sine" (DCS) excitation. The spatial angle chosen was 45^o in the tests which is equal to the normal value ($=\frac{360^o}{4n}$) for 2 ND modes. The spatial angle would be -90^o for generating a backward travelling wave. If $\phi_t = +90^o$ is chosen then, the direction of the generated wave is reversed but it should not be thought that the forward travelling wave has been simulated, as explained in section 3.4.2.

Two methods are proposed to find the response to the DCS excitation. In the first method, which is fully experimental, a phase and amplitude shifter (PHASH) has been developed to control and adjust the two input forces at each frequency.The second method is a hybrid procedure. By carrying out two ordinary sine-sweep tests, A and B, we can measure the corresponding response vector $\{x\}$ and input force vector (F) . Then, we can calculate the FRF matrix [H] by using the general response formula $\{x\}=[H]\{F\}$. Having obtained [H], the response can be calculated for the DCS excitation.

4.3.1 Experimental method (EM)

In this method, the simulation is applied directly to the test structure. At the frequency of excitation, the relative amplitude and spatial phase angle of the two input forces must be adjusted to meet the predefined values. An acceptable tolerance for forces ratio ($\frac{F_2}{F_1}$) is

chosen as ± 0.1 which is within 10% ; and the acceptable tolerance for the temporal phase angle is assumed to be $\pm 2^{o}$ for $\phi_t = 90^{o}$. In figure 4.5, the instrumentation layout for this method is shown and specifications of the equipment are presented in Appendix D.

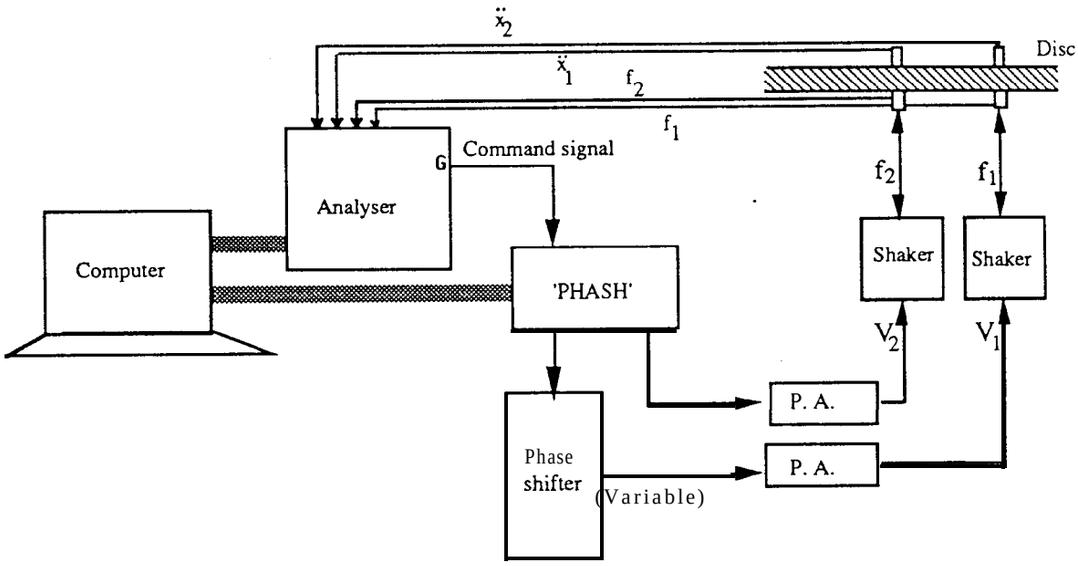

Figure 4.5 Instrumentation in the Experimental method for the simulation of a travelling wave

Two sinusoidal forces f_1 and f_2 are applied at points 1 and 2. The command signal from the generator goes to the power amplifiers through the phase shifters. A standard phase shifter is in series with one channel of 'PHASH' for manual phase controlling in difficult situations. The PHASH is used for fine control through a computer and the phase shifter is just for manual large phase shifting when it is necessary. The program POLAR, which is for a single-sine sweep test, has been modified to control two shakers with the hardware 'PHASH'. The details of the controller 'PHASH' and the corresponding program are presented in Appendix C.

4.3.2 Hybrid method (HM)

The second method is a hybrid procedure in which two tests are performed without applying any restriction or control on the two sinusoidal excitations. The FRF matrix [H] is calculated from these measurements. Finally, the response to the DCS excitation can be obtained using $\{x\}=[H]\{F\}$.

In the following, the analysis used in the hybrid method is summarised

Applying equation $\{x\}=[H]\{F\}$ for the measurement points 1 and 2 in the tests A and B, we will have:

$$\left.\begin{aligned} \begin{Bmatrix} x_1 \\ x_2 \end{Bmatrix}_A &= \begin{bmatrix} H_{11} H_{12} \\ H_{21} H_{22} \end{bmatrix} \begin{Bmatrix} F_1 \\ F_2 \end{Bmatrix}_A \\ \text{and} \quad \begin{Bmatrix} x_1 \\ x_2 \end{Bmatrix}_B &= \begin{bmatrix} H_{11} H_{12} \\ H_{21} H_{22} \end{bmatrix} \begin{Bmatrix} F_1 \\ F_2 \end{Bmatrix}_B \end{aligned}\right\} \quad (4.2)$$

Combining these two matrix equations, we have:

$$\left[\{x\}_A \{x\}_B\right] = [H]\left[\{F\}_A \{F\}_B\right] \quad (4.3)$$

In the measurement, normally f_2 and the responses are measured relative to f_1, which is received at channel 1 of the analyser. Therefore, both sides of equation (4.2) are divided by F_1 and so equations (4.3) after combination will become:

$$\left[\begin{Bmatrix} (\frac{x_1}{F_1}) \\ (\frac{x_2}{F_1}) \end{Bmatrix}_A \begin{Bmatrix} (\frac{x_1}{F_1}) \\ (\frac{x_2}{F_1}) \end{Bmatrix}_B\right] = [H]\left[\begin{Bmatrix} 1 \\ (\frac{F_2}{F_1}) \end{Bmatrix}_A \begin{Bmatrix} 1 \\ (\frac{F_2}{F_1}) \end{Bmatrix}_B\right]$$

If $(\frac{F_2}{F_1})_A \neq (\frac{F_2}{F_1})_B$, the second matrix on the right hand side can be inverted and the FRF matrix [H] is calculated:

$$[H] = \frac{\begin{bmatrix} \left(\frac{F_2}{F_1}\right)_B & -1 \\ -\left(\frac{F_2}{F_1}\right)_A & 1 \end{bmatrix}}{\left(\frac{F_2}{F_1}\right)_B - \left(\frac{F_2}{F_1}\right)_A} \left[\begin{Bmatrix} \left(\frac{x_1}{F_1}\right) \\ \left(\frac{x_2}{F_1}\right) \end{Bmatrix}_A \quad \begin{Bmatrix} \left(\frac{x_1}{F_1}\right) \\ \left(\frac{x_2}{F_1}\right) \end{Bmatrix}_B \right] \tag{4.4}$$

In the abovementioned method, two excitations are used simultaneously. However, it may be more convenient if we use just one shaker when the other is disconnected in each test. By this method, we can measure the elements of the FRF matrix directly. Assuming that in test C, excitation is at point 1 and the response is measured at points 1 and 2 then, we will obtain:

$$H_{11}=\left(\frac{x_1}{F_1}\right)_C \quad \text{and} \quad H_{21}=\left(\frac{x_2}{F_1}\right)_C$$

Similarly, in test D, excitation is at point 2 and response is measured at points 1 and 2 then, the other two elements of FRF matrix are obtained:

$$H_{12}=\left(\frac{x_1}{F_1}\right)_D \quad \text{and} \quad H_{22}=\left(\frac{x_2}{F_1}\right)_D$$

Therefore, in this method [H] is measured directly.

Having obtained [H] by either of the hybrid methods, two-excitation or single-excitation tests, then, we can calculate the response due to the simulation condition.

Each of these two hybrid methods has some advantages. Using two excitations at the same time takes less measurement time, since the shakers are aligned and connected just once. The effects of shaker, push rod and force gauge are almost equal for both modes when applying two exciters. However, using one shaker in each test may cause different effects, although it has the advantage of avoiding interaction between the second shaker and structure. Let us suppose that a mistuned disc is vibrating at a frequency near to one of the ND modes. The response will be dominated by this single mode. The forces are applied at two points which could be relatively out of phase for the excited mode while

the temporal phase angles of the forces are the same. Then, one of the forces will be opposing the vibration which is to be generated and this is a contradiction to our aim, which is to excite the disc.

Also, when we are using two exciters , the ratio of $(\frac{F_2}{F_1})$ should be different in test A and test B to avoid singularity of the forces matrix. This may be another disadvantage of the two-excitation hybrid method compared with applying a single shaker.

In this work, two exciters have been used for the hybrid method, using the same number as have been applied in the direct (or experimental) procedure.

4.4 EXTRACTION OF MODAL PROPERTIES

In the previous sections, the methods for simulating a travelling wave response have been presented. Now, the question is: if we simulate a travelling wave for a range of frequencies around the diametral mode, how can these data be used to extract modal properties - can the conventional modal testing methods be applied?

Assuming that two harmonic excitations F_1 and F_2 have been applied on the disc, then the response at a point j on the rim x_j will be:

$$x_j = H_{j1} F_1 + H_{j2} F_2$$

or

$$\left(\frac{x_j}{F_1}\right) = H_{j1} + H_{j2} \left(\frac{F_2}{F_1}\right) \qquad (4.5)$$

where H_{j1} and H_{j2} are the receptances between points 1,2 and j respectively. Remembering that the term on the left hand side is measurable and, also, in single-point excitation modal testing, the second term on the right hand side is zero.

Substituting the general FRF formula into equation (4.5), we have:

$$\left(\frac{x_j}{F_1}\right) = \sum_{r=1}^{2} \frac{{}_r\phi_j \, {}_r\phi_1}{\omega_r^2-\omega^2+i\eta_r\omega_r^2} + \sum_{r=1}^{2} \frac{{}_r\phi_j \, {}_r\phi_2}{\omega_r^2-\omega^2+i\eta_r\omega_r^2}\left(\frac{F_2}{F_1}\right) \tag{4.6}$$

where r=1 and 2 represent the dual diametral modes which are being investigated. Adding two parts of equation (4.6) we get:

$$\frac{x_j}{F_1} = \sum_{r=1}^{2} \frac{{}_r\phi_j \left[{}_r\phi_1+{}_r\phi_2\left(\frac{F_2}{F_1}\right)\right]}{\omega_r^2-\omega^2+i\eta_r\omega_r^2} \tag{4.7}$$

This equation is similar to the FRF formula for H_{j1}, the only difference is in the numerator. It seems that the modal analysis routines such as the circle-fitting method can still be applied for $\frac{x_j}{F_1}$ if the ratio $\left(\frac{F_2}{F_1}\right)$ can be held constant during the measurements. The denominator is the same as for the standard FRF formula. Thus, the calculated natural frequencies ω_r and damping factors η_r will yield the natural frequencies and damping loss factors of the diametral modes. The numerator represents a complex quantity which is called 'pseudo modal constant' ${}_rA_{je}$.

$${}_rA_{je} = {}_r\phi_j \left[{}_r\phi_1+{}_r\phi_2\left(\frac{F_2}{F_1}\right)\right] \tag{4.8}$$

According to the simulation criterion, $\left(\frac{F_2}{F_1}\right)$ is equal to +i when ϕ_t=+90 and the spatial phase angle is equal to the nominal value ($\phi_s=\frac{360}{4n}$). In the general application of simulation, ϕ_s can be any applicable angle so that equation (4.8) can be written as:

$${}_rA_{je} = {}_r\phi_j \left[{}_r\phi_1+a\,{}_r\phi_2+ib\,{}_r\phi_2\right] \tag{4.9}$$

where a and b are defined as: a=cos ϕ_t, b=sin ϕ_t.

If the nodal diameter mode shapes of the disc are assumed to be real, ${}_r\phi_1$ and ${}_r\phi_2$ will be real. Then, from equation (4.9), the phase of the pseudo-modal constant will be:

$$\angle {}_rA_{je} = \tan^{-1}\left(\frac{b\ {}_r\phi_2}{{}_r\phi_1 + a\ {}_r\phi_2}\right)$$

This implies that this angle does not depend on the position on the disc and for any two points on the rim, say points 1 and 2, we can write:

$$\left|\angle {}_rA_{1e} - \angle {}_rA_{2e}\right| = m\pi ; \qquad m=0, 1, \cdots$$

This means that the pseudo-modal constants have 0^o or 180^o phase difference for any two points. This is similar to the behaviour of real modes despite the (pseudo-) modal constants being complex.

If ${}_rA_{j1}$ and ${}_rA_{j2}$ are the modal constants relating points 1, 2 and j, then from equation (4.9), we can write:

$${}_rA_{je} = {}_rA_{j1} + a\ {}_rA_{j2} + i b\ {}_rA_{j2}$$

For this equation, the real and imaginary parts in the both sides should be equal. Again, if the modes are assumed to be real, the modal constants (which are also real) can be obtained from:

$$\left.\begin{aligned} {}_rA_{j1} &= \mathrm{Real}({}_rA_{je}) - \frac{a}{b}\,\mathrm{Im}({}_rA_{je}) \\ \text{and} \qquad {}_rA_{j2} &= \frac{\mathrm{Im}({}_rA_{je})}{b} \end{aligned}\right\} \qquad (4.10)$$

Thus, using equation (4.10) and assuming that the modes are real, the modal constants can be calculated from the 'pseudo modal constants'.

A special case is considered: when $\phi_t = -90^o$ as the result a=0 and b=-1, then the following relations can be applied for this case:

$$\left.\begin{aligned} {}_rA_{j1} &= \mathrm{Real}({}_rA_{je}) \\ {}_rA_{j2} &= -\,\mathrm{Im}({}_rA_{je}) \end{aligned}\right\}$$

Another point from the definition of pseudo-modal constant, equations (4.7) and (4.8), is that the phase difference between two modes can be obtained:

If $_1\phi$ and $_2\phi$ are real, and assuming that $\phi_t = +90^\circ$ then:

$$\angle_1 A_{je} = \tan^{-1}\left(\frac{_1\phi_2}{_1\phi_1}\right) \quad \text{and} \quad \angle_2 A_{je} = \tan^{-1}\left(\frac{_2\phi_2}{_2\phi_1}\right)$$

By assuming that $_1\phi = \cos n(\theta-\alpha)$ and $_2\phi = \sin n(\theta-\alpha)$, and substituting for $\theta_1 = 0^\circ$ and $\theta_2 = 45^\circ$, we can show that:

$$\frac{1\%}{1\%} = \tan na \quad \text{and} \quad \frac{2\phi_2}{2\%} = \tan(n\alpha - 90^\circ)$$

Therefore, the phase angle between two modes are obtained:

$$\angle_2 A_{je} - \angle_1 A_{je} = (n\alpha - 90^\circ) - na$$

or:

$$\angle_2 A_{je} - \angle_1 A_{je} = -90^\circ$$

It is seen that this angle is -90° between the second and first conjugates of the diametral mode.

4.5 SENSITIVITY OF THE SIMULATION TO THE EXCITATION PARAMETERS

As mentioned in section 3.4.2, the travelling wave response of a particular ND mode pair can be simulated using two harmonic excitations provided that the spatial and temporal phase angles, ϕ_s and ϕ_t satisfy the relation $n\,\phi_s - \phi_t = \pi$ and also that the relative amplitude of the forces to be equal, $(\frac{F_2}{F_1} = 1)$. The parameters ϕ_s, ϕ_t and $(\frac{F_2}{F_1})$ are called the excitation parameters.

In practice and in the experimental work, it is possible that an excitation parameter will not have its desired value precisely but will contain some error. Hence, a tolerance has to be given for each of the excitation parameters as in many other practical techniques. Here, the effect of the excitation parameters' deviation on the travelling wave response is investigated. A simple tuned system with just a single pair of ND modes is considered. The response at different points on the disc are calculated and then the component of the travelling wave can be estimated using the method mentioned in section 3.8. However, for the tuned case, we can obtain the amplitude of travelling wave directly using equation (3.10) in section 3.4.1.

Different values of the excitation parameters around their nominal values have been chosen and then the travelling wave amplitude relative to the amplitude of the total response is calculated for each case. Figure 4.6 shows the variation of the travelling wave against the excitation parameters. It is seen that for a certain value on the horizontal axis for every parameter, the deviation of the forces ratio has less influence than the spatial and temporal phase angles. The chosen tolerances in the experiments in section 4.6.1 have been derived from figure 4.6. The tolerance of $\pm 10\%$ in $(\frac{F_2}{F_1})$ makes the travelling wave component to be at least 90% of the total response. There is more than 97% travelling wave component in the response if $\pm 2^{o}$ tolerance is used for the temporal or spatial phase angles.

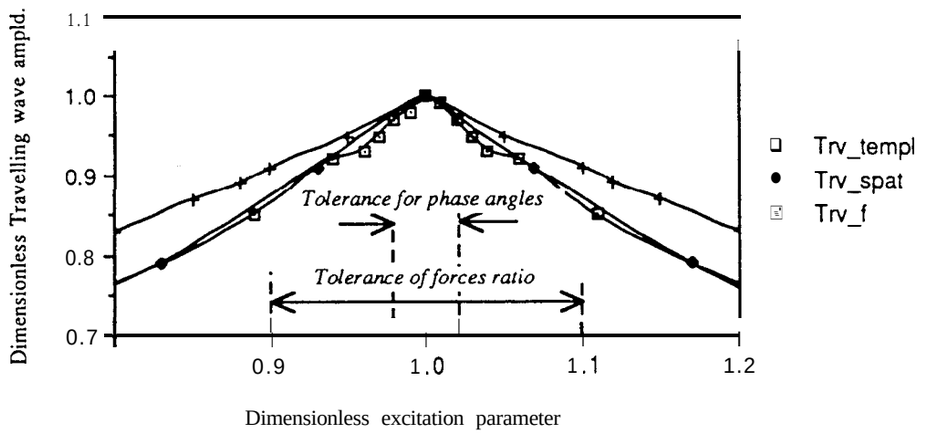

Figure 4.6 Normalised travelling wave amplitude vs normalised excitation parameters

4.6 EXPERIMENTAL RESULTS AND DISCUSSION

The same disc which was used in the tests with one shaker (in section 4.2.3) is chosen for the simulation of travelling waves. The experiments are concentrated on 2 ND modes although similar tests may be carried out on the other ND modes. Two excitations have been used and two different methods of simulation - experimental (EM) and hybrid (HM) - have been applied to the disc. The results are presented in the following sections

4.6.1 The Experimental Method (EM) Results

Two equal sinusoidal forces with predefined temporal phase angle were applied to the disc at a certain spatial phase angle. For two diametral mode and spatial phase angle equal to 45°, ϕ_t should be equal to -90° for simulating the (backward) travelling wave. Remembering that by choosing $\phi_t=+90^{\circ}$ instead we just change the direction of the wave.

The test is consisted of sine-sweep at frequencies around the 2 ND natural frequencies. At each frequency the magnitudes of two forces and the temporal phase angle are checked to be within the acceptable tolerances mentioned in section 4.3.1. The measured responses are shown in figure 4.7 in the form of $(\frac{X_1}{F_1})$ and $(\frac{X_2}{F_1})$ together with $(\frac{T_2}{F_1})$ plotted against frequency.

These are not in fact standard FRFs due to the fact that more than one exitation is applied to the structure. As mentioned in section 4.4, although these are not normal FRFs, we can apply the standard modal analysis methods on these data, regarding the obtained modal constants as pseudo-modal constants. The program MODENT was used and the results obtained are presented in table 4.2.

Table 4.2 Modal properties from EM at points 1 and 2

	2 ND mode No.	Natural frequency [Hz]	Pseudo-Modal Constant [1/Kg]	Phase [Deg.]	Damping loss factor; η
Data from point 1 (X1_F21)	1	157.14	0.0257	-59.4	0.00208
	2	158.39	0.0593	+24.9	0.00164
Data from point 2 (X2_F21)	1	157.16	0.0680	+117.9	0.00224
	2	158.40	0.0315	+16.6	0.00164

4.6.2 The Hybrid Method (HM) Results

In the other method also, two exciters were used but there was no control on the temporal phase angle or on the amplitude ratio of the forces. The measured data for both tests A and C are shown in the Appendix B. Again, these are not standard FRFs; however, they can be used to calculate the special FRFs to represent the simulation of travelling wave as

mentioned in section 4.3.2. The results are shown in figure 4.8 and the modal data are presented in table 4.3.

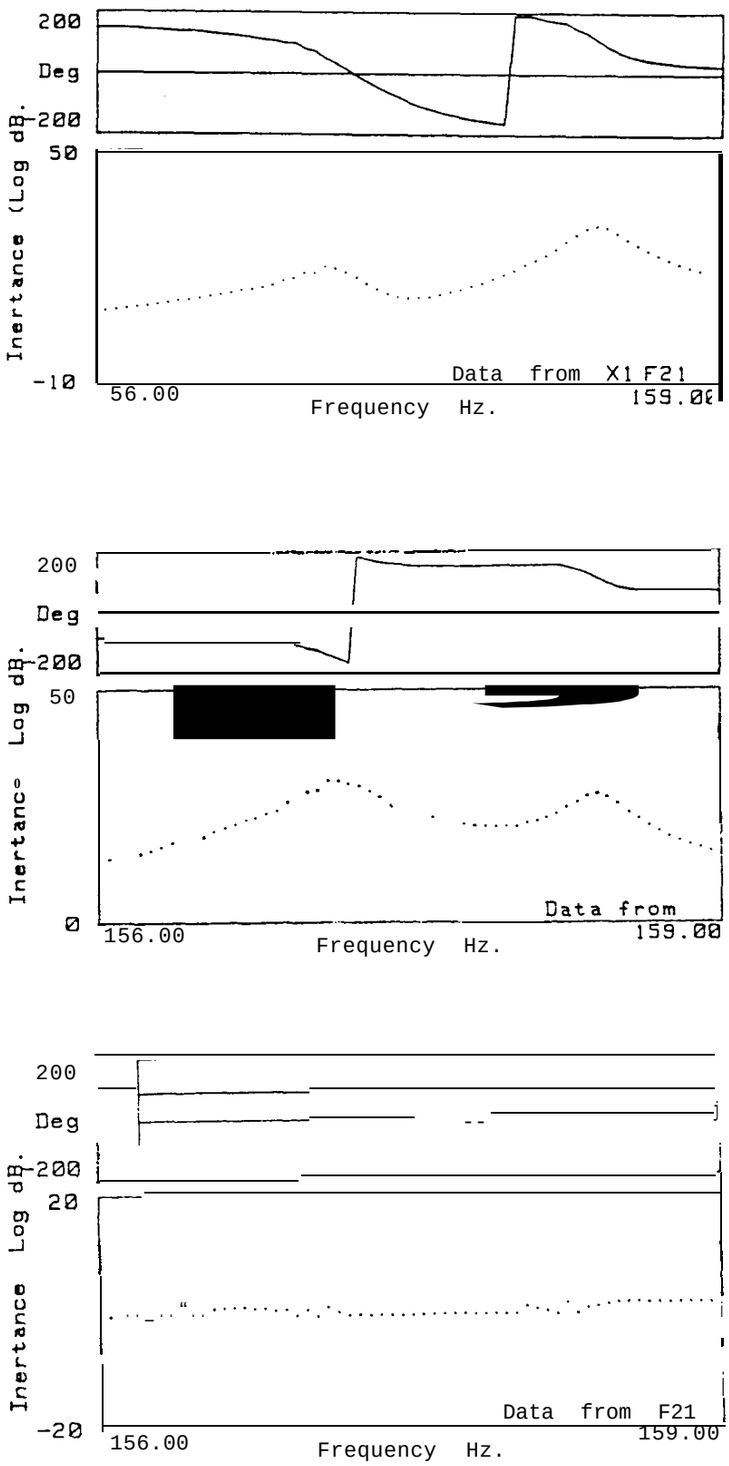

Figure 4.7 Results in the Experimental Method of simulation

Table 4.3 Modal properties from HM at points 1 and 2

	2 ND mode No.	Natural frequency [Hz]	Pseudo-Modal constant [1/Kg]	Phase [Deg.]	Damping loss factor ; η
Data from point 1 (W1_AC)	1	157.16	0.0272	-69.6	0.00200
	2	158.39	0.0538	+21.0	0.00133
Data from point 2 (W2_AC)	1	157.15	0.0696	+115.2	0.00209
	2	158.39	0.0270	+16.2	0.00129

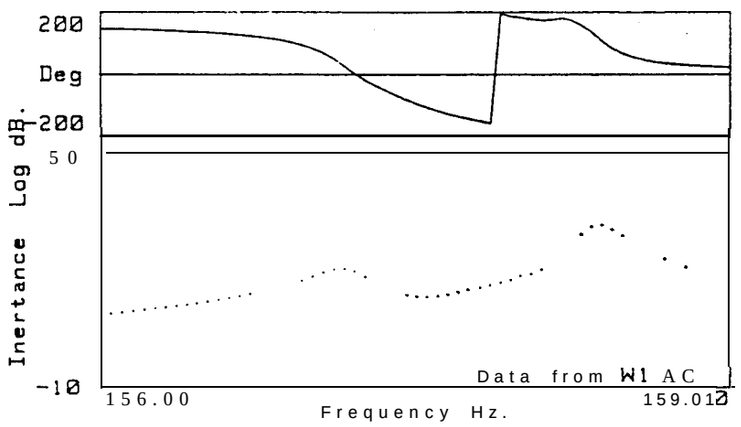

a)

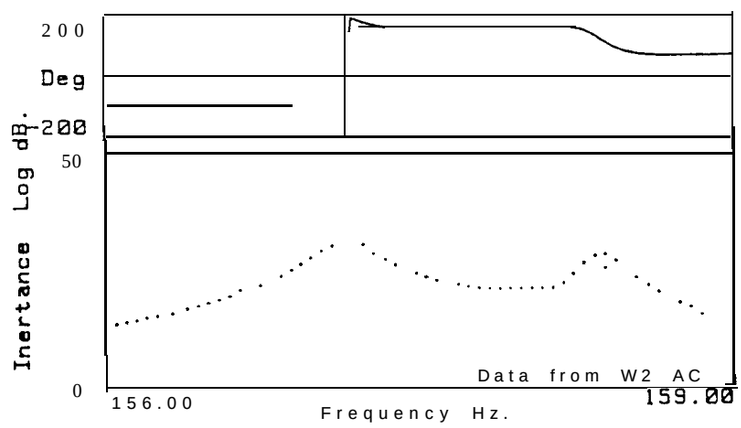

b)

Figure 4.8 Results in Hybrid Method of simulation

4.6.3 Discussion

In previous sections, the simulation of a travelling wave has been carried out in a disc for a range of different frequencies. The responses at two points 1 and 2 on the disc were measured for the frequencies around the natural frequencies. Two methods, the fully experimental and the hybrid methods, have been used and the results shown in figures 4.7, 4.8 and tables 4.2 and 4.3.

The disc behaved as a mistuned system since the natural frequencies of the two 2 ND modes are not the same. The separation of these frequencies has also appeared in the single-excitation test results shown in figure 4.4. Some part of this frequency-splitting is due to the influence of the attached transducers and shakers. Since the mode is mistuned, the travelling wave at frequencies adjacent to the natural frequencies will be contaminated with the other sorts of vibration, even though the conditions of the simulation are met. As mentioned in the earlier sections, the modal properties can be obtained from the measured response using conventional modal analysis. The natural frequencies and damping factors obtained are almost the same as the original ones (in table 4.1), although there are 'pseudo-modal constants' which can be used to find the true modal constants if the modes are assumed to be real.

In order to interpret the results, a numerical example is examined. Assuming a disc has two pairs of diametral modes, 2 ND and 3 ND, whose modal properties are shown in table 4.4. Two sinusoidal excitations are used and the temporal phase angles are set to be $+90^{o}$ in order to excite the 2 ND modes.

The responses at points 1 and 2 are shown in figure 4.9 and the modal properties have been obtained (using MODENT) and they are presented in table 4.5. This numerical example is for a mistuned case similar to the disc in the experiment. In another numerical study, a tuned system is examined. This system is similar to the mistuned case but the natural frequency and damping factor

Table 4.4 Modal data for numerical example (mistuned system)

Natural frequencies		Damping factors		Excitation parameters			
2ND	3ND	2ND	3ND	ϕ_s	ϕ_t	α, 2 ND	α, 3 ND
100, 101	130, 130	0.001, 0.002	0.001, 0.001	45	+90	10	0

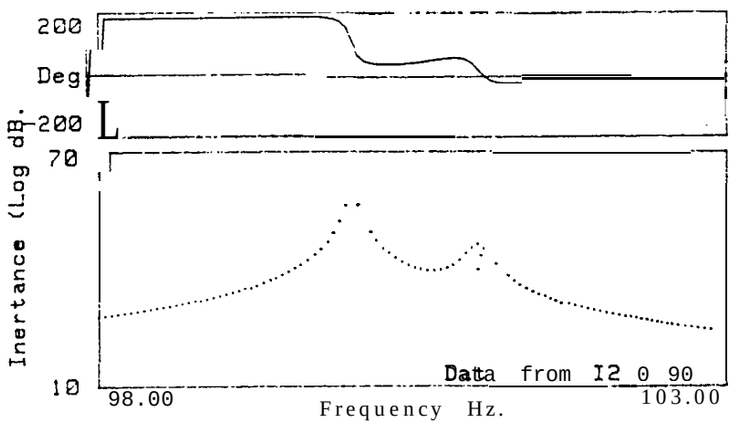

a)

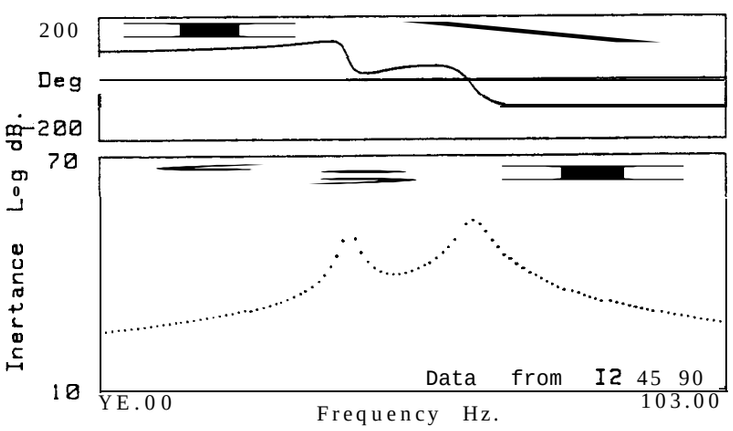

b)

Figure 4.9 Results from numerical example (mistuned system)

a) at point 1 (θ=0°); b) at point 2 (θ=45°)

Table 4.5 Modal properties from measurements at points 1 and 2; (mistuned system)

	2NDmode No.	Natural frequency [Hz]	Psedo_modal constant [1/Kg]	Phase [Deg.]	Damping loss factor; η
Data from point 1 (I2_0_90)	1	100	0.9397	+20.0	0.00100
	2	101	0.3419	-70.0	0.00200
Data from point 2 (I2_45_90)	1	100	0.3426	-20.0	0.00100
	2	101	0.9396	-110.0	0.00200

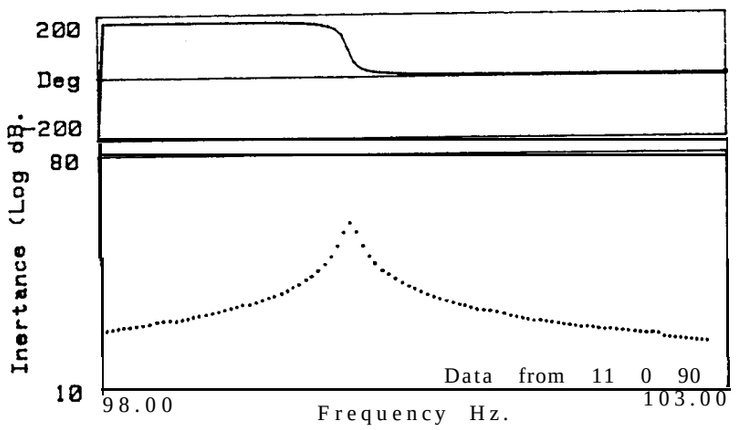

a)

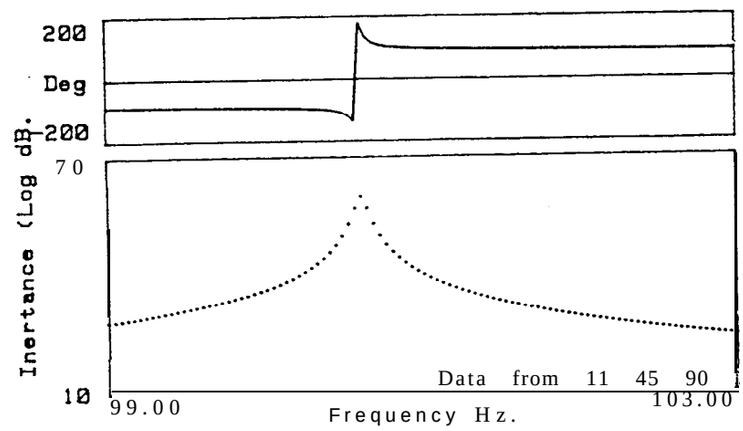

b)

Figure 4.10 Results from numerical example (tuned system)

a) at point 1 ($\theta=0^o$); b) at point 2 ($\theta=45^o$)

Table 4.6 Modal properties from measurements at points 1 and 2; (tuned system)

	2NDmode No.	Natural frequency [Hz]	Modal constant [1/Kg]	Phase [Deg.]	Damping loss factor; η
Data from point 1 (I2_0_90)	1	100	0.9999	0.0	0.00100
	2				
Data from point 2 (I2_45_90)	1				
	2	100	0.9998	+90.0	0.00100

are 100 Hz and 0.001 respectively for both 2 ND modes. Of course, in this system a is equal to zero since it is a tuned case. For this tuned system, the responses to the DCS excitations have been presented in figure 4.10 and the modal properties are given in table 4.6.

There is a pure travelling wave at each frequency shown in figure 4.10. By comparison of the phase angle curves for points 1 and 2, it is seen that at each frequency the phase lag of point 2 relative to point 1 is +90°. This is for inertances which is same for the phase difference of the receptances. It implies that the wave travels from point 2 towards point 1 on the rim. This is correct, since ϕ_t was chosen to be +90° which is the opposite sign to the temporal phase angle for generating a **backward** travelling wave which would go from point 1 towards point 2.

For the mistuned system shown in figure 4.9, the phase difference around the two natural frequencies is not 90° but away from the natural frequencies, where the effect of mistuned modes is reduced, the phase angle **is 90°**. In the actual mistuned system, figures 4.7 and 4.8, similar interpretation can be made. At frequencies very close and equal to the natural frequencies, the travelling wave disappears, while at frequencies away from natural frequencies, the condition of the response returns to the travelling wave.

From the calculated modal parameters, the phase difference between two modes corresponding to the pseudo-modal constants is 90° for the numerical system (table 4.5). However, these are about 10° off for the actual systems (tables 4.2 and 4.3).This is because the measurements and modal analysis of the data is carried out with the inevitable inclusion of some errors.

The phase of the pseudo-modal constant shows that the phase difference for each mode at two different points on the rim is 0° or 180°, as it was expected from the theory. This shows that the modes are originally real, even though they have appeared as complex modes.

The results from the experimental or direct simulation method and results from the hybrid simulation method are in general agreement. As mentioned earlier, each method has some advantages and disadvantages. The direct simulation method needs more testing time and a controller such as 'PHASH', which makes for more complicated instrumentation for the test. However, in this method we can have the simulated travelling wave on the real structure while in the hybrid method the response to the DCS excitation **is calculated.**

Another disadvantage in the hybrid method is the requirement of different $(\frac{F_2}{F_1})$ in the two tests. When the disc is mistuned and the damping is low, the two diametral modes behave as two separate modes. In this situation, near resonance, it is not easy to apply different $(\frac{F_2}{F_1})$ in two tests since one of the forces (which is more involved in the excitation of the first mode) will be at a low level due to the frequency dependency of the input force. We cannot increase it by increasing the input voltage. For the similar situation in the experimental method, it is also difficult to excite the other mode by adjusting the forces at frequencies close to a natural frequency of a mistuned lightly-damped system.

The test disc is a very lightly-damped structure. Its damping had to be increased by adding a wire to the blades in order to carrying out the two excitation tests. The inherent damping is about four times less than the values measured with the additional damping

material. A single-shaker test on the disc without additional damping and the corresponding modal data have been shown in Appendix B for comparison with the other modal data which have been obtained from the wired disc.

4.6 CONCLUSIONS

It has been shown that travelling waves can be simulated on an axisymmetric structure by applying two harmonic excitations. Two methods have been applied: in the first , conditions of the simulation are applied directly on the structure. This method has been called the experimental method. The second method is a hybrid procedure in which the FRF matrix is calculated from the data of two sets of measurements on the structure. Then the response to the special excitation for the simulation (DCS excitation) is calculated.

In a tuned system, the response is a pure travelling wave. However, in the case where the structure is mistuned and very lightly-damped, a pure travelling wave can not be established at frequencies close or equal to a natural frequency. The experimental method has some advantages subject to having a proper controller for the amplitude ratio and the temporal phase angle between the two forces.

As a result of simulating the travelling wave at frequencies around a set of diametral modes, two modes will emerge from the analysis with phase angles at 90° relative to each other. The standard modal analysis routines such as the circle-fitting can be applied on the responses despite the application of more than one exciter. In the case of real modes in the disc, the modal constants can be obtained from the pseudo-modal constants.

Chapter 5

TRAVELLING WAVE RESPONSE IN A LUMPED-MASS MODEL

5.1 INTRODUCTION

In chapter 1, it was mentioned that non-uniformity in the static pressure distribution exerted on a rotating disc in a gas or steam turbine could excite the disc in different engine orders. Furthermore, each nodal diameter mode of the disc rotating past a non-rotating and static force may be simulated on a stationary disc using a dual harmonic excitation. On the other hand, for a disc as an axisymmetric structure, most of the modes are double, so that at one frequency there are two modes with same mode shapes but orthogonal in space. Simulation of double modes is carried out by applying two harmonic forces separated by a spatial angle of $\phi_s = \frac{360^o}{4n}$, where n is the number of nodal diameters (ND), and by a temporal phase angle $\phi_t = 90^o$. In chapter 3, it was shown that different temporal and spatial phase angles can be chosen provided they satisfy the following relation:

$$n\phi_s - \pi = \phi_t$$

In the present chapter, a discrete mass model of a disc is considered for further analysis on the forced vibration of rotating discs. The simulation criterion which has already been

5.3 EIGENVECTORS FOR REPEATED EIGENVALUES

As mentioned in the previous section, for repeated eigenvalues any linear combination of their eigenvectors is itself also an eigenvector. However, a particular eigenvector can be introduced which is unique relative to a chosen eigenvector of the family of eigenvectors of the repeated eigenvalues. In the following, the method which has been developed in reference [47] is used.

Supposing that $\{\psi\}_k$ and $\{\psi\}_l$ are two eigenvectors corresponding to the equal eigenvalues λ_k^2 and λ_l^2. Alternative eigenvectors $\{\psi'\}_k$ and $\{\psi'\}_l$ are introduced such that at a certain coordinate, x_i, one of them is zero :

$$_k\psi_i' = 0 \qquad (5.5)$$

Also, the new eigenvectors are to fulfii the orthogonality condition:

$$\{\psi'\}_k^T [M] \{\psi'\}_l = 0 \qquad (5.6)$$

Setting $\{\psi'\}_k$ and $\{\psi'\}_l$ as a combination of the initial eigenvectors, we can write :

$$\left.\begin{aligned} \{\psi'\}_k &= p\ \{\psi\}_k + \{\psi\}_l \\ \{\psi'\}_l &= q\ \{\psi\}_k + \{\psi\}_l \end{aligned}\right\} \qquad (5.7)$$

where p and q are two constants which are to be determined.

Substituting into equation (5.6) gives :

$$p\,q\,m_k + m_l = 0 \qquad (5.8)$$

where :

$$m_k = \{\psi\}_k^T [M] \{\psi\}_k$$

$$m_l = \{\psi\}_l^T [M] \{\psi\}_l$$

On the other hand, by using equation (5.5) for coordinate i, we will get :

$$P_k\psi_i - {}_l\psi_i = 0$$

or :

$$p = -\frac{{}_l\psi_i}{{}_k\psi_i} \qquad (5.9)$$

Now, q will be obtained from equation (5.8) :

$$q = \frac{m_l}{m_k} \cdot \frac{{}_k\psi_i}{{}_l\psi_i} \qquad (5.10)$$

The new eigenvectors possess the properties of orthogonality and are unique in direction (or phase). However, they should be normalized in magnitude to be the same as the original ones. For simplicity, if the eigenvectors are represented by vectors $\mathbf{u}$ and $\mathbf{u}'$:

$$\{\psi\}_k = \mathbf{u} \quad \text{and} \quad \{\psi'\}_k = \mathbf{u}' \qquad (5.11)$$

they can be written in term of unit vectors and norms :

$$\hat{\mathbf{u}} = \frac{\mathbf{u}}{\|\mathbf{u}\|} \quad \text{and} \quad \hat{\mathbf{u}}' = \frac{\mathbf{u}'}{\|\mathbf{u}'\|}$$

The normalised eigenvector $\mathbf{u}_n'$ is in the direction to $\mathbf{u}'$ and is equal to $\mathbf{u}$ in magnitude, that is:

$$\mathbf{u}_n' = \|\mathbf{u}\| \hat{\mathbf{u}}'$$

or :

$$\mathbf{u}_n' = \frac{\|\mathbf{u}\|}{\|\mathbf{u}'\|} \cdot \mathbf{u}'$$

Substituting the original vectors from equation (5.11) will give:

$${}_n\{\psi'\}_k = \frac{(\text{norm}\{\psi'\}_k)}{(\text{norm}\{\psi\}_k)} \cdot \{\psi\}_k \qquad (5.12)$$

Similarly, we can obtain the normalized eigenvector for the other mode:

$$ {}_n\{\psi'\}_1 = \frac{(\text{norm}\{\psi'\}_1)}{(\text{norm}\{\psi\}_1)} \cdot \{\psi\}_1 \qquad (5.13) $$

5.4 DUAL-EXCITATION RESPONSE

In the previous section, the eigenvalues and eigenvectors of the assumed lumped mass system have been obtained. Now, the response to any set of harmonic forces can be calculated; although particular interest is on the response to the two harmonic excitations with specific spatial and temporal phase angles. The general formula for the response [3] is:

$$ \{X\} = [H]\{F\} \qquad (5.14) $$

where $[H]$ is the FRF matrix whose general element H_{ij} is given by:

$$ H_{ij} = \sum_{r=1}^{N} \frac{{}_r\phi_i \cdot {}_r\phi_j}{\lambda_r^2 - \omega^2} $$

N is the number of modes and is assumed to be equal to the coordinates. ${}_r\phi_i$ is the mass normalised eigenvector element at point i, and is equal to:

$$ {}_r\phi_i = \frac{{}_r\psi_i}{\sqrt{m_r}} $$

The input forces, $f_1(t)=F_0 \cos \omega t$ and $f_2(t)=F_0 \cos(\omega t+\phi_t)$, should have equal magnitudes and hence the force vector for the case of interest is

$$ \{F\} = \begin{Bmatrix} F_1 \\ F_2 \end{Bmatrix} = \begin{Bmatrix} F_0 \\ F_0 \angle +\phi_t \end{Bmatrix} \qquad (5.15) $$

where ϕ_t is the temporal phase angle which is equal to -90° with the spatial angle $\phi_s = \frac{360^\circ}{4n}$. In the general case, the following relation is applicable between ϕ_t and ϕ_s as shown in chapter 3:

$$n\,\phi_s - \phi_t = \pi \qquad (5.16)$$

Now, using equation (5.14) and assuming different numerical data for the model, the response can be calculated and the simulation criterion examined for different conditions such as mistuned systems, complex modes and general spatial phase angle.

5.5 NUMERICAL STUDY

Program DISC4 has been written for the analysis of the lumped mass system shown in figure 5.1. It is assumed that the system consists of 16 elements and all the masses and stiffness are the same unless they have been modified in the input data. This means that, for example, the mass, stiffness or damping loss factor of element i can be p% above or below its nominal value. In this way we can introduce any kind of mistuning or non-proportionality in the system.

The program first calculates the eigenvalues and eigenvectors of the system, then, in the case of repeated eigenvalues, obtains proper eigenvectors for such eigenvalues using the method mentioned in section 5.3. Finally, it calculates the response at all the coordinates for the desired mode, for a given spatial angle (between the two exciters) and at the given excitation frequency.

In another subroutine of the program, the multi-input sine dwell test method has been considered to isolate one mode. In this method mono-phase forces are applied at all

coordinates. Their amplitudes are selected such that a particular mode -but **only** that mode- will be excited. Using this method any mode can be isolated at the excitation frequency.

In the following section, seven particular cases of mistuned systems with different damping and forcing inputs are presented.

CASE **1 : Mistuned system with real modes**

In this case all the masses are equal to unity except those at coordinates 1, 5, 6 and 12 which are increased by 2%, 3%, 4% and 2.5% respectively. Also, the stiffness for all the springs is 1.E+4 (N/m) except for elements 3, 8 and 9 which are changed by +1%, +2% and +1% respectively. The damping loss factors for all elements are assumed to be 0.05. The first 7 eigenvalues and eigenvectors are shown in table 5.1. A rigid body mode has been found at 4.46 rad/s and the rest of the modes are nodal diameter modes which are in pairs with close natural frequencies. This table shows that although the modes are close, they are real modes since proportional damping has been assumed for the model.

The 2 ND modes are plotted in figure 5.2; they correspond to the eigenvalues λ_4 and λ_5. This figure shows that despite the mistuning in [M] and [K], the mode shapes are very close to sinusoidal forms.

To simulate the 2 ND travelling wave on the system, two excitations with a temporal phase angle of 90^o are located at coordinates 1 and 3. The angle between these two coordinates is 45^o for 16 elements around the disc. The total response due to this excitation at frequency equal to 76.3 rad/s (identical to the lower 2 ND natural frequency) is shown in figure 5.3 (c). The response to the different wave orders can be analysed as mentioned in section 3.8. Figure 5.3 (b) shows the contribution of the 2 ND mode

Table 5.1 Eigenvalues and eigenvectors for case study 1

$\lambda_1^2=$ 4.46^2 (1+.05 i)	$\lambda_2^2=$ 39.14^2 (1+.05 i)	$\lambda_3^2=$ 39.22^2 (1+.05 i)	$\lambda_4^2=$ 76.34^2 (1+.05 i)	$\lambda_5^2=$ 76.64^2 (1+.05 i)	$\lambda_6^2=$ 110.73^2 (1+.05i)	$\lambda_7^2=$ 111.16^2 (1+.05i)
0.250	0.029	0.353	0.353	-0.003	0.351	-0.064
0.250	-0.108	0.336	0.252	0.249	0.073	-0.343
0.250	-0.228	0.269	0.004	0.356	-0.294	-0.199
0.250	-0.314	0.161	-0.243	0.255	-0.301	0.187
0.250	-0.353	0.028	-0.352	0.004	0.061	0.346
0.250	-0.336	-0.109	-0.250	-0.249	0.346	0.066
0.250	-0.267	-0.229	0.003	-0.351	0.191	-0.299
0.250	-0.158	-0.315	0.254	-0.247	-0.198	-0.295
0.250	-0.027	-0.352	0.356	-0.004	-0.341	0.066
0.250	0.109	-0.336	0.254	0.244	-0.073	0.350
0.250	0.230	-0.269	0.004	0.352	0.288	0.205
0.250	0.316	-0.161	-0.249	0.253	0.296	-0.193
0.250	0.353	-0.029	-0.353	0.003	-0.067	-0.347
0.250	0.337	0.109	-0.252	-0.249	-0.348	-0.073
0.250	0 270	0.229	-0.005	-0.355	-0.203	0.291
0.250	0.162	0.315	0.245	-0.254	0.191	0.296

backward wave, which is the largest of the various orders in the total response. This is expected as the excitation is set for 2 ND modes. Figure 5.3 (a) represents the rest of the response when the contribution of the backward wave of 2 ND modes is removed. Note that when the wave travels in the direction of the excitation point 1 to the excitation point 2 it is a backward travelling wave. In contrast, if it travels from point 2 towards point 1, it is a forward travelling wave. This terminology is based on the earlier description of the simulation where the direction of disc rotation, Ω, was assumed to be in the opposite direction to θ. Therefore, a wave is a backward one if travels in the direction of θ.

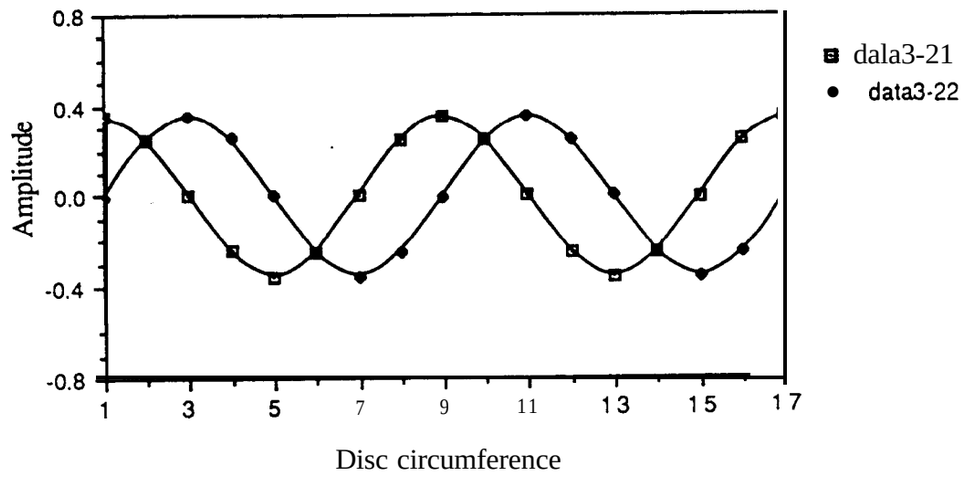

Figure 5.2 2ND modes of mistuned system; case study 1

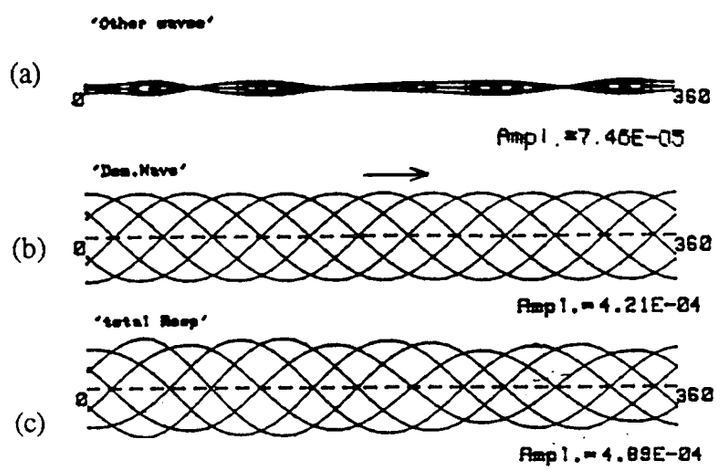

Figure 5.3 Response of the disc in case study 1

CASE 2: Mistuned disc with complex modes

Table 5.2 shows the first 7 eigenvalues and eigenvectors of the system with the same mass and stiffness data as in the previous case but with the damping loss factors at elements 3, 8 and 9 changed by -50%, +50% and -20% respectively. This variation in the damping loss factors results in non-proportional damping in the model and, consequently, the modes are complex as seen in table 5.2. The response to the two excitations is calculated for this system and the results are shown in figure 5.4. It is seen that the backward wave of 2 ND modes is dominant in the response as in the previous case, and that the modal complexity had no significant effect on the response to this excitation.

Table 5.2 Eigenvalues and eigenvectors for case study 2

$\lambda_1^2=$ 4.46^2 (1+.05 i)		$\lambda_2^2=$ 39.16^2 (1+.051i)		$\lambda_3^2=$ 39.2^2 (1+.047i)		$\lambda_4^2=$ 76.34^2 (1+.047i)		$\lambda_5^2=$ 76.64^2 (1+.051i)		$\lambda_6^2=$ 110.7^2 (1+.049i)		$\lambda_7^2=$ 111.1^2 (1+.049i)	
.250	0^o	.18	137.0^o	.36	7.6^o	.35	-2.0^o	.016	-113.9^o	.36	-2.1^o	.096	-129.3^o
.250	0^o	.27	159.4^o	.29	18.4^o	.24	-2.3^o	.26	-177.6^o	.11	$-44.^o$	.35	-177.4^o
.250	0^o	.35	171.0^o	.20	38.2^o	.013	-113.5^o	.35	-179.9^o	.30	-171.3^o	.22	163.4^o
.250	0^o	.37	179.4^o	.13	84.6^o	.25	-176.9^o	.25	$177.^o$	.31	172.8^o	.20	21.3^o
.250	0^o	.35	-172.4^o	.18	137.4^o	.35	-179.8^o	.017	71.1^o	.096	53.0^o	.35	-2.5^o
.250	0^o	.29	-161.7^o	.28	159.7^o	.24	177.4^o	.26	2.2^o	.35	2.8^o	.11	-49.5^o
.250	0^o	.19	-141.8^o	.35	171.1^o	.021	53.2^o	.35	$-.4^o$	.21	-17.9^o	.31	-171.7^o
.250	0^o	.13	-93.5^o	.37	179.5^o	.26	2.7^o	.24	-3.3^o	.21	-161.4^o	.31	170.8^o
.250	0^o	.18	-43.1^o	.36	-172.3^o	.35	$-.1^o$	.013	-118.3^o	.35	177.7^o	.095	48.9^o
.250	0^o	.28	-20.6^o	.29	-161.8^o	.25	-2.7^o	.25	-177.6^o	.11	135.3^o	.36	3.1^o
.250	0^o	.35	$-.9^o$	.2	-142.1^o	.016	-111.7^o	.35	-179.8^o	.29	8.7^o	.22	-15.8^o
.250	0^o	.38	$-.6^o$	.13	-95.0^o	.25	$-178.^o$	.25	177.9^o	.31	-8.2^o	.2	-161.4^o
.250	0^o	.36	7.6^o	.18	-43.0^o	.35	179.7^o	.016	63.9^o	.1	-129.7^o	.36	178.1^o
.250	0^o	.29	18.4^o	.28	-20.6^o	.24	177.5^o	.26	2.4^o	.35	-177.4^o	.11	136.9^o
.250	0^o	.20	38.0^o	.35	-9.1^o	.014	71.5^o	.36	$.1^o$	.22	163.0^o	.30	8.6^o
.250	0^o	.13	85.0^o	.38	$-.6^o$	.25	1.9^o	.25	-2.2^o	.20	19.1^o	.31	-7.4^o

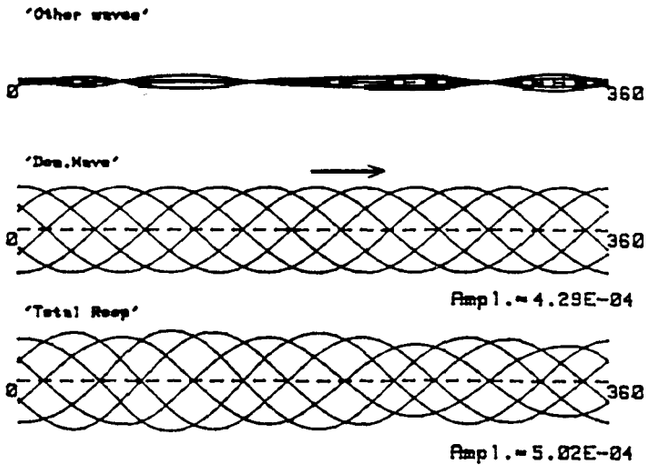

Figure 5.4 Response of the disc in case study 2

CASE 3 : Excitation at frequencies different from the natural frequency

According to theory, the response of the dual diametral modes to the excitation preset for the simulation of a travelling wave is a pure travelling wave if the disc is tuned. This is independent of the excitation frequency, whether it is equal to, below or above the natural frequency. However, in a mistuned case, the component of the travelling wave increases if the excitation frequency is away from the natural frequency, since at frequencies away from the natural frequencies, the effects of the two modes are almost the same. This argument is always true whether we consider just one set ND modes or more. But in the latter *case,* the other modes are also excited more or less depending on the excitation frequency.

In case study 3, excitation at a frequency away from the natural frequency is investigated. The same model as was used in case 1 is used again here and an excitation frequency of

80 rad/s is chosen which is higher than 2 ND natural frequencies of 76.34 and 76.64 rad/s. The response is shown in figure 5.5 and indicates a backward travelling wave of 2 ND modes.

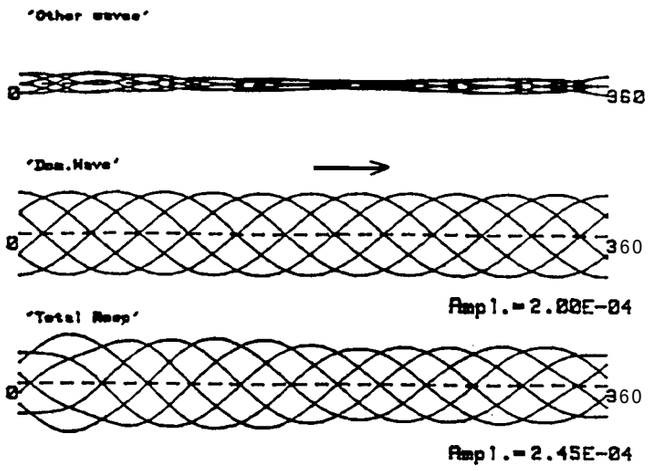

Figure 5.5 Response of the disc at 80 rad/s in case study 3

The investigation is continued further at an excitation frequency of 110 rad/s, which is very close to the 3 ND natural frequencies of 110.75 and 111.16 rad/s, while the two exciters are properly selected for excitation of the 2 ND modes. In *figure* **5.6** the response is shown in which the 3 ND modes are seen to be dominant. It is concluded that a mode cannot be isolated at a frequency equal to the natural frequency of another nodal diameter modes even if the excitation forces are set such as to excite that mode. As a result, the modes which are not easy to identify by their number of nodal diameters can be recognized by applying a different excitation pattern at the suspected natural frequency. By changing the excitation pattern, if it still responds to the previous modes, then this mode is the right one.

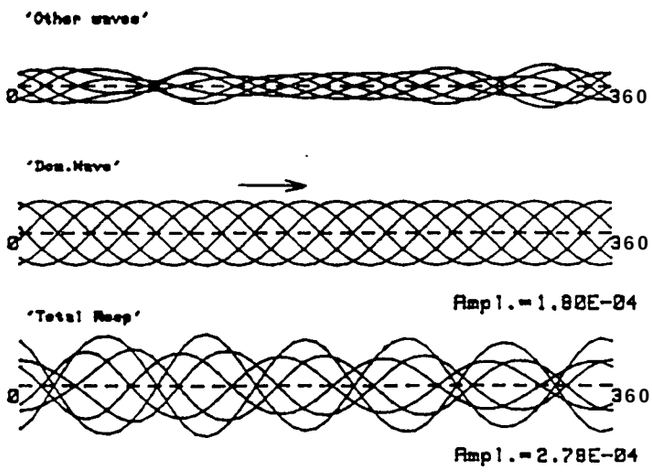

Figure 5.6 Response of the disc at 110 rad/s in case study **3**

CASE 4 The effects of frequency split and damping level on the response

In the excitation of n ND modes, the response approaches a backward travelling wave if the corresponding natural frequencies are close together and the level of damping is high enough. Figure 5.7 shows the response of the same system as discussed in figure **3.5** but with a damping loss factor of 0.005 instead of 0.05. It is seen that the total response is close to a fixed vibration (vibration of one mode), rather than a travelling wave.

The effects of damping level and the closeness of natural frequencies in the simulation are studied comprehensively below, in section 5.6.

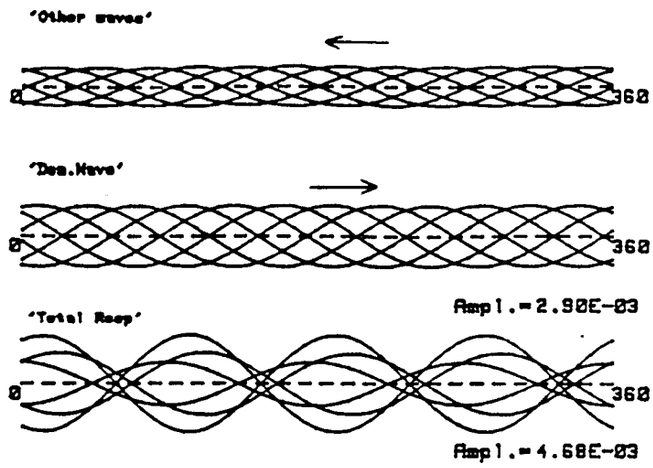

Figure 5.7 Response of the disc in case study 4

CASE 5 : Excitation with the forces at an arbitrary spatial phase angle

The same data as were applied in case 2 are considered here and the second excitation force is applied at point 4 so that $\phi_s=67.5^o$. By using the relation (5.16) for 2 ND modes, temporal phase angle ϕ_t would be required to be $+45^o$ in order to simulate the travelling wave of 2 ND mode. The response and its two components are shown in figure **5.8,** representing almost a backward travelling wave of 2 ND mode, the same as figures 5.3 and 5.4, when $\phi_s=45^o$. Hence, any applicable spatial angle can be used, subject to satisfying relation (5.16).

CASE 6 : Dependency of modes location on the mass distribution

A set of data is considered in which all the masses are the same except at point 3 where it is 5% more than the others. The mode shapes of the 2 ND modes are shown in figure 5.9. It is seen that the anti-node of the lower natural frequency mode coincides with point 3 while the node of the other mode is at this point. This is the same conclusion that has been mentioned in references [7]

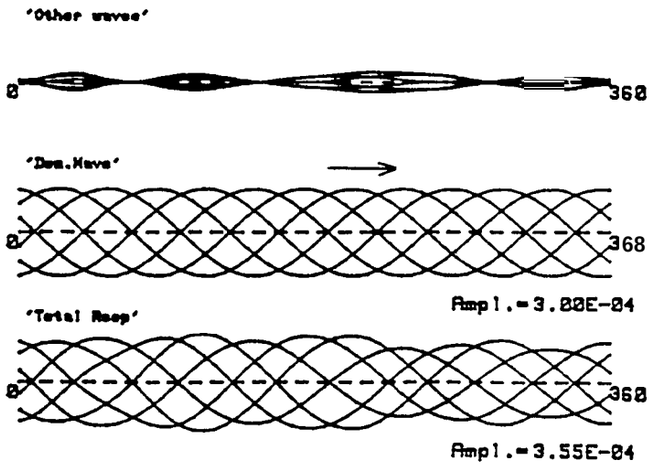

Figure 5.8 Response of the disc in case study 5

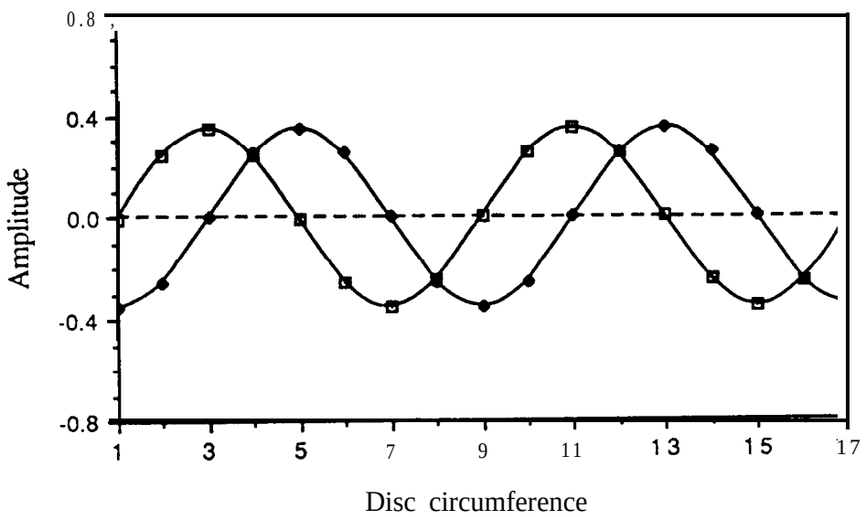

Figure 5.9 2 ND modes when there is concentrated mass at coordinate 3

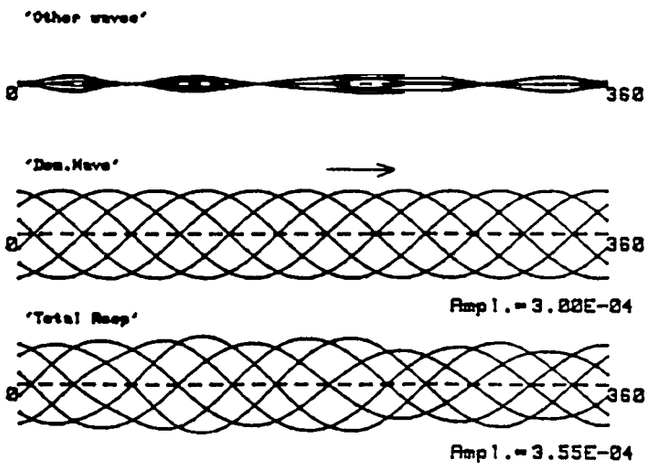

Figure 5.8 Response of the disc in case study 5

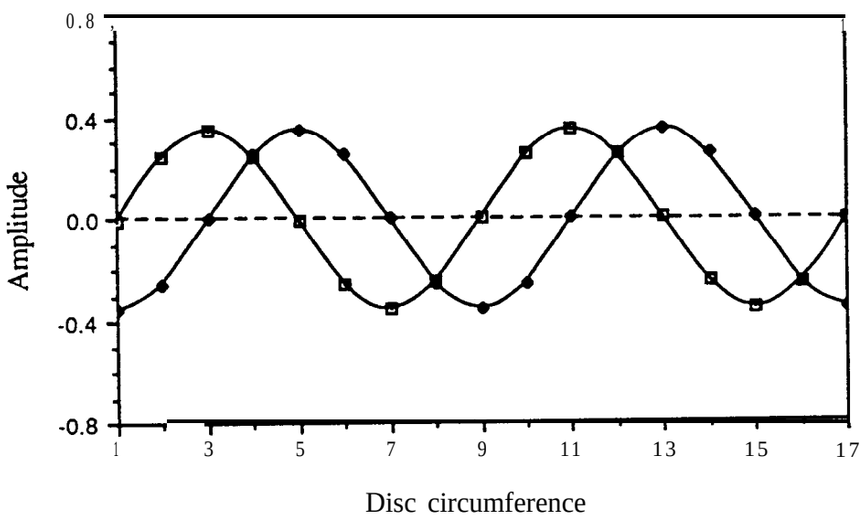

Figure 5.9 2 ND modes when there is concentrated mass at coordinate 3

and [19] and states that in mistuned axisymmetric systems, the modes are located such that the masses are effectively on the nodes of higher frequency mode and at the anti-nodes of the lower frequency mode. By referring to figure 5.2 and comparing with figure 5.9, it is seen that the position of the modes has been changed due to different mass distributions around the disc, although the same excitation positions were used for both simulations.

CASE 7 : Applying simulation using more than two excitations

As mentioned in section 3.6, it is feasible to apply more than two excitations in the simulation provided that they are located and synchronised with respect to the two original excitations. In this case, four excitations which are two identical pairs, are applied to the disc in a similar way to the case shown in figure 3.4 of chapter 3. The response of the system to the four excitations is shown in figure 5.10. Here, the same data as had been used in case 1 were applied, and so figure 5.10 is comparable with figure 5.3. In figure 5.10, the relative maximum amplitude of 'other waves' to the total response is 0.10 while for the two excitation case figure 5.3, it is 0.15.

These figures imply that by increasing the number of exciters there will be a significant reduction of the 'other waves' components in the response. In the other words, by using more excitation locations, the response approaches the response of the mode of interest and this is beneficial from a quality point of view.

Practically, the application of more than two excitations does not necessarily mean that the controlling procedure becomes more complex. This is because by choosing proper locations and similar temporal and spatial phase angles to the two set exciters for the required mode shape there is no need for extra controllers and more complex procedures.

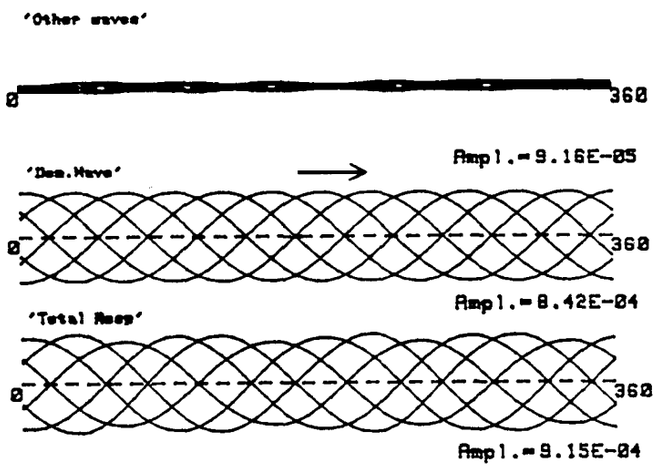

Figure 5.10 Response of the disc in case study 7; (4 excitations were used)

5.6 GENERAL STUDY ON THE EFFECTS OF THE NATURAL FREQUENCY SPLIT AND DAMPING FACTOR ON THE SIMULATION

In this section, the sensitivity of the simulation of a travelling wave response to the damping and also to the frequency splitting is investigated. In chapter 3, it has been explained that the travelling wave can be simulated in an axisymmetric structure by applying the special set of harmonic forces. The basis for establishing a travelling wave in a disc is the existence of dual modes. Here, it is intended to study the effect of natural frequency splitting and damping level on the simulation.

Eigenfunctions of a dual ND mode are assumed to be of the form:

$$\phi^{(1)}(\theta) = \cos n(\theta - \alpha)$$

$$\phi^{(2)}(\theta) = \sin n(\theta - cx)$$

The response x_3 at a point on the rim to the two harmonic excitations F_1 and F_2 can be expressed as:

$$x_3 = H_{31} F_1 + H_{32} F_2$$

In an analytical investigation, x_3 can be calculated since the receptances H_{31} and H_{32} are obtained using the general FRF formula:

$$H_{jk} = \sum_{r=1}^{\infty} \frac{{}_r\phi_j \, {}_r\phi_k}{\omega_r^2 - \omega^2 + i\eta_r \omega_r^2}$$

Responses at some other points, (say 15 points), can be calculated in the similar way. Then, the travelling wave component in the total response is estimated by using the technique mentioned in section 3.8.

Consider a disc with 2 ND modes for this analysis. Two harmonic exciters are applied on the disc with a spatial phase angle $\phi_s = 45°$, temporal phase $\phi_t = -90°$ and relative magnitudes equal to 1. The excitation frequency is assumed to be 95 Hz while the lower natural frequency is 100 Hz. Different frequency splits can be studied by considering different values for the second natural frequency. The effect of damping loss factor on the development of the travelling wave is also investigated. In each case, damping is assumed to be the same for both of the 2 ND mode.

To illustrate the results, a 3 dimensional diagram has been shown in figure 5.11. It can be seen that the travelling wave component increases with lower frequency spacing and with higher damping. The effect of the frequency spacing is more than the effect of damping in the low damping value range ($\eta < 0.2$). This range of damping covers most of the structures which are encountered in practice. Thus, the frequency splitting has a significant role in the formation of a travelling wave at a certain frequency.

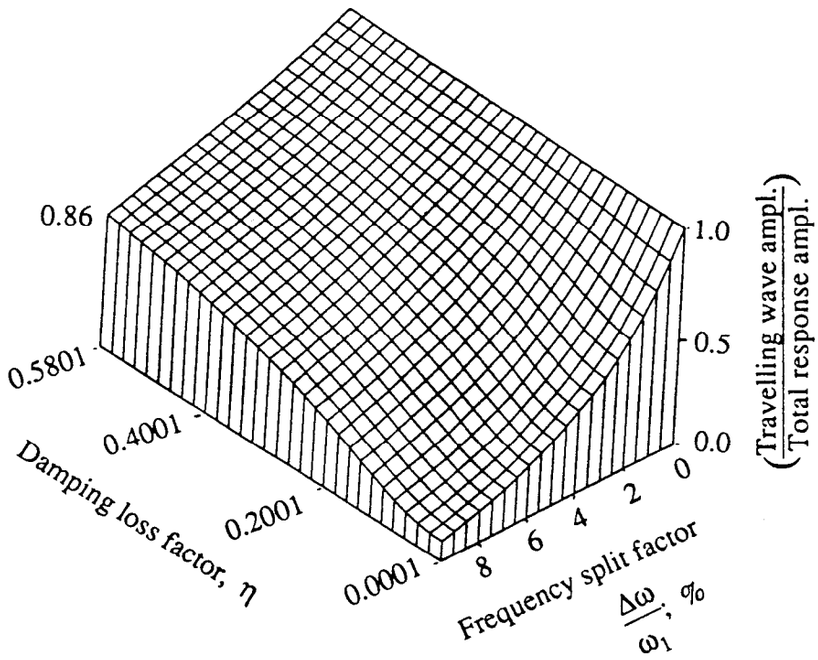

Figure 5.11 Travelling wave component vs nat. frequency split and damping

5.7 CONCLUDING REMARKS

In the analysis of the assumed lumped mass model of the disc the following conclusions can be drawn:

1- By introducing non-proportional damping to the model, complex modes are achieved and for this system and the considered case, the travelling wave can be simulated by using DCS exciters, similar to the system with real modes.

2- Various spatial phase angles for two excitation forces can be chosen, subject to the satisfying the relation of: n $\phi_s - \phi_t = \pi$.

3- Orientation of a ND mode shape depends on the distribution of the mass and stiffness in the mistuned disc. The point with a higher effective mass will coincide with an anti-node of the lower natural frequency mode while it will be on the nodal line of the higher natural frequency mode.

4- The response of an n ND mode to the two excitations (DCS exciters) is a travelling wave with order n. This is true for a tuned disc; however, in a mistuned disc, the contribution of the travelling wave to the total response at a certain excitation frequency will be decreased by increasing the natural frequency-splitting or by reducing the damping.

Chapter 6

VIBRATION INTERACTION OF A ROTATING DISC AND AN ADJACENT STATOR -

Part I Excitation applied to the disc

6.1 INTRODUCTION

It is well understood that at critical speeds as shown on the Campbell diagram, the n ND mode of a disc, or bladed disc, can be excited by n EO excitation and resonant vibration can occur leading to possible fatigue failure. Hence these critical speeds are avoided in the design and operation of the rotating discs. Kushner [15] has shown that even minor resonances can become significant if the critical points are to be avoided in the running speed ranges. These minor resonance points are determined by the difference between the number of blades in the disc and the number of vanes in the stator. Jay et al [17] also have shown that the difference between the number of blades and vanes defines the order of the forcing function and hence determines the order of the excited nodal diameter mode. There are several kinds of interaction between a rotating disc and the stator in which the number of vanes and blades are concerned. There is the possibility of vibration

interaction between a rotating disc and an adjacent stator in a gas or steam engine where vibration in one of the structures is transferred to the other one. In figure 6.1 two possibilities for vibration transmission between the rotating disc and the stator have been illustrated. Figure 6.1a) shows a typical seal between the stator and the rotating disc which is used, for example, to separate the gas passage and the adjacent section in the rotor disc construction. Supposing that the rotating disc is vibrating at nth EO-excitation, a dynamic force can be transmitted to the stator through the seal due to this vibration.

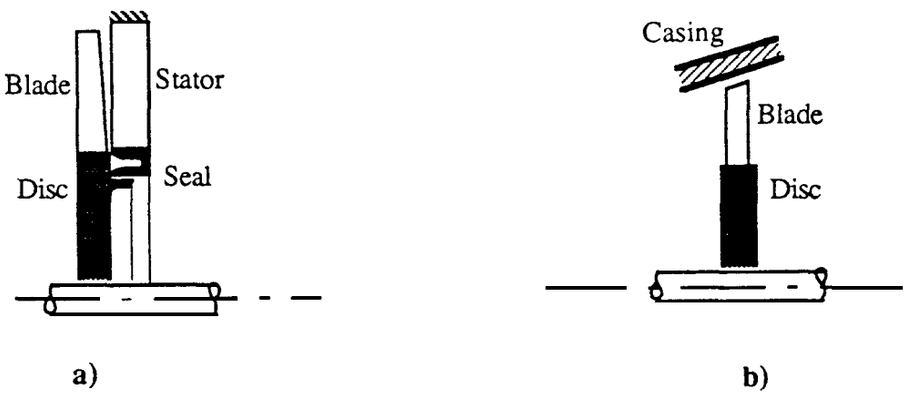

Figure 6.1 Two possible situations which could cause a vibration interaction between the rotating disc and the stator

Figure 6.1b) represents another configuration in which the surface of the casing (stator) of the engine is not parallel to its axis. When the disc vibrates, it is possible that the gap between the rotor and the stator changes with the same order as the excited ND mode in the disc. The pressure of the gas-flow is related to the thickness of the gap and as a result, the dynamic pressure on the stator causes vibration. Hence, there is a similar situation for the possibility of vibration interaction between the rotating disc and the stator.

In order to investigate the vibration interaction between a rotating disc and the stator, two distinct analyses are considered according to the source of the excitation. In this chapter,

it is assumed that the initial excitation is the n EO excitation on the disc and in the next chapter, the excitation is assumed to be exerted on the stator. In the both cases, it is assumed that the vibration is transmitted between the disc and the stator through a soft spring so that the displacement in one causes a proportional force on the other structure.

In this chapter, the response of a pair of ND modes of a rotating disc due to nth EO excitation is obtained, then the response of the stator due to the vibration interaction is determined. It will be explained in section 6.3 that the total analytical solution for the vibration interaction is not possible and we only obtain the part of the stator response due to the interaction.

6.2 RESPONSE OF THE ROTATING DISC TO nth ENGINE ORDER EXCITATION

One of the most significant sources of excitation of diametral modes in a rotating disc is engine order excitation. This kind of excitation can be expressed as $F_n(\theta_o,t)=F_o \cos n\theta_o$, which could be the effect of the static gas pressure behind n stationary vanes or nozzles to the rotating disc, (Remembering that θ_o is the stationary coordinate and θ is a coordinate rotating with disc). A static force applied to the rotating disc is also, in fact, an engine order excitation to which all the diametral modes are susceptible to resonance and not just, for example, n ND modes in the case of n EO excitation.

In the following section, the response of a pair of ND modes of the disc to nth EO excitation is obtained.

6.2.1 Analysis in terms of coordinates rotating with disc

Consider a rotating disc subjected to nth EO excitation, $F_n(\theta_o,t)=F_o \cos n\theta_o$. By substituting θ_o by $(\theta-\Omega t)$, and expanding, the forcing function in terms of coordinates rotating with the disc is obtained:

$$F_n(\theta,t) = F_o \sin n\theta \sin n\Omega t + F_o \cos n\theta \cos n\Omega t \qquad (6.1)$$

By setting the eigenfunctions of the two n ND modes as: $\Phi_{n1}=\sin n\theta$ and $\Phi_{n2}=\cos n\theta$, the generalized forces in these two modes can be calculated.

According to the definition, if $F_n(\theta,t)$ is a dynamic distributed force applied on a system, the generalized force formula for mode i of that system is :

$$Q_i = \int_0^{2\pi} (F(\theta,t)\ \phi_i(\theta)\ d\theta) \qquad (6.2)$$

Therefore, for the first n ND mode of the disc, the generalized force will be:

$$Q_{n1} = \int_0^{2\pi} F_o (\sin^2 n\theta \sin n\Omega t + \sin n\theta \cos n\theta \cos n\Omega t\, d\theta)$$

$$= F_o \int_0^{2x} \frac{1-\cos 2n\theta}{2} \sin n\Omega t\, d\theta + F_o \int_0^{2x} \frac{\sin 2 n\theta}{2} \cos n\Omega t\, d\theta$$

or :

$$Q_{n1} = \pi F_o \sin n\Omega t \qquad (6.3)$$

Similarly, for the other mode:

$$Q_{n2}(t) = F_o \int_0^{2\pi} (\sin n\theta . \cos n\theta \sin n\Omega t + \cos^2 n\theta \cos n\Omega t\, d\theta) \qquad (6.4)$$

or:

$$Q_{n2}(t) = \pi F_o \cos n\Omega t \qquad (6.5)$$

Having obtained the generalized forces, the generalized (or normal) responses are calculated by using the convolution integral, as used in chapter 2. If m_{n1} and ω_{n1} are the

$$q_{,}(t) = W_{21} \cos n\Omega t + W_{22} \cos \omega_{n2} t$$

where:
$$W_{21} = \frac{-\pi F_o}{m_{n2} (n^2\Omega^2 - \omega_{n2}^2)}$$

and
$$W_{22} = \frac{\pi F_o}{m_{n2} (n^2\Omega^2 - \omega_{n2}^2)}$$

and the steady-state solution will be deduced:

$$q_{,}(t) = W_{21} \cos n\Omega t \qquad (6.11)$$

Knowing the generalized coordinates for the n ND modes, the response is calculated using the mode-summation formula:

$$X_{dn}(\theta,t) = \sum_{i=1}^{2} \phi_{ni}(\theta)\, q_{ni}(t) \qquad (6.12)$$

Substituting from equations (6.10) and (6.11) into equation (6.12), the response of the rotating disc due to n EO excitation is obtained:

$$X_{dn}(\theta,t) = W_{11} \sin n\theta \sin n\Omega t + W_{21} \cos n\theta \cos n\Omega t \qquad (6.13)$$

6.2.2 Analysis in terms of stationary coordinates

Equation (6.13) represents the response of the rotating disc in terms of a coordinate rotating with it. However, from the stator point of view, the response of the disc should be obtained in terms of the stationary coordinate 8,. By assuming that rotation is in the opposite direction to 8, the relation between the rotating and a stationary coordinates is:

Equation (6.23) represents the steady-state response of the stator due to interaction with the disc subjected to EO excitation. Supposing that the stator is tuned, then the parameters A and P would be equal and hence:

$$X_{sn}(\theta_o,t) = \frac{A}{m_s\ \omega_s} \cos n(\theta_o + 2\Omega t)$$

which expresses a forward travelling wave with speed of '2Ω'.

Another result from this analysis is that the frequency of vibration in the stator is twice the vibration frequency in the disc. Also, it is deduced from equations (6.22) and (6.23) that for a system in which natural frequency of the n ND mode of the stator is equal to '$2n\Omega$', a resonance coincidence in the stator would occur as a consequence of the interaction.

6.4. NUMERICAL STUDY

The analysis has been used in a computer program to investigate different situations in the disc-stator interaction. The program 'IN_PLT' has been developed to simulate the interaction of n EO excitation of the disc and stator. In this program, different data for the disc and the stator are entered. The program calculates the response of the rotating disc in terms of coordinates rotating with the disc, $X_{dn}(\theta,t)$, and then the responses of the rotating disc and of the stator from the view point of a stationary observer, $X_{dn}(\theta_o,t)$ and $X_{sn}(\theta_o,t)$, are calculated. An animation display of the responses is shown on the computer screen and a hard copy of these displays can be obtained. In one time period ($T= 60./n\Omega$), the response is plotted at six time intervals successively. In the case of a travelling wave, different colours and/or numbering of the curves can help to indicate in which direction it is travelling. The direction of the travelling waves can also be shown by an arrow above the curves, similar to the cases shown in figures 6.4 to 6.10.

In figure 6.3, a frequency-speed diagram for the 3 ND modes of a disc and stator is shown. The natural frequencies of the 3 ND modes are assumed to be 100.0 and 101.0 Hz for the disc and 80.0 and 80.5 Hz for the stator. Also, it is assumed that the natural frequencies of the disc do not change with the speed of rotation. The generalised masses for the 3 ND modes of the disc are supposed to be m_{n1}=1.O and m_{n2}=1.1 kg and of the stator, m_{s1}=0.9 and m_{s2}=1.O kg. The various responses of the disc and the stator for the interface stiffness equal to K=1.E+6 (N/m) are calculated and examined at six rotational speeds shown in figure 6.3. The results will be discussed in the next section but the conditions for each case are as follows:

Ω_A : At this speed the lower natural frequency of the 3 ND modes of the stator coincides one of the resonant frequencies of a 3 ND mode of the rotating disc, that is: $\omega_{s1}=\omega_{n1}-3\Omega_A$. Hence Ω_A is equal to 400 rev/min and the responses for this speed are as shown in figure 6.4.

Ω_B : The interaction is examined at an ordinary speed Ω_B=500 rev/min for comparison of the results with other particular cases. Figure 6.5 illustrates the responses for this speed.

Ω_D : At this speed, the '3Ω' line (or 3 EO line) intersects one of the resonant frequency lines of the rotating disc. For this case $(\omega_{n1}-3\Omega_D)=3\Omega_D$ and hence Ω_D=1000 rev/min. In figure 6.6 the responses of the disc and the stator are illustrated when the rotation speed is at Ω_D.

Ω_E : It is worth examining the interaction at the rotating speed for which the excitation line (3 EO line) intersects one of the stator natural frequency lines. As an example of this case, consider Ω_E in figure 6.3 for which we can write $(3\Omega_E)=\omega_{s1}$ and hence, Ω_E=1610 rev/min. The responses for this speed are illustrated in figure 6.7.

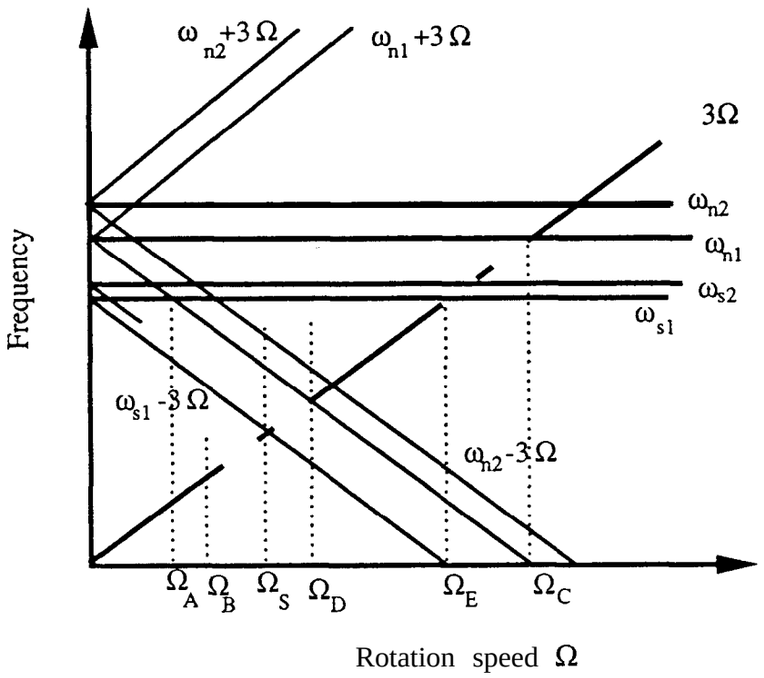

Figure 6.3 Natural frequencies and the rotation speeds studied in the vibration interaction between the disc and the stator

Ω_S: In the analysis, it has been realized that at a certain rotating speed the stator will be at resonance . That speed is given by $\Omega_S = \frac{\omega_s}{2n}$. At one of these speeds Ω_S=800 rev/min , the interaction has been examined and corresponding responses are shown in figure 6.8.

Ω_C : Let us consider one of the critical speeds. Theoretically, at the critical speed of n EO excitation, the response of the disc is very high and in an undamped case goes to infinity. In order to make calculation feasible at speeds such as Ω_C, the denominator of the amplitudes in equations (6.13) and (6.15) is assumed to be a small value rather than zero.

At this critical speed, $\omega_{d1} - n\Omega_C = 0$ and with the assumption of ω_{d1}=100 Hz, then Ω_C becomes 2000 rev/min. The results of these data are shown in figure 6.9.

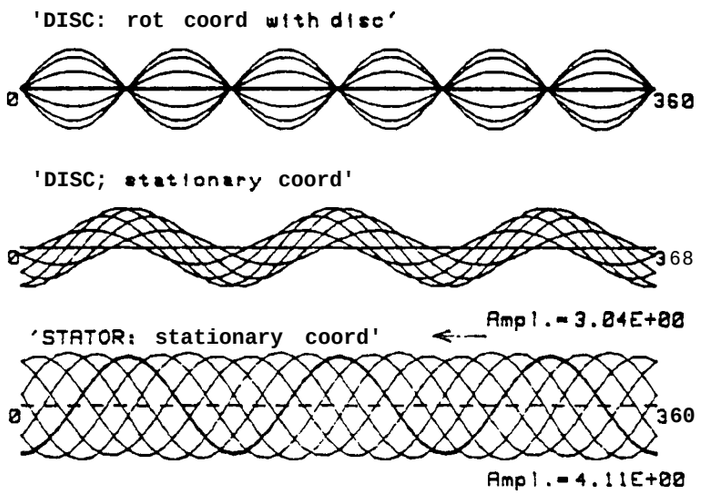

Figure 6.9 Responses at Ω_C=2000 rev/min.

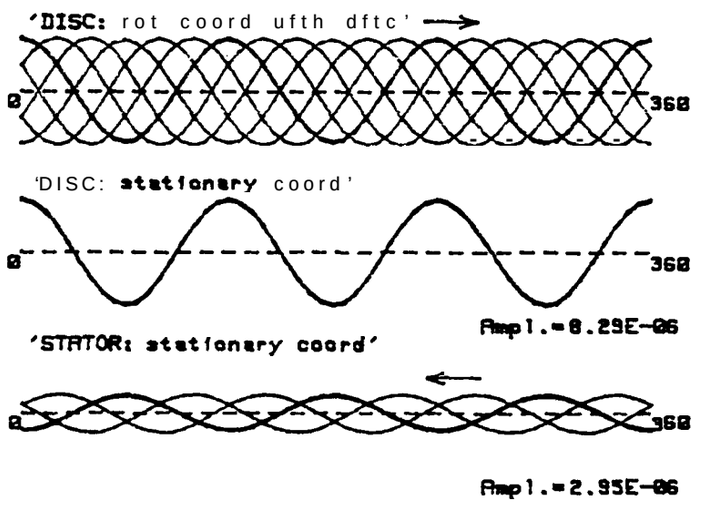

Figure 6.10 Responses at 400 rev/min.and with reduction of the detuning in the disc

this figure. The responses for different cases are presented in figures 6.4 to 6.10. In each figure, two upper families of curves represent the disc responses in terms both of stationary coordinates and of coordinates rotating with the disc. The lowest family of curves illustrates the response of the stator. In almost all figures, the response of the disc to 3 EO excitation is very close to a backward travelling wave in the rotating coordinate or a 'standing wave' in the stationary coordinate. Since the disc has been assumed to be mistuned, it is not a pure standing wave but a standing wave oscillating in its position as shown, for example, in figure 6.7. In fact, this slight deviation from a pure standing wave is responsible inducing vibration to the stator.

The response of the stator is almost a forward travelling wave with a speed twice that of the travelling wave on the disc. At Ω_A=400 rev/min and Ω_B=500 rev/min there is no resonance coincidence, (figures 6.4 and 6.5). Also, resonance does not occur either when the 3 EO line intersects the disc resonance frequency line, (ω_{d1}-3Ω), (that is at Ω_D=1000 rev/mitt), or at the speed of Ω_E=1610 rev/min where the 3 EO line intersects the stator natural frequency line. However, the level of response is higher than in figures 6.4 and 6.5 as these speeds are closer to a critical speed. In figure 6.9, the response at one of the critical speeds of the disc has been illustrated. The level of response indicates that the resonances coincide . In this figure, the response of the disc in terms of coordinates rotating with the disc is a fixed vibration which means one of the pair of 3 ND modes of the disc dominates in the response due to the detuning assumption made for the disc.

At Ω_S=800 rev/min, where the 3 EO line intersects the (ω_{s1}-3Ω) line the coincidence of resonance occurs in the stator as seen in figure 6.8. This speed is equal to $\Omega=\frac{\omega_s}{2n}$ in general, which has been obtained in the analysis and is introduced as a minor resonance in the vibration interaction between a rotating disc and an adjacent stator.

Another point examined in the analysis is the effect of detuning on the interaction. Figure 6.10 shows the responses for the case in which the modal masses of 3 ND mode of the disc are closer than in the case whose responses are illustrated in figure 6.4. Due to the

lower detuning, a reduction in the level of vibration in the stator is observed and, as mentioned before, because of this effect, no vibration will be induced to the stator in the case of a perfectly tuned disc.

6.6 CONCLUSIONS

The vibration interaction between a stator and a disc subjected to n EO excitation has been investigated. In general, a forward travelling wave with a speed of '2Ω' and effective vibration frequency equal to '$2n\Omega$' exists in the response of the stator. There is a resonance coincidence for the stator when the natural frequency of the structure is equal to '$2n\Omega$'; in other words, in the interaction a critical speed for the stator is equal to $(\frac{\omega_s}{2n})$. This point can be seen in the frequency - speed diagram where the assumed '$\omega_s - n\Omega$' line intersects the excitation line(n EO).

The response of the disc is almost a standing wave from the viewpoint of a stationary observer, such as the stator. It is the slight deviation from a pure standing wave which excites a travelling wave response in the stator. However, for a tuned rotating disc the response to the n EO excitation is an exact ‘standing wave’ so that it could not introduce any vibration to the stator.

Chapter 7

VIBRATION INTERACTION BETWEEN A ROTATING DISC AND AN ADJACENT STATOR- Part II: The excitation applied to the stator

7.1 INTRODUCTION

In chapter 6, the first part of an analysis of the vibration interaction between a rotating disc and the adjacent stator was reported in which the excitation was a static stationary force applied on the disc. Another possibility for vibration interaction is when the stator vibrates due to a harmonic force and the movement of the stator transfers to the rotor and makes the rotor vibrate. This kind of excitation is quite possible in practice since there are different accessory devices and equipment mounted on the stator or nearby, such as an oil pump, which could generate a harmonic excitation in the stator.

In this chapter, the response of a stator due to a harmonic excitation is investigated and its interaction with an adjacent rotor is examined. The steady-state responses have been calculated in both a stationary coordinate system and in terms of coordinates rotating with

disc. A computer program has been developed to display and plot the responses of the disc and stator in order to examine the interaction .

Analysis is started by assuming a harmonic force applied to a stator as shown schematically in figure 7.1. The vibration of the stator can be transferred to the adjacent rotating disc through the seal as described in section 6.1. In the following, an analysis is carried out for one pair of modes of the nodal diameter family to examine the vibration interaction between the stator and rotor.

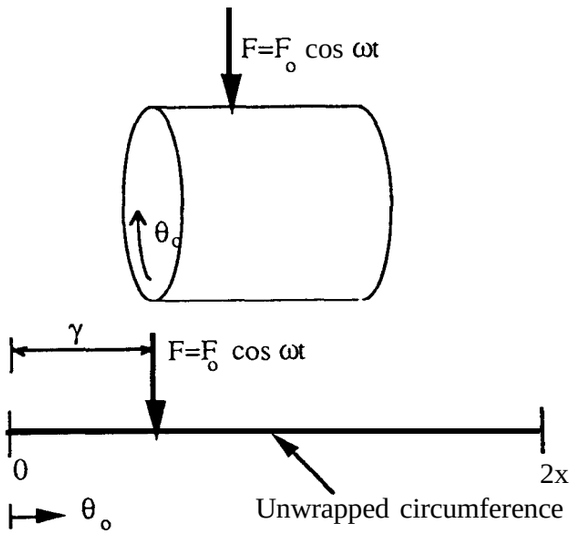

Figure 7.1 Schematic diagram of the stator and applied force

7.2 RESPONSE OF THE STATOR

In order to analyse the response of a stator to a harmonic excitation, it is assumed that the eigenfunctions of the n ND modes are:

$$\left.\begin{aligned}\phi_{S1} &= \sin n\theta_o \\ \phi_{s2} &= \cos n\theta_o\end{aligned}\right\} \qquad (7.1)$$

In fact these equations represent the n ND mode shapes on a circle of the stator and in the interface area with the adjacent rotating disc The excitation point may not coincide with a nodal diameter and the spatial angle between the excitation point and the adjacent nodal point is assumed to be γ; figure 7.1. By these assumptions, the forcing function will be $(F_o \cos \omega t)\,\delta[\theta_o-\gamma]$ and the generalised forces can be obtained as follows:

$$Q_{s1}(t) = \int_0^{2\pi} F_o(\cos \omega t)\delta[\theta_o-\gamma] \sin n\theta_o \, d\theta_o \qquad (7.2)$$

$$Q_{s2}(t) = \int_0^{2\pi} F_o(\cos \omega t)\delta[\theta_o-\gamma] \cos n\theta_o \, d\theta_o \qquad (7.3)$$

or :

$$\left.\begin{aligned}Q_{s1}(t) &= F_o \sin ny \cos \omega t \\ Q_{s1}(t) &= F_o \cos ny \cos \omega t\end{aligned}\right\} \qquad (7.4)$$

Now, the modal responses are calculated by using the convolution integral .

$$\left.\begin{aligned}q_{,,}(t) &= \frac{1}{m_{s1}\omega_{s1}} \int_0^t (F_0 \sin ny \cos \omega\tau) \sin \omega_{s1}(t-\tau)\, d\tau \\ q_{s2}(t) &= \frac{1}{m_{s2}\omega_{s2}} \int_0^t (F_0 \cos ny \cos \omega\tau) \sin \omega_{s2}(t-\tau)\, d\tau\end{aligned}\right\} \qquad (7.5)$$

After integration and considering the steady-state terms only, will give:

$$\left.\begin{aligned} q_{s1}(t) &= -\left[\frac{F_o \sin n\gamma}{m_{s1}(\omega^2 - \omega_{s1}^2)}\right] \cos \omega t \\ q_{s2}(t) &= -\left[\frac{F_o \cos n\gamma}{m_{s2}(\omega^2 - \omega_{s2}^2)}\right] \sin \omega t \end{aligned}\right\} \qquad (7.6)$$

The response of the stator is obtained by using the mode-summation formula:

$$X_{sn}(\theta_o,t) = q_{s1}(t)\,\phi_{s1}(\theta) + q_{s2}(t)\,\phi_{s2}(\theta_o) \qquad (7.7)$$

or:

$$X_{sn}(\theta_o,t) = -A_1 \cos \omega t \sin n\theta_o - A_2 \cos \omega t \cos n\theta_o \qquad (7.8)$$

where:

$$\left.\begin{aligned} A_1 &= \frac{F_o \sin n\gamma}{m_{s1}[\omega^2 - \omega_{s1}^2]} \\ A_2 &= \frac{F_o \cos n\gamma}{m_{s2}(\omega^2 - \omega_{s2}^2)} \end{aligned}\right\} \qquad (7.9)$$

Equation (7.8) can be written in another form:

$$X_{sn}(\theta_o,t) = -A, \cos \omega t \sin n(\theta_o - a) \qquad (7.10)$$

where $A_s = +\sqrt{A_1^2 + A_2^2}$ and $\alpha = \text{atan}(-\frac{A_2}{A_1})$

which represents the response of the stator to the harmonic force and it is seen to represent a 'fixed vibration'. Since at a certain value of θ_o, the response is zero and these points are time independent (nodal points) which implies to a fixed vibration.

7.3. RESPONSE OF THE ROTATING DISC

The excitation of the *n* ND modes on the stator can be transferred to the disc through the seal and generate a distributed dynamic force on the disc. The interface force is assumed to be proportional to the difference of the disc and stator displacements. The block diagram of the vibration interaction has been illustrated in figure 7.2. Similar to part I (chapter 6), this system has no complete analytical solution but it is possible to analyse some parts of the response by assuming that

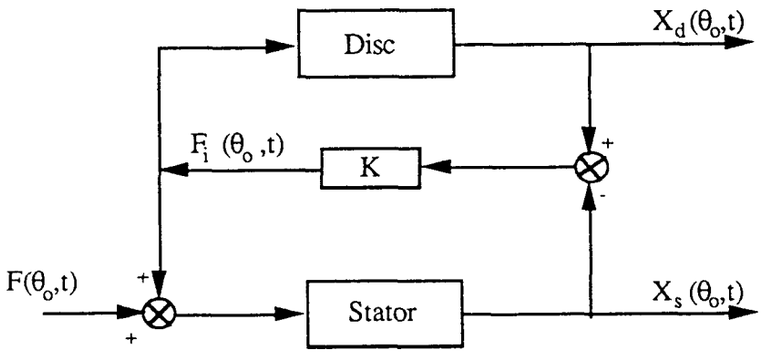

Figure 7.2 Block diagram for vibration interaction when the excitation force applied to the stator

the system is linear. For the stator, the response to the force $F(\theta_o,t) = F_o \cos \omega t$ has already been obtained and for disc, the response to $F_{i1}(\theta_o,t) = K X_{sn}(\theta_o,t)$ is analysed. These disc and stator responses are a part of the total response due to the vibration interaction.

Substituting from equation (7.10) gives:

$$F_{i1}(\theta_o,t) = -K A, \cos \omega t \sin n(\theta_o - \alpha) \qquad (7.11)$$

This is the equation of the dynamic force induced on the rotating disc by the vibrating stator.

7.3.1 The generalised forces

The rotating disc with the applied stationary dynamic force is shown schematically in figure 7.3. Coordinate θ is rotating with the disc which spins with an angular speed of Ω in the opposite direction to θ_o. The dynamic load (F_{i1}) is stationary in space as presented in equation (7.11). The analysis is carried out in terms of the rotating coordinate θ. Thus, the forcing function relative to

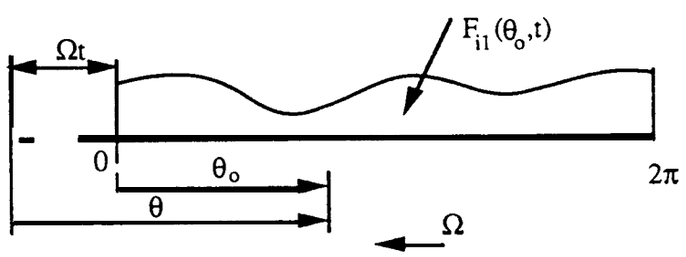

Figure 7.3 Schematic of the rotating disc and the dynamic force on it

the coordinate on the rotating disc is obtained by substituting θ_o with $(0 - \Omega t)$ in equation (7.11):

$$f_d(\theta,t) = - K A, \cos \omega t \sin n(\theta - \Omega t - a) \qquad (7.12)$$

In the general case we consider the m ND modes of the disc and later we will see that m has to be equal to n, the number of nodal diameters in the mode considered in the stator. The eigenfunctions of the m ND modes of the disc are assumed to be:

$$\phi_{m1} = \sin m\theta \quad \text{and} \quad \phi_{m2} = \cos m\theta \tag{7.13}$$

Now, the generalized forces can be obtained:

$$Q_{d1}(t) = \int_0^{2\pi} [-K\ A,\ \cos \omega t\ \sin n(\theta - \Omega t - \alpha)]\ \sin m\theta\, d\theta$$

It can be shown that this integral has a non-trivial solution only when m=n. Setting m=n and after simplification, we find:

$$Q_{d1}(t) = -\pi\ K\ A,\ \cos \omega t\ \cos n(\Omega t + a) \tag{7.14}$$

Similarly, for the other mode:

$$Q_{d2}(t) = +\pi\ K\ A,\ \cos \omega t\ \sin n(\Omega t + a) \tag{7.15}$$

7.3.2 Analysis of the response in terms of coordinates rotating with disc

Using equations (7.14) , (7.15) and the convolution integral, the modal responses are obtained:

$$q_{d1}(t) = \frac{1}{m_{d1}\,\omega_{d1}} \int_0^t [-\pi K A_s \cos \omega\tau \cos n(\Omega\tau + \alpha) \sin \omega_{d1}(t-\tau)]\, d\tau$$

and

$$q_{d2}(t) = \frac{1}{m_{d2}\,\omega_{d2}} \int_0^t [+\pi K A_s \cos \omega\tau \sin n(\Omega\tau + \alpha) \sin \omega_{d2}(t-\tau)]\, d\tau$$

After integration and considering the steady-state terms, this gives:

$$\left.\begin{aligned} q_{d1}(t) &= W_{11} \cos[(\omega + n\Omega)t + n\alpha] + W_{12} \cos[(\omega - n\Omega)t + n\alpha] \\ \text{and} \quad q_{d2}(t) &= -W_{21} \sin[(\omega + n\Omega)t + n\alpha] + W_{22} \sin[(\omega - n\Omega)t + n\alpha] \end{aligned}\right\} \tag{7.16}$$

where :

$$W_{11} = \frac{+\pi K A_s}{2m_{d1}[(\omega+n\Omega)^2 - \omega_{d1}^2]} \quad , \quad W_{12} = \frac{+\pi K A_s}{2m_{d1}[(\omega-n\Omega)^2 - \omega_{d1}^2]}$$

$$W_{21} = \frac{+\pi K A_s}{2m_{d2}[(\omega+n\Omega)^2 - \omega_{d2}^2]} \quad , \quad W_{22} = \frac{+\pi K A_s}{2m_{d2}[(\omega-n\Omega)^2 - \omega_{d2}^2]}$$

(7.17)

Using the mode-summation formula , the response of the disc is derived:

$$X_{dn}(\theta,t) = q_{d1}(t)\,\phi_{d1}(\theta) + q_{d2}(t)\,\phi_{d2}(\theta)$$

Substituting from equations (7.13) and (7.16) gives:

$$X_{dn}(\theta,t) = W_{11}\cos[(\omega+n\Omega)t+n\alpha]\sin n\theta + W_{12}\cos[(\omega-n\Omega)t+n\alpha]\sin n\theta$$

$$-W_{21}\sin[(\omega+n\Omega)t+n\alpha]\cos n\theta + W_{22}\sin[(\omega-n\Omega)t+n\alpha]\cos n\theta \qquad (7.18)$$

Equation (7.18) represents the response of the rotating disc expressed in terms of the coordinate rotating with the disc. This equation can be presented in two parts to show the backward and the forward travelling wave components:

$$X_{dn}(\theta,t) = X_b(\theta,t) + X_f(\theta,t)$$

where:

$$X_b(\theta,t) = W_{11}\sin[n\theta-(\omega+n\Omega)t-n\alpha] + (W_{11}-W_{21})\sin[(\omega+n\Omega)t+n\alpha]\cos n\theta$$

and $$X_f(\theta,t) = W_{22}\sin[n\theta+(\omega-n\Omega)t-n\alpha] + (W_{12}-W_{22})\cos[(\omega-n\Omega)t+n\alpha]\sin n\theta$$

(7.19)

Recalling equations (7.17), it is concluded that resonances will occur if $\omega \pm n\Omega = \omega_{d1}$ and/or $\omega \pm n\Omega = \omega_{d2}$. This means that at the following excitation frequencies, a resonance coincidence happens :

$$W_{11} = \frac{+\pi K A_s}{2m_{d1}[(\omega+n\Omega)^2 - \omega_{d1}^2]} \quad , \quad W_{12} = \frac{+\pi K A_s}{2m_{d1}[(\omega-n\Omega)^2 - \omega_{d1}^2]}$$

$$W_{21} = \frac{+\pi K A_s}{2m_{d2}[(\omega+n\Omega)^2 - \omega_{d2}^2]} \quad , \quad W_{22} = \frac{+\pi K A_s}{2m_{d2}[(\omega-n\Omega)^2 - \omega_{d2}^2]}$$

(7.17)

Using the mode-summation formula , the response of the disc is derived:

$$X_{dn}(\theta,t) = q_{d1}(t)\,\phi_{d1}(\theta) + q_{d2}(t)\,\phi_{d2}(\theta)$$

Substituting from equations (7.13) and (7.16) gives:

$$X_{dn}(\theta,t) = W_{11}\cos[(\omega+n\Omega)t+n\alpha]\sin n\theta + W_{12}\cos[(\omega-n\Omega)t+n\alpha]\sin n\theta$$

$$-W_{21}\sin[(\omega+n\Omega)t+n\alpha]\cos n\theta + W_{22}\sin[(\omega-n\Omega)t+n\alpha]\cos n\theta \qquad (7.18)$$

Equation (7.18) represents the response of the rotating disc expressed in terms of the coordinate rotating with the disc. This equation can be presented in two parts to show the backward and the forward travelling wave components:

$$X_{dn}(\theta,t) = X_b(\theta,t) + X_f(\theta,t)$$

where:

$$X_b(\theta,t) = W_{11}\sin[n\theta-(\omega+n\Omega)t-n\alpha] + (W_{11}-W_{21})\sin[(\omega+n\Omega)t+n\alpha]\cos n\theta$$

and $$X_f(\theta,t) = W_{22}\sin[n\theta+(\omega-n\Omega)t-n\alpha] + (W_{12}-W_{22})\cos[(\omega-n\Omega)t+n\alpha]\sin n\theta$$

(7.19)

Recalling equations (7.17), it is concluded that resonances will occur if $\omega \pm n\Omega = \omega_{d1}$ and/or $\omega \pm n\Omega = \omega_{d2}$. This means that at the following excitation frequencies, a resonance coincidence happens:

$$\omega=\omega_{d1}\pm n\Omega \quad \text{and} \quad \omega=\omega_{d2}\pm n\Omega \tag{7.20}$$

Each of these frequencies is called a 'resonance frequency' of the n ND mode in the rotating disc.

7.3.3 Response of the rotating disc in terms of stationary coordinates

An expression for the response in terms of the stationary coordinate θ_o, is obtained by replacing 'θ' by '$\theta_o+\Omega t$' in the equation (7.18).

$$X_{dn}(\theta_o,t) = W_{11}\cos[\omega+n\Omega)t+n\alpha]\sin n(\theta_o+\Omega t)+W_{12}\cos[\omega-n\Omega)t+n\alpha]\sin n(\theta_o+\Omega t)$$

$$-W_{21}\sin[\omega+n\Omega)t+n\alpha]\cos n(\theta_o+\Omega t)+W_{22}\sin[\omega-n\Omega)t+n\alpha]\cos n(\theta_o+\Omega t)$$

After rearranging the terms of this equation, we obtain:

$$X_{dn}(\theta_o,t) = 0.5(W_{11}+W_{21})\sin[n\theta_o-\omega t-n\alpha]+0.5(W_{12}-W_{22})\sin[n\theta_o-(\omega-2n\Omega)t-n\alpha]$$

$$+ 0.5(W_{12}+W_{22})\sin[n\theta_o+\omega t+n\alpha]-0.5(W_{21}-W_{11})\sin[n\theta_o+(\omega+2n\Omega)t+n\alpha] \tag{7.21}$$

Equation (7.21) represents the response of the disc in terms of the stationary coordinate. It shows that the response consists of four travelling waves; two backward and two forward waves. Comparing equation (7.21) with equation (7.18), we see that although the response frequencies are different in the two coordinates, the resonance frequencies are the same and are as presented in equation (7.20).

Equation (7.21) can be separated into the two parts; backward and forward travelling waves ;

$$X_{dn}(\theta_o,t) = X_b(\theta_o,t) + X_f(\theta_o,t)$$

where $X_b(\theta_o,t) = 0.5(W_{11}+W_{21})\sin[n\theta_o-\omega t-n\alpha]$

$$+0.5(W_{12}-W_{22})\sin[n\theta_o-(\omega-2n\Omega)t-n\alpha]$$

and $X_f(\theta_o,t) = 0.5(W_{12}+W_{22})\sin[n\theta_o+\omega t+n\alpha]$

$$-0.5(W_{21}-W_{11})\sin[n\theta_o+(\omega+2n\Omega)t+n\alpha]$$

For the special case where the disc is tuned, $m_{d1}=m_{d2}$ and $\omega_{d1}=\omega_{d2}$, it is deduced from equation (7.17) that $W_{12}=W_{22}$ and $W_{11}=W_{21}$ and therefore:

$$\left.\begin{aligned} X_b(\theta_o,t) &= W_{11}\sin[n\theta_o-\omega t-na] \\ \text{and} \quad X_f(\theta_o,t) &= W_{22}\sin[n\theta_o+\omega t+n\alpha] \end{aligned}\right\} \quad (7.22)$$

which are single backward and forward travelling waves. Although equation (7.22) represents the response components for a tuned disc, it can also be used to estimate the components of the response for a mistuned disc if the excitation frequency is far enough from the resonance frequencies.

From equation (7.22) we can deduce that when $\omega=0$ (i.e. a static force excitation which, here, has physically no sense), the response of the disc is:

$$X_{dn}(\theta_o,t) = (2W\cos na)\sin n\theta_o$$

which represents a ‘standing wave’ and it is expected from the excitation of a rotating disc with a static force.

7.4 NUMERICAL STUDY

The results obtained in the previous sections can be used in a computer program to investigate different situations in the disc-stator interaction process. A program 'IN_PLTD' has been developed to simulate the vibration interaction of the stator with the disc when a harmonic force excites the stator. In this program, different data for the disc and the stator are entered and the responses of the stator and the disc are calculated. Different excitation frequencies and rotating speeds are examined on two assumed systems. The two systems are similar and consist of a disc and stator with 3 ND modes. The modal parameters used for system I are shown in table 7.1. The only difference between the two systems is the second natural frequency of the disc, which is assumed to be 202.0 Hz in system II, compared with 200.5 Hz in system I. The interface stiffness is assumed K=1.E+6 (N/m) in all cases.

Table 7.1 Modal data for 3 ND modes (systems I and II)

	Generalized masses, [kg]		Natural frequencies, [Hz]	
	System I	System II	System I	System II
DISC	1.00, 1.02	1.00, 1.02	200.0, 200.5	200.0, 202.0
STATOR	1.20, 1.30	1.20, 1.30	150.0, 152.0	150.0, 152.0

Different cases which have been considered for System I are summarized in table 7.2. For system II, only one case has been considered and the other situations are similar to the cases in system I hence they are not considered.

Table 7.2 Different cases considered for system I

Case symbol	A	B	C	D	E	F	G	H
Excitation frequency, Hz	100	150	152	152	150	152	200	152
Rotation speed rev/min	1000	1000	960	970	1010	1000	1000	2500
Relevant figure No.	7.4	7.5 & 7.6	7.7	7.8	7.9	7.10	7.11	7.12

The disc response is obtained in terms of the stationary coordinates and also in terms of the coordinate rotating with the disc and the results are illustrated in figures 7.4 to 7.13 for the different cases. In each figure the maximum amplitudes obtained in the analysis are written at the bottom of the curves. The general format and idea behind this style of presentation has been explained in previous chapters and the only difference here is that there are different components with different frequencies for the response of the disc in the stationary coordinate. In displaying a disc response which consists of more than one frequency component, it is usually impractical to select a period to cover all the components' periods. The display will be more representative of the response if the longer period (corresponding to the lower frequency) is used. However, if the amplitude of the lower frequency term is much less than the amplitude of the higher frequency term, we would present the response in the basis of the period of the higher frequency component.

Following the above considerations, nine cases studied and the results have been displayed in figures 7.4 to 7.13 and are discussed in the next section.

7.5 RESULTS AND DISCUSSION

The possibility of vibration interaction in a stator-disc system with a harmonic excitation on the stator has been studied. The response of the stator has been presented in equations (7.8) and (7.10). It is seen that the stator response is a 'fixed vibration' and there are no travelling waves since the excitation is simply one harmonic stationary force. The position of the exciter on the stator has been shown by an arrow, in figures 7.4 to 7.13. In all the

case studies, the spatial position for the exciter has been assumed to be $\gamma=10^{o}$ which has been illustrated in the schematic responses of the stator, figure 7.1. In those cases where the excitation frequency coincides with one of the natural frequencies of the stator (e.g. in figures 7.5 and 7.7), the response is exactly the same mode shape assumed earlier in the analysis , i.e.a 'sin 3θ' or a 'cos 3θ' shape. But at the other excitation frequencies, both 3 ND modes have effective influence in the response of the stator and hence, the response is a $\sin(3\Omega+\alpha_1)$ or a $\cos(3\Omega+\alpha_2)$ shape, e.g. in figures 7.4 and 7.11.

Equation (7.11) represents the forcing function applied to the disc which is due to the interaction with the vibration in the stator. The rotating disc response to this excitation has been presented in equation (7.18) and also in the two separate parts in equation (7.19). This response has been calculated in terms of the coordinate rotating with the disc. The disc response has also been obtained in terms of the stationary coordinate and presented in equation (7.21). The general conclusion is that when the excitation frequency coincides with the disc resonance frequencies, $\omega=\omega_d\pm n\Omega$, a resonance coincidence will occur.

Different cases studied have been summarised in table 7.2; moreover, a special case of system II has also been examined where at one rotating speed there are two possible resonances. All the responses for different cases have been shown in figures 7.4 to 7.13 and are discussed respectively. In figure 7.4 the responses at ω= 100 Hz and Ω=1000 rev/min are shown. In this case, the excitation frequency is below the natural frequency of the stator (150 Hz) and also is different from the resonant frequency of the rotating disc. The response of the stator is a 'fixed vibration' while for the disc it is a travelling wave with varying amplitude.

The responses for the excitation frequency equal to 150 Hz and at the speed of Ω=1000 rev/min are shown in figure 7.5. This excitation frequency is equal to the natural frequency of the stator and, also, for the assumed speed it coincides with the resonant frequency of the disc. It is seen that here resonance occurs in the stator as well as in the disc. However, the amplitude in the disc is much higher than in the stator as the figures

below the plots show. Figures 7.5 illustrates that the response of the disc is a fixed vibration in the coordinate rotating with the disc. This response can be decomposed into the two components X_f and X_b according to equation (7.19). For this case, the term of $(W_{11}-W_{21})\sin[(\omega+n\Omega)t+n\alpha]\cos n\theta$ is dominant which represents a fixed vibration and is shown in figure 7.6.

There are three other cases where the the excitation frequencies and the speed are such that the stator and the disc are at resonance. These situations and their responses have been shown in figures 7.7, 7.8 and 7.9. It is seen that the disc response for all of these cases are in the same shape as in figure 7.5 and they represent the fixed vibration in the disc.

Figure 7.10 shows the case in which the excitation frequency is equal to the stator natural frequency but the speed is such that the response frequency does not coincide with the disc's resonance frequency. In this case, although the stator is at resonance, the disc itself is not and the response is a large backward travelling wave. In figure 7.11 the excitation frequency is assumed to be 200 Hz which is equal to one of the disc natural frequencies. This figure represents the responses for this case and shows that the disc is not at resonance. The interpretation is that for the rotating disc its 'resonance frequencies' should be considered in the comparison with the excitation frequency and not its actual natural frequencies.

Another case considered is shown in figure 7.12 where the excitation frequency is equal to one of the stator natural frequencies and the speed is much greater than for the resonance frequency. In this case, the disc is not at resonance, similar to the case shown in figure 7.10 and the response is a backward travelling wave with varying amplitude.

The last case considered is on system II, which is similar to the previous system but the second natural frequency of the 3 ND of the disc is 202 Hz rather than to 200.5 Hz. This change makes the system have two distinct coincidences of resonance at the speed of

1000rev/min; see figure 7.13. Comparison of the responses with the relevant case in the previous system (figure 7.5), we see that there is no significant differences.

7.6 CONCLUSION

There is the possibility of vibration interaction between the stator and an adjacent rotating disc if the stator is excited by a harmonic force. Owing to this interaction, the analysis showed that the effective excitation force for the rotating disc is in terms of two frequencies 'ω' and '$n\Omega$' rather than a single frequency. The response in the n ND modes of the stator to this excitation is a fixed vibration with frequency equal to the excitation frequency, ω. However, the disc response is a combination of 'fixed vibrations' and 'travelling waves'. The frequencies of the disc response are $\omega \pm n\Omega$ in the view of an observer on the disc, and hence the resonance frequencies are $\omega_d \pm n\Omega$ for the rotating disc. In a frequency-speed diagram of a diametral mode, there are four points where the coincident of the resonance will occur. At these points the excitation frequency is equal to the both stator natural frequency and the disc resonance frequency.

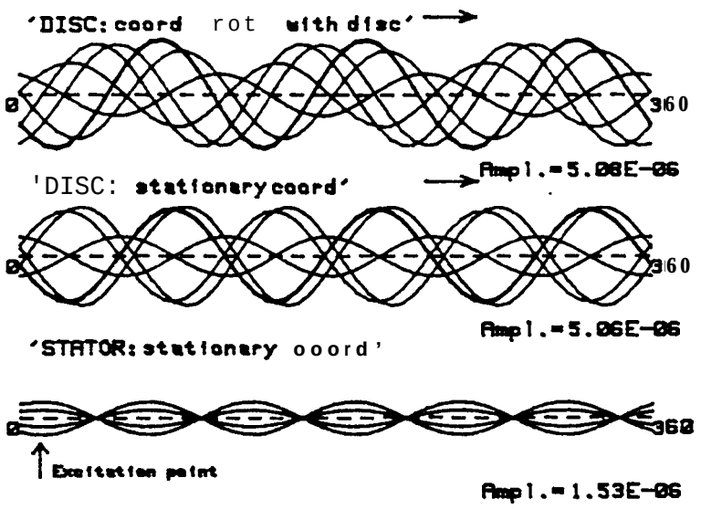

(a)

Modal data for 3 ND modes

	Generlized masses, [kg]	Natural Frequencies, [Hz]
DISC	1.00, 1.02	200.0, 200.5
STATOR	1.20, 1.30	150.0, 152.0

Excitation frequency ω = 100 [Hz]

Running speed Ω = 1000 [rev./min]

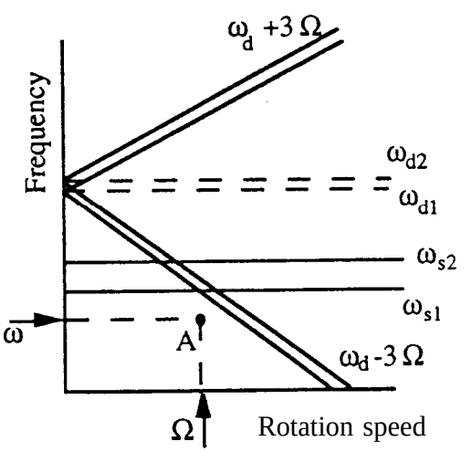

(b)

Figure 7.4 (a) **The** responses of disc and stator; **(b)** Relevant data about them

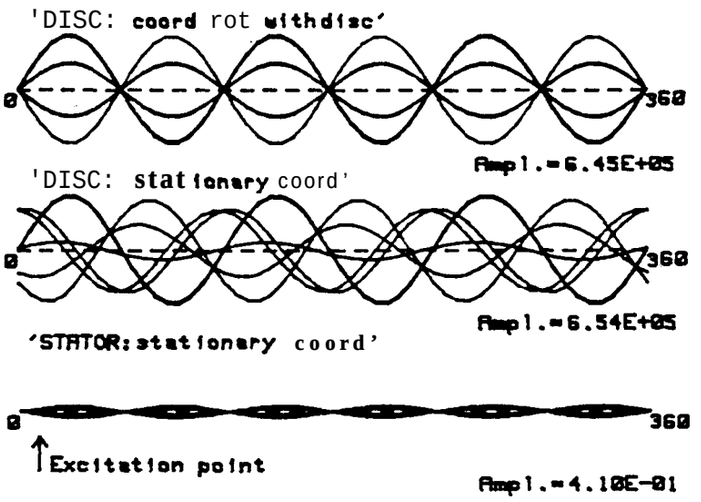

(a)

Modal data for 3 ND modes

	Generlized masses, [kg]	Natural Frequencies, [Hz]
DISC	1.00, 1.02	200.0, 200.5
STATOR	1.20, 1.30	150.0, 152.0

Excitation frequency ω = 150 [Hz]

Running speed Ω = 1000 [rev./min]

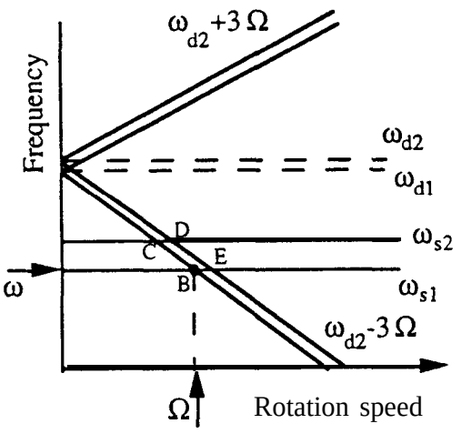

(b)

Figure 7.5: (a) **The** responses of disc and stator; **(b)** Relevant data about them

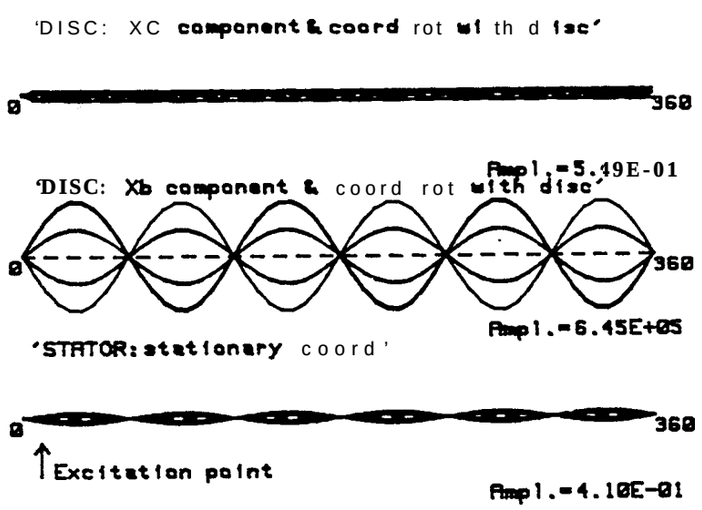

(a)

Modal data for 3 ND modes

	Generlized masses, [kg]	Natural Frequencies, [Hz]
DISC	1.00, 1.02	200.0, 200.5
STATOR	1.20, 1.30	150.0, 152.0

Excitation frequency ω = 150 [Hz]

Running speed Ω = 1000 [rev./min]

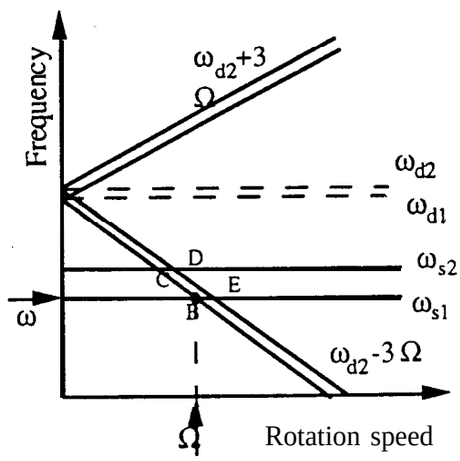

(b)

Figure 7.6: (a) The response components of the disc and the stator response;
(b) Relevant data about them which are the same as in figure 7.5

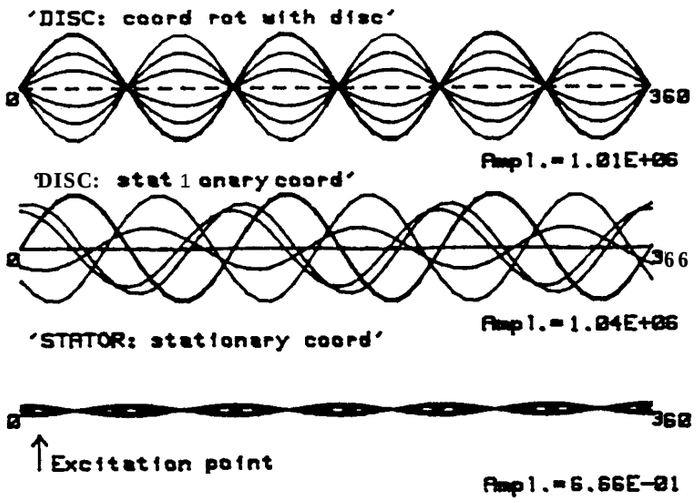

(a)

Modal data for 3 ND modes

	Generlized masses, [kg]	Natural Frequencies, [Hz]
DISC	1.00, 1.02	200.0, 200.5
STATOR	1.20, 1.30	150.0, 152.0

Excitation frequency $\omega = 152$ [Hz]

Running speed $\Omega = 960$ [rev./min]

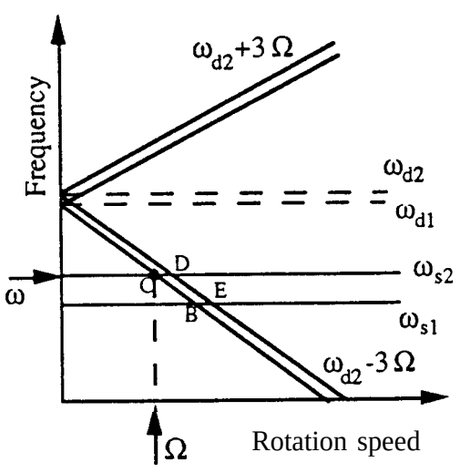

(b)

Figure 7.7: (a) **The** responses of disc and stator; **(b)** Relevant data about them

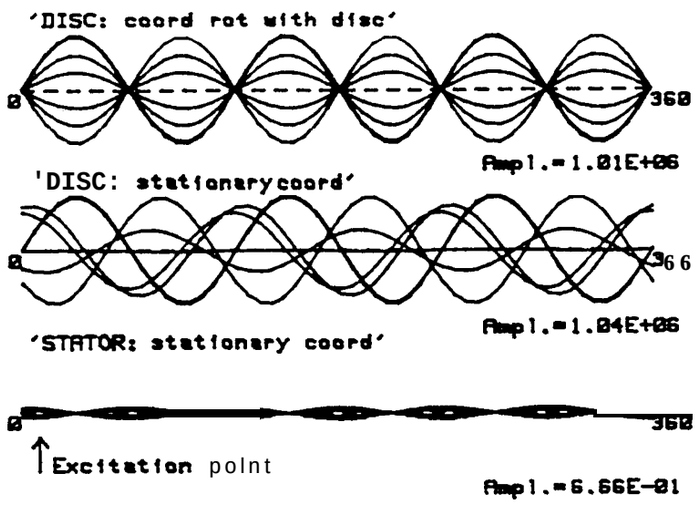

(a)

Modal data for 3 ND modes

	Generlized masses, [kg]	Natural Frequencies, [Hz]
DISC	1.00, 1.02	200.0, 200.5
STATOR	1.20, 1.30	150.0, 152.0

Excitation frequency $\omega = 152$ [Hz]

Running speed $\Omega = 960$ [rev./min]

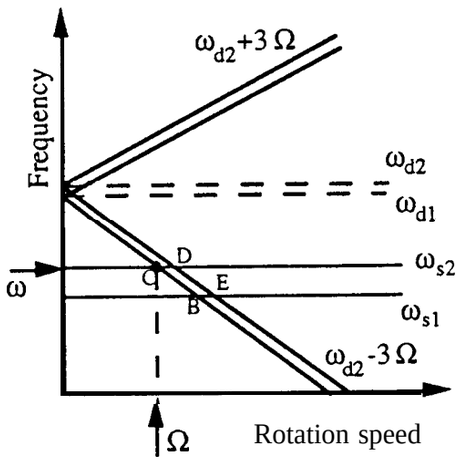

(b)

Figure 7.7: (a) **The** responses of disc and stator; **(b)** Relevant data about them

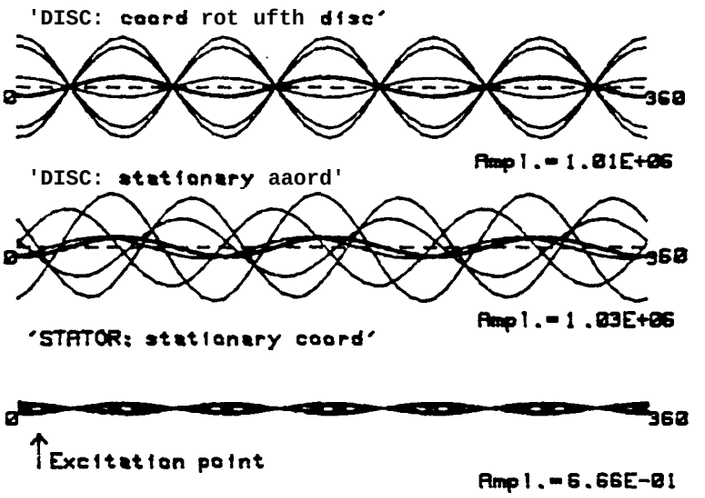

(a)

Modal data for 3 ND modes

	Generlized masses, [kg]	Natural Frequencies, [Hz]
DISC	1.00, 1.02	200.0, 200.5
STATOR	1.20, 1.30	150.0, 152.0

Excitation frequency ω = 152 [Hz]

Running speed Ω = 970 [rev./min]

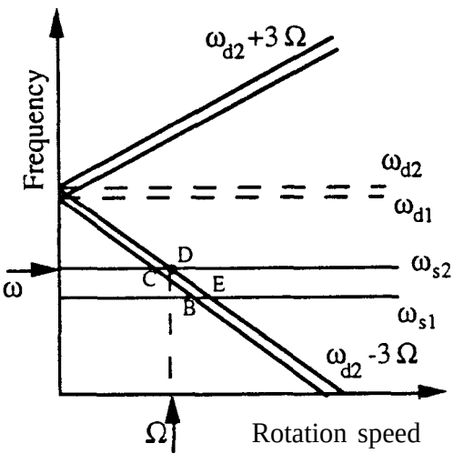

(b)

Figure 7.8: (a) **The** responses of disc and stator; **(b)** Relevant data about them

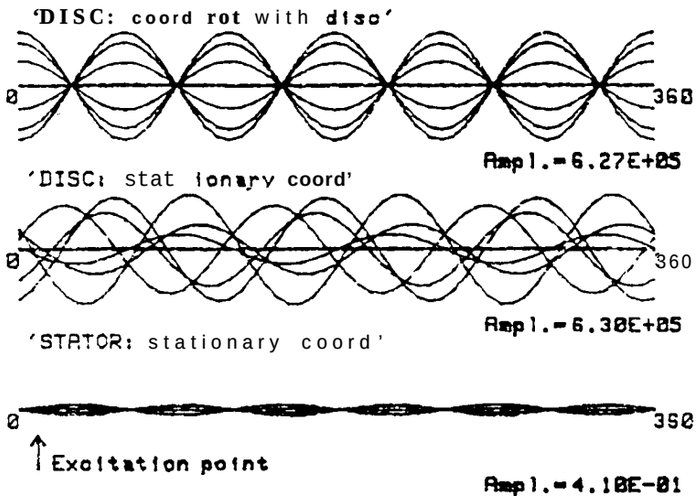

(a)

Modal data for 3 ND modes

	Generlized masses, [kg]	Natural Frequencies, [Hz]
DISC	1.00, 1.02	200.0, 200.5
STATOR	1.20, 1.30	150.0, 152.0

Excitation frequency ω = 150 [Hz]

Running speed Ω = 1010 [rev./min]

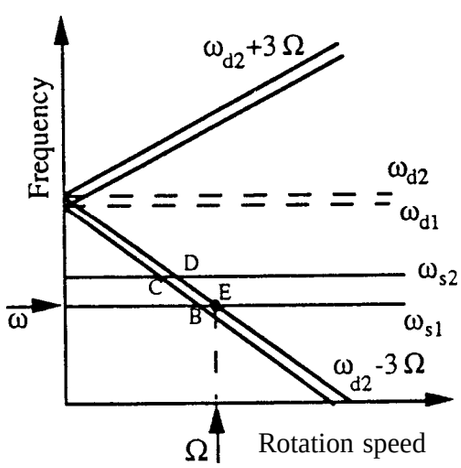

(b)

Figure 7.9: **(a)** **The** responses of disc and stator; **(b)** Relevant data about them

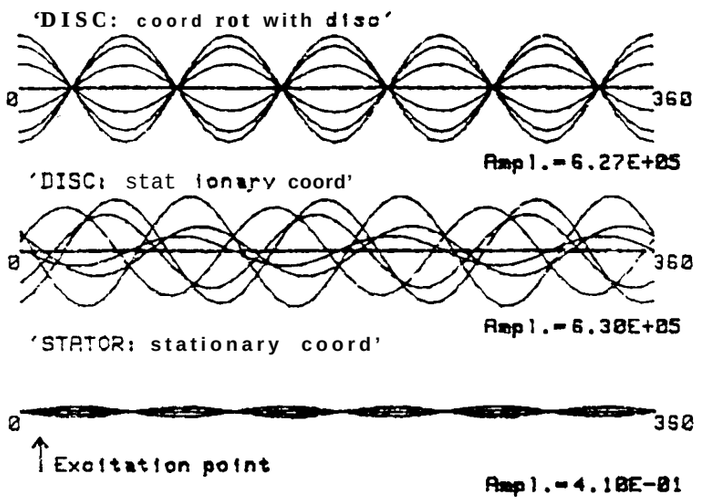

(a)

Modal data for 3 ND modes

	Generlized masses, [kg]	Natural Frequencies, [Hz]
DISC	1.00, 1.02	200.0, 200.5
STATOR	1.20, 1.30	150.0, 152.0

Excitation frequency ω = 150 [Hz]

Running speed Ω = 1010 [rev./min]

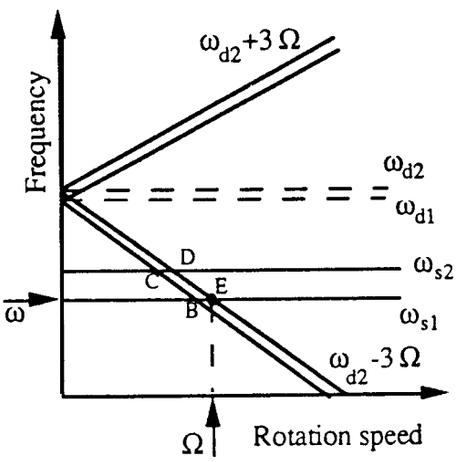

(b)

Figure 7.9: (a) **The** responses of disc and stator; **(b)** Relevant data about them

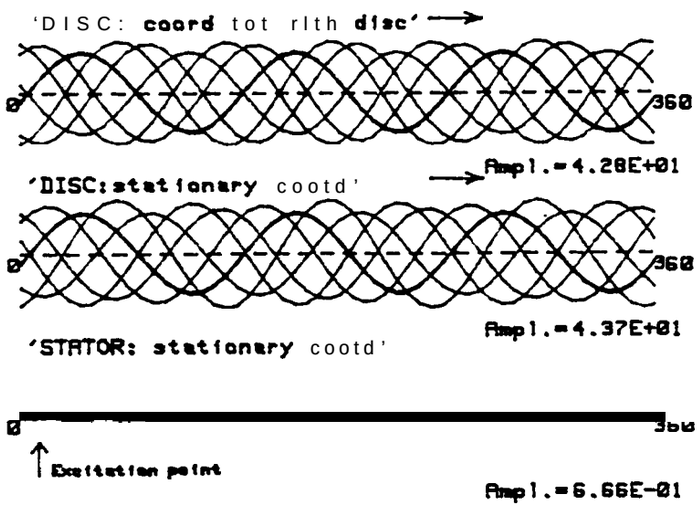

(a)

Modal data for 3 ND modes

	Generlized masses, [kg]	Natural Frequencies, [Hz]
DISC	1.00, 1.02	200.0, 200.5
STATOR	1.20, 1.30	150.0, 152.0

Excitation frequency ω = 152 [Hz]

Running speed Ω = 1000 [rev./min]

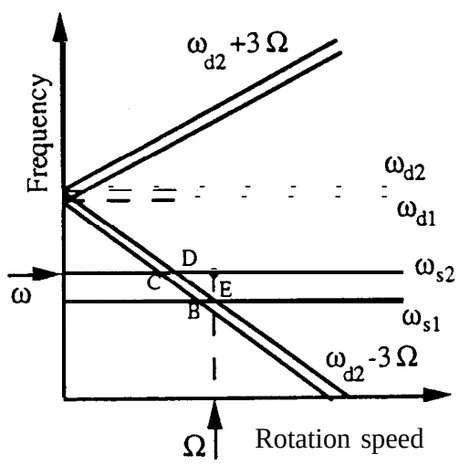

(b)

Figure 7.10: (a) **The** responses of disc and stator; **(b)** Relevant data about them

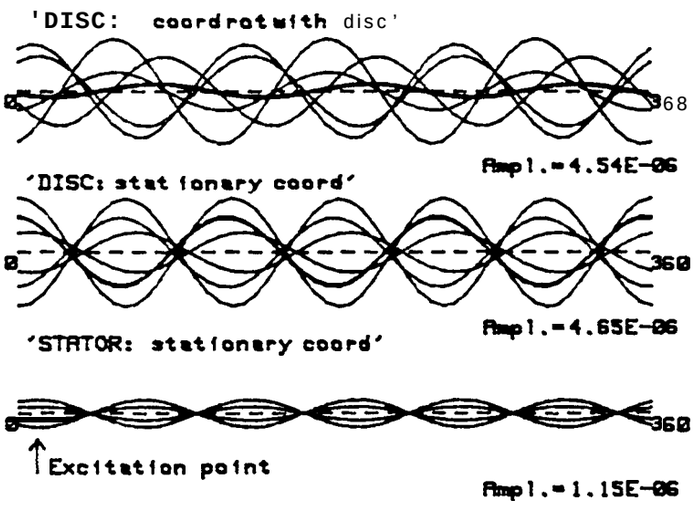

(a)

Modal data for 3 ND modes

	Generlized masses, [kg]	Natural Frequencies, [Hz]
DISC	1.00, 1.02	200.0, 200.5
STATOR	1.20, 1.30	150.0, 152.0

Excitation frequency ω = 200 [Hz]

Running speed Ω = 1 o o 0 [rev./min]

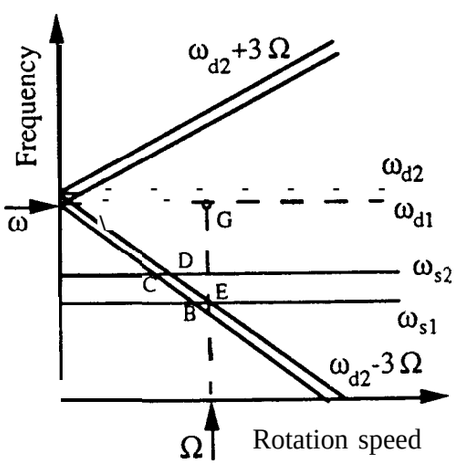

(b)

Figure 7.11: (a) **The** responses of disc and stator; **(b)** Relevant data about them

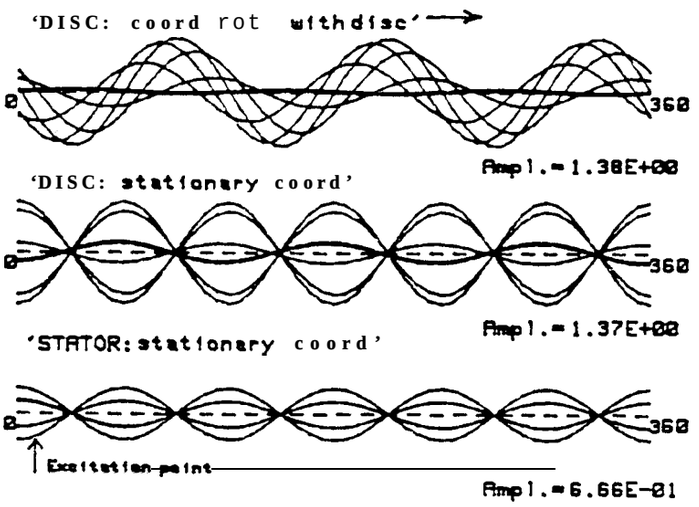

(a)

Modal data for 3 ND modes

	Generlized masses, [kg]	Natural Frequencies, [Hz]
DISC	1.00, 1.02	200.0, 200.5
STATOR	1.20, 1.30	150.0, 152.0

Excitation frequency ω = 152 [Hz]

Running speed Ω = 2500 [rev./min]

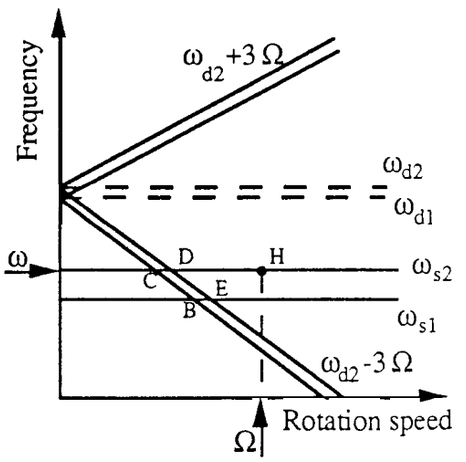

(b)

Figure 7.12: (a) The responses of disc and stator; (b) Relevant data about them

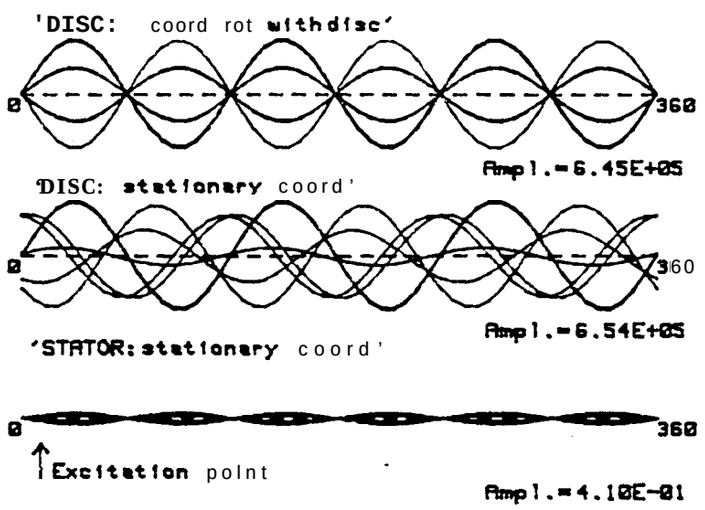

(a)

Modal data for 3 ND modes

	Generlized masses, [kg]	Natural Frequencies, [Hz]
DISC	1.00, 1.02	200.0, 202.0
STATOR	1.20, 1.30	150.0, 152.0

Excitation frequency ω = 150 [Hz]

Running speed Ω = 1000 [rev./min]

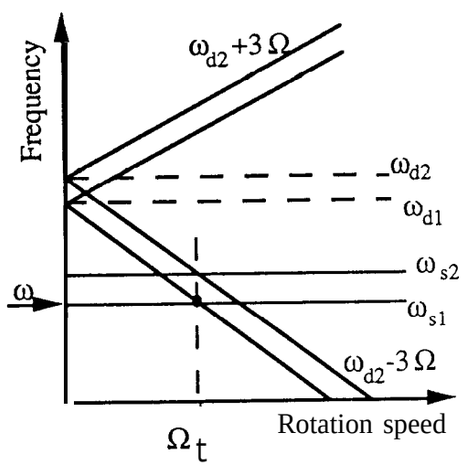

(b)

Figure 7.13: (a) **The** responses of disc and stator; **(b)** Relevant data about them

- Collection of different terms and definitions used in rotating disc study such as backward and forward travelling waves, standing waves and fixed vibration;
- Analysis of the frequency response of a rotating disc in rotating coordinates and in stationary coordinates. The analysis was confirmed by experiments;
- Presenting a more genera1 relationship for excitation parameters - forces ratio, spatial and temporal phase angles - in the simulation of a disc rotating past a static force;

$$n\phi_s - \phi_t = k\,\pi \qquad k=\cdots -1,1,3,\cdots$$

- Development of hardware (PHASH) and a software to control and adjust two forces for simulation of travelling wave. The program is written for H.P. computers and can be run to control the relative force ratio to the desired value through the PHASH;
- Presenting a technique using more than two excitations for simulation of travelling waves which use the same control system as used in the dual-controlled sine excitation method. A four-excitation method was applied to a discrete mass model of a disc to simulate travelling waves. This application resulted in increasing the relative amplitude of the travelling wave component about 6% compared with using dual excitations;
- Development of a format for displaying the travelling wave and animated response of a disc. The unwrapped rim response was used. This method can give a clear picture of a vibrational rotating disc;

- Study of possibilities of vibration interaction between a rotating disc and an adjacent stator. The vibration initiated in the rotating disc might transfer to the stator or vice versa.

8.3 RECOMMENDATIONS FOR FURTHER WORK

The work studied here is the development of a method which can be very effective in the modal testing of rotating discs. The models of a disc used in this study have been simple ones. This was necessary as an early stage to achieve the main theoretical relationships.

APPENDICES

APPENDIX

FURTHER DATA OF NON-CONTACTING EXCITER AND PROBES

A.1 Non-Contacting Electra-Magnetic Exciter

An electro-magnetic exciter is one of the non-contact devices which may be used in experiments on rotating structures. The problem with these exciters is that in high amplitude vibration, they produce some harmonics of excitation frequency rather than just a single frequency equal to the input frequency [55]. Before any harmonic excitation measurement on the rotating disc, the spectrum of the response of stationary disc has been obtained to check the harmonics of excitation frequency. It was realized that second harmonic is stronger and so in all measurements, this harmonic has been considered as the excitation frequency. In figure A. 1 the spectrum of response of a stationary disc to the excitation frequency set equal to 98 Hz has been shown. In the figure the measured spectrum have been obtained by using two different non-contact devices a) Laser and b) Proximeter.

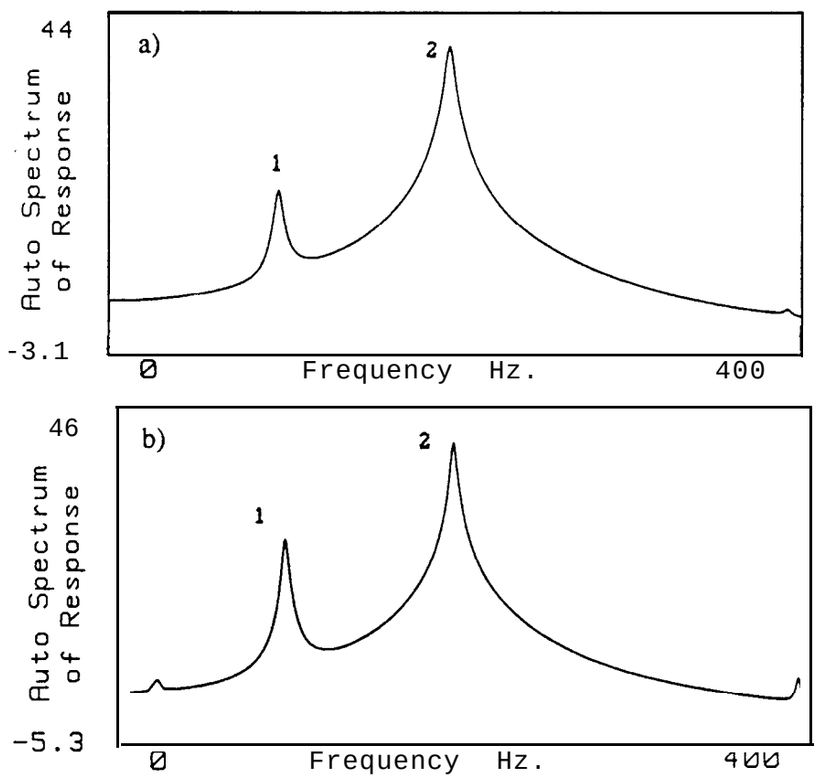

No.	Fre
1	98
2	196

Figure A.1 Response of the stationary disc to a non-contacting electro-magnet excitation Using: a) Laser doppler VPI, b) Proximeter probe (Generator frequency setting =98.0 Hz)

A.2 Comparison of Proximeter and Accelerometer in a hammer

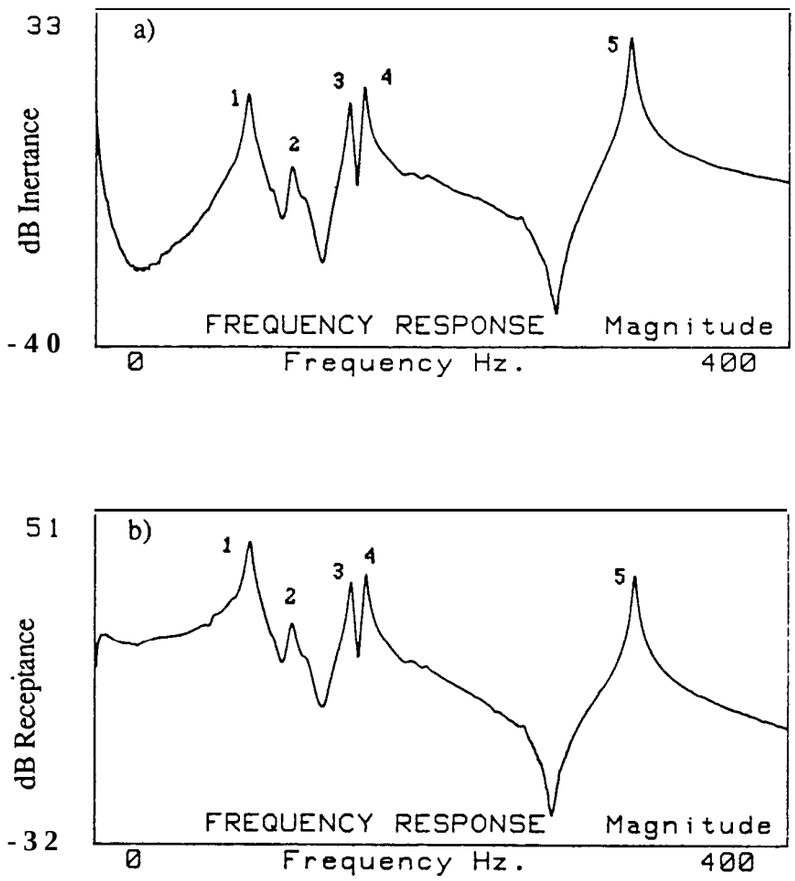

Figure A.2 **FRF** from hammer test. Using a) Accelerometer b) Proximeter

APPENDIX B

SECONDARY RESULTS IN THE SIMULATION METHODS

In this Appendix, some of the results related to the simulation of travelling waves which have been explained in chapter 4 are illustrated. These are for the cases where more details about the results are required.

B.1 Circle fitting on the data

In the following, some of the results are illustrated in Nyquist plots in order to give a better idea for the phases of the dual modes and also to present the modal analysis procedure.

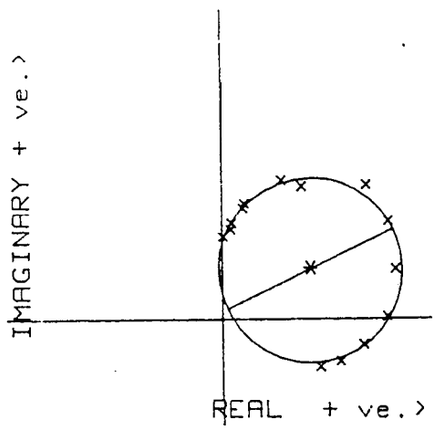

Res.Freq.= 157. 16 Hz.
Phase = +115.5 deg
Damping = .00216
P.S.Modal C.= 6.46940E-02 1/kg

X2_F21 Lower 2 ND mode

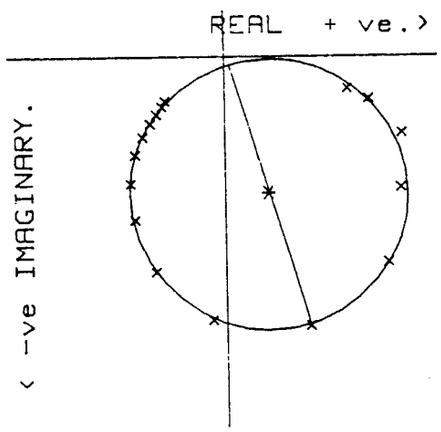

158.40 Hz.
+16.6 deg
.00168
3.24569E-02 1/kg

X2_F21 Higher 2 ND mode

Figure B.l Using circle-fitting of MODENT on the data of X2_F21

(Receptance plot - removing effect of other mode)

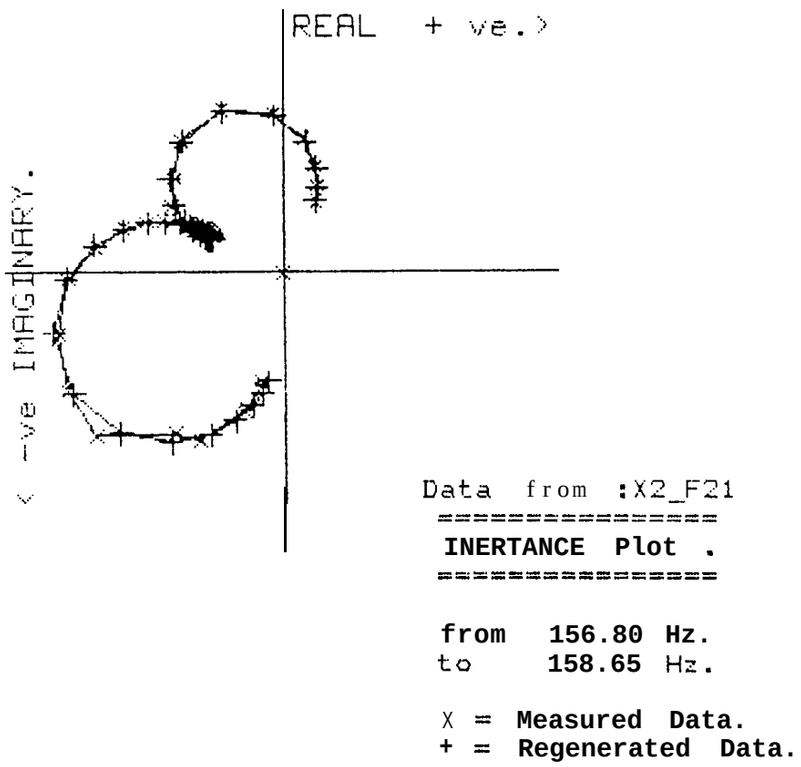

Figure B.2 Regenerating data X2_F21 after circle-fitting (in Nyquist plot)

B.2 Numerical results when spatial phase angle is -90°

As mentioned in chapter 4, in the simulation of a travelling wave we can either use $+\phi_t$ or $-\phi_t$ as the temporal phase angle of the excitation forces. In section 4.5.3, two numerical examples have been presented to examine the relative phases of the pseudo-modal constants. Here, the results for the similar cases but for ϕ_t=-90° are shown.

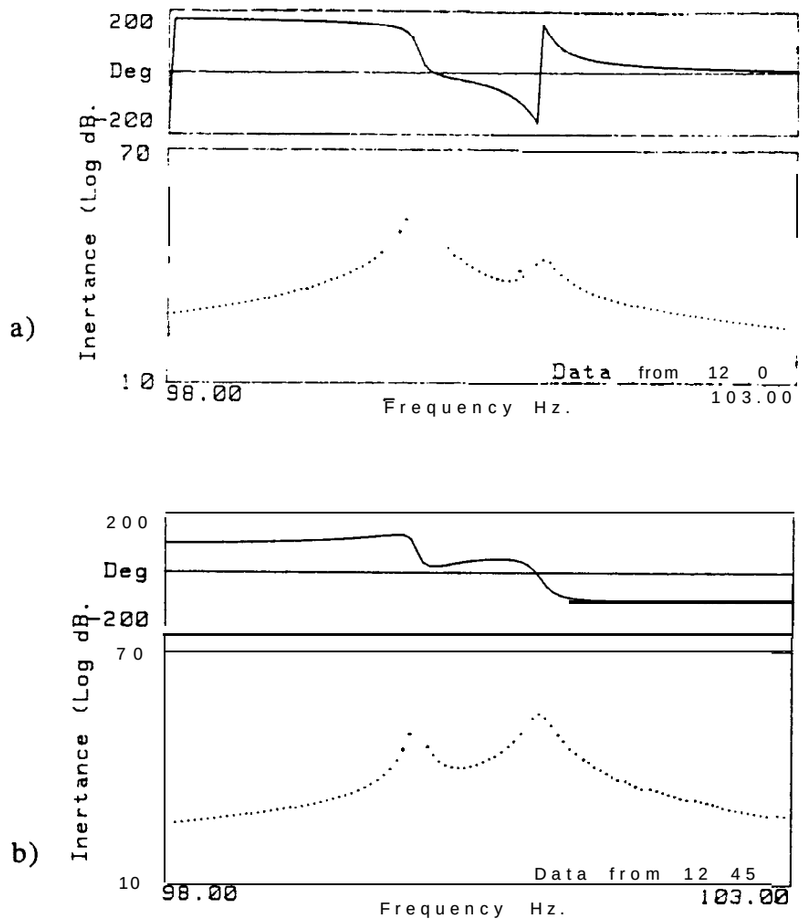

Figure B.3 Results from a numerical example of a mistuned system
(Similar system as introduced in table 4.4; but here ϕ_t=-90°)
a) At point 1 (WY'); b) At point 2 (θ=45°)

Table B.l Modal properties from data presented in figure B.3

	2NDmode No.	Natural frequency [Hz]	Pseudo-modal constant [1/Kg]	Phase [Deg.]	Damping loss factor; η
Data from point 1 (12_0)	1	100	0.9394	-20.0	0.00100
	2	101	0.3418	+70.0	0.00200
Data from point 2 (12_45)	1	100	0.3425	-20.0	0.00100
	2	101	0.9395	-110.0	0.00200

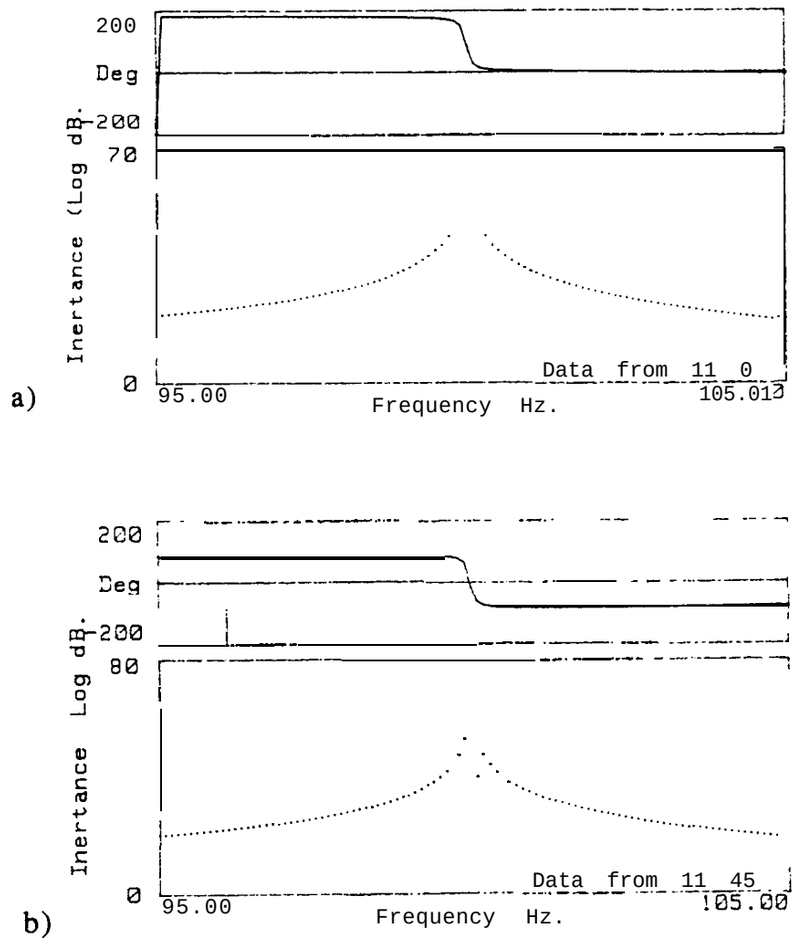

Figure B.4 Results from a numerical example of a tuned system
(Similar system as introduced in section 4.5.3; but here ϕ_t=-90°)
a) At point 1 (θ=0°); b) At point 2 (θ=45°)

Table B.2 Modal properties from data presented in figure B.4

	2 ND mode No.	Natural frequency [Hz]	Modal constant [1/Kg]	Phase [Deg.]	Damping loss factor ; η
Data from point 1 (I1_0)	1	100	0.9995	0.0	0.00100
	2	-	-	-	-
Data from point 2 (I1_45)	1	-	-	-	-
	2	101	0.9395	-110.0	0.00200

B.3 Raw data in the Hybrid Method

In the Hybrid Method, two sets of experimental data have been used to calculate the simulation responses at points 1 and 2 on the disc. These experimental data are illustrated in figures B.5 and B.6.

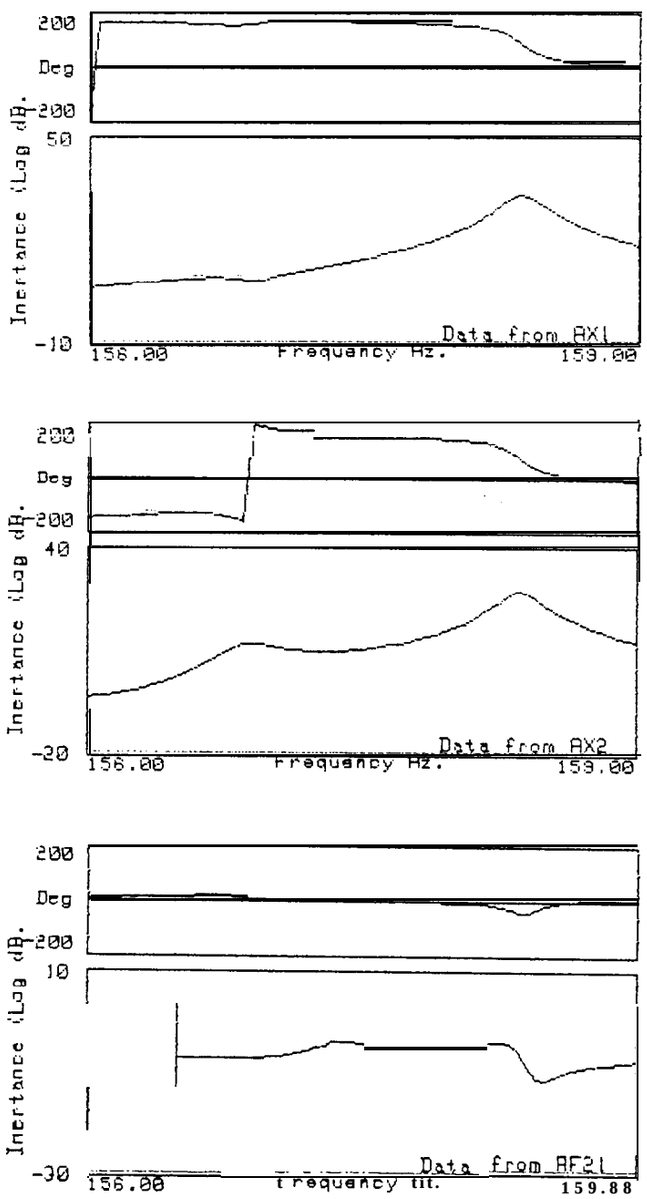

Figure B.5 Response at points 1 and 2; together with force ratio in test A of Hybrid Method

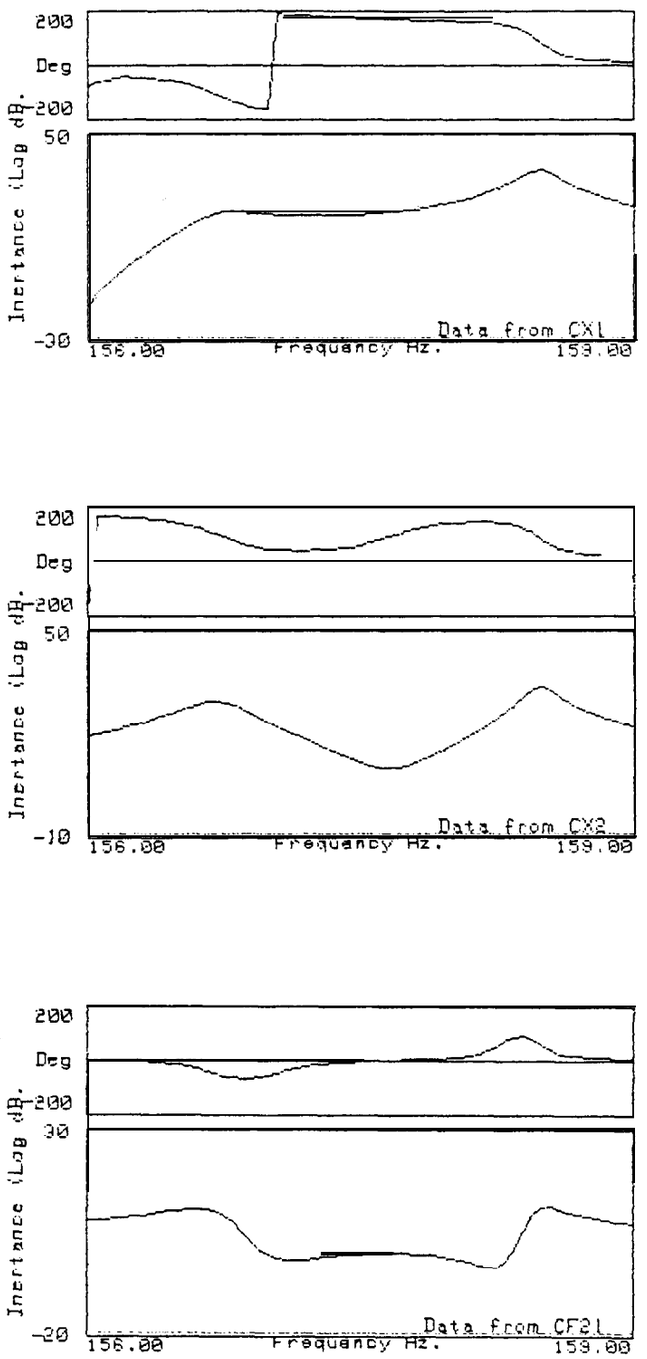

Figure B.6 Response at points 1 and 2; together with force ratio in test C of Hybrid Method

B.4 An earlier experiment for simulation on the disc

In this section the results of the earlier experimental simulation on the disc are presented. These experiments had been carried out using the phase shifter in a manually-controlled test. The results from both methods have been shown in figure B.7, tables B.3 and B.4. Although the test structure had been suspended in a different way and the technique had been not as accurate compared with the experiments in chapter 4, we can see similar relative relationship for the phases.

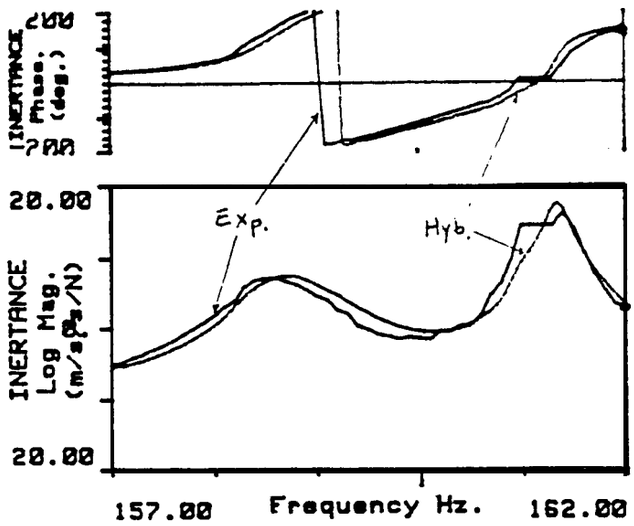

Response at point 1

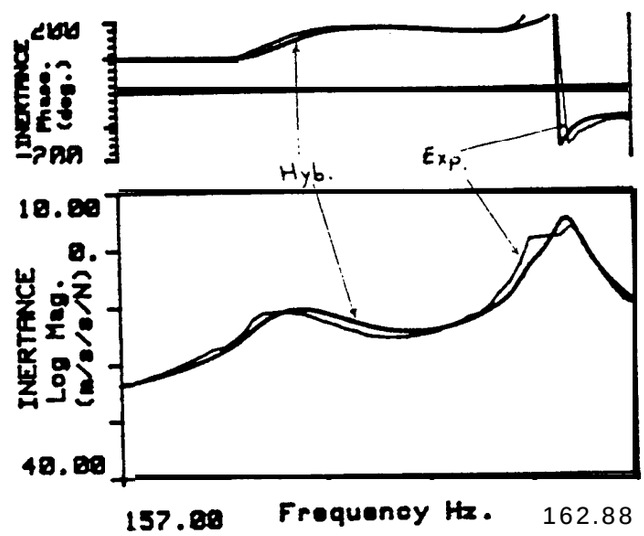

Response at point 2

Figure B.7 Experimental and Hybrid method's results from the earlier test (ϕ_t=-90°)

Table B.3 Modal parameters from the EM

	2 ND mode No.	Natural frequency [Hz]	Pseudo_modal constant [1/Kg]	Phase [Deg.]	Damping loss factor ; η
Data from point 1 (WAV1)	1	158.5	0.0134	+140.0	0.00496
	2	161.4	0.0145	-132.3	0.00228
Data from point 2 (WAV2)	1	158.5	0.0012	+162.9	0.00514
	2	161.4	0.0030	+51.2	0.00224

Table B.4 Modal parameters from the HM

	2 ND mode No.	Natural frequency [Hz]	Pseudo_modal constant [1/Kg]	Phase [Deg.]	Damping loss factor ; η
Data from point 1 (WAVE1)	1	158.69	0.0173	+143.2	0.00590
	2	161.35	0.0129	-136.4	0.00168
Data from point 2 (WAVE2)	1	158.68	0.0013	+155.7	0.00582
	2	161.35	0.0027	+51.9	0.00166

B.5 Results for the very lightly-damped disc

Figure B.8 and table B.4 show the results of a single-sine test on the disc without additional damping. It is seen that compared with the value of damping in chapter 4, here the damping loss factor is very low.

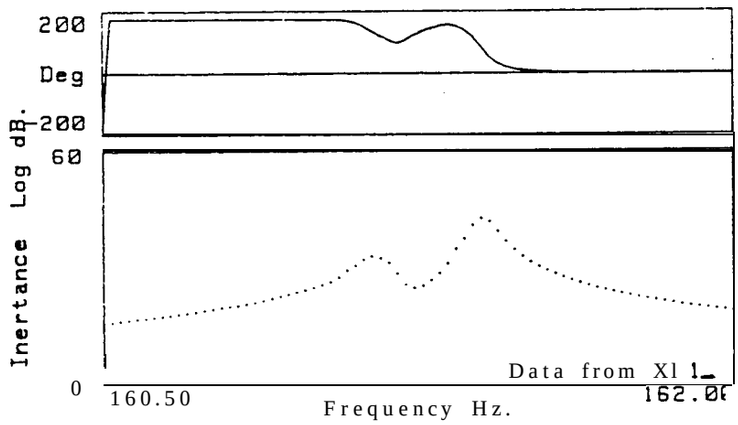

Figure B.8 Point measurement in the single-excitation test of the disc

Table B.5 Modal parameters from data in figure B.8

	2 ND mode No.	Natural frequency [Hz]	Modal constant [1/Kg]	Phase [Deg.]	Damping loss factor: η
Data from point 1 (X11_)	1	161.16	0.0198	+9.5	0.00054
	2	161.40	0.0510	-0.1	0.00036

APPENDIX C

PHASE AND AMPLITUDE SHIFTER (PHASH)

In chapter 4, it was mentioned that vibration in a disc rotating past a non-rotating static force can be simulated for each mode in a stationary disc excited by two harmonic forces. These two harmonic forces should be equal in magnitude and their temporal phase angle should be equal to a specific value. On the other hand, during a sine sweep test, the magnitude and the phase of the excitation will change even if the input voltage to the shaker does not change. The electrical impedance of the shaker is a function of its coil displacement and, hence, it is a function of the frequency response of the structure. This function can not be simply defined but it is complex. As long as one excitation is used, changes of the excitation force do not make the test difficult, since normally the ratio of the response to the input force is required at each frequency. However, in the two excitation test, where some special conditions should be fulfilled, a controller has to be used to keep the input forces at the desired levels. In the simulation of a travelling wave, the controller must be able to control the magnitudes of the two input forces, and also their phases, by changing the input to the shakers accordingly.

Since the function relating the input voltage to the excitation frequency is not available, the two forces must be controlled using a trial and error procedure with the input voltages.

C.1 Hardware of the shifter

A shifter (PHASH) has been developed which is controlled by a H.P. computer. The PHASH has been made using four different components as shown in Figure Cl. They

are the DAC, BBDs, VCO , and Multipliers which are described briefly in the following sections:

C.l.l Digital to Analogue Converter (DAC)

A four-channel digital to analogue converter interface provides four independent voltage outputs with 12-bit resolution. In this application, three channels are used: V_0 for the 'voltage controlled oscillator' (VCO) and V_1, V_2 for controlling the amplitudes of the forces.

An H.P. computer program controls the output voltages of the DAC independently. The DAC has different options for its output voltage: in this application, the O-10 volt range has been chosen for all channels.

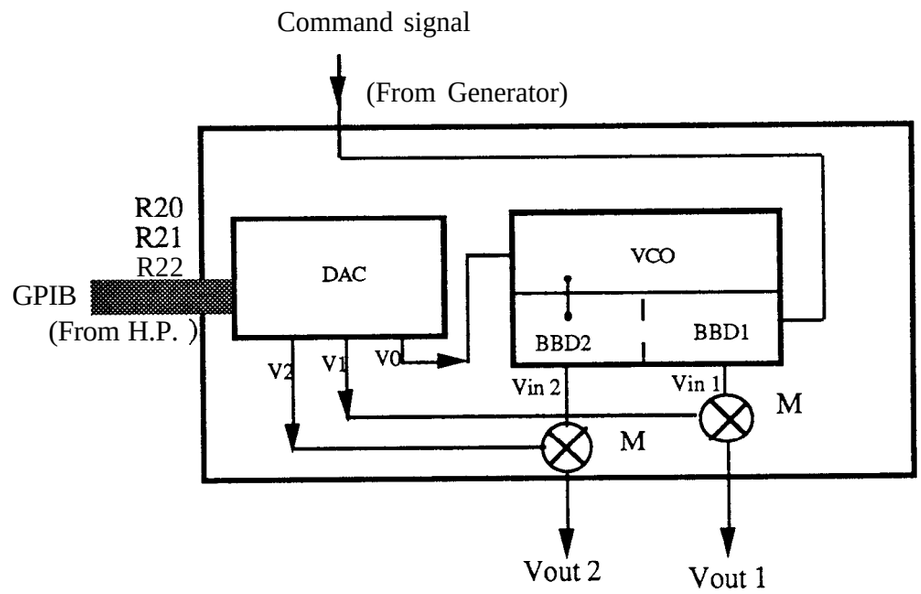

Figure C.l Components in the 'PHASH'

C.1.2 Phase Controllers (BBD and VCO) :

This instrument has been made using two bucket brigade delays (BBD) and a voltage controlled oscillator (VCO). The time delay of the signal passing through the BBD, and hence the signal phase, is controlled by the frequency of the clock input to the BBD. The signal from the generator goes to the BBDs. One of these, (BBD1), gives a signal with a fixed phase angle while the other can give the signal with variable phase angle using the VCO. In the first BBD, the clock works with a pre-set value set by a potentiometer and in the second BBD, the clock is controlled by a signal from the VCO which in turn responds to V_0 from the DAC.

A schematic diagram of the circuits of BBD1, VCO and BBD2 are shown in figures C.2, C.3.and C.4.

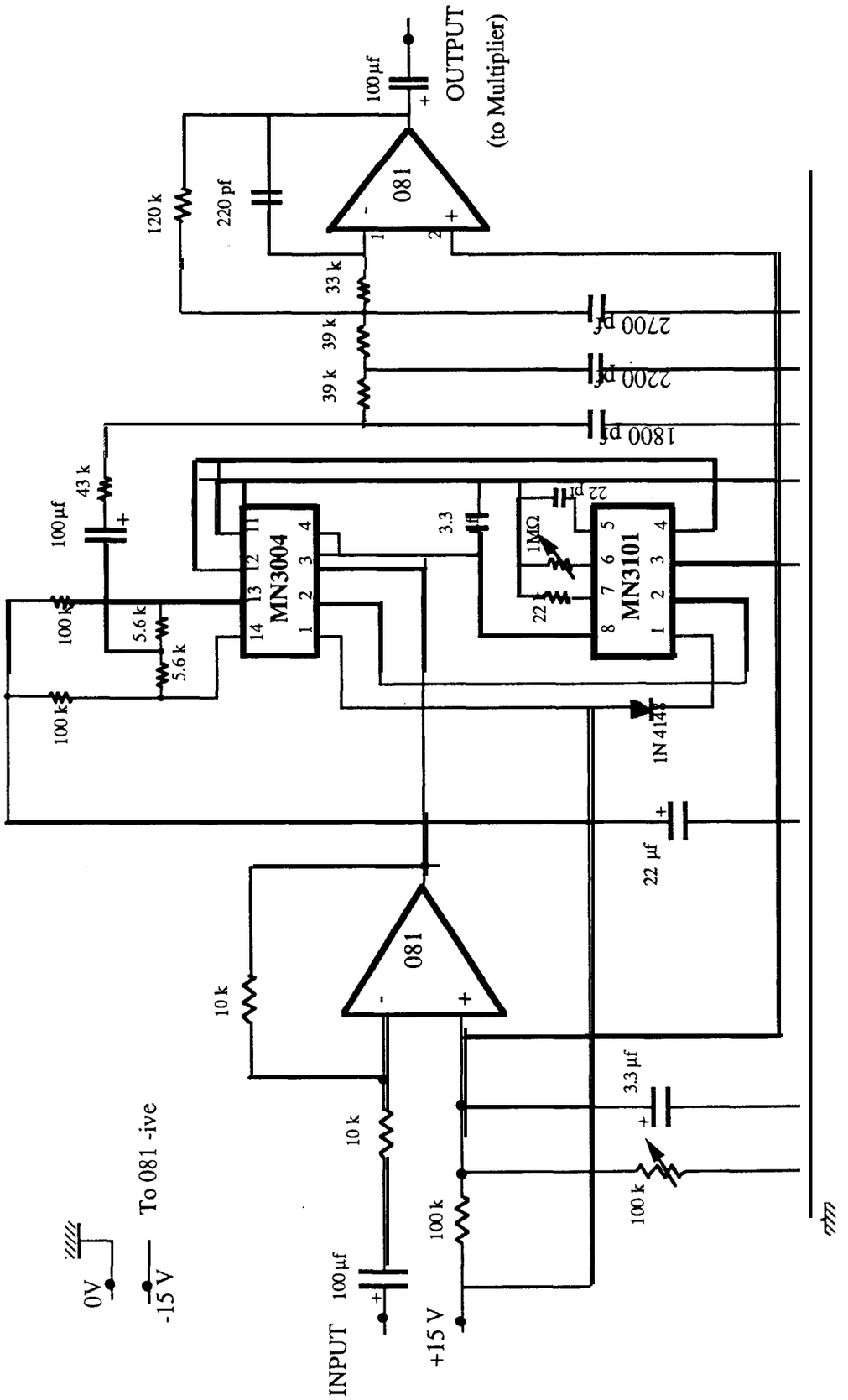

Figure C. 2 BBD1 which has fixed clock frequency

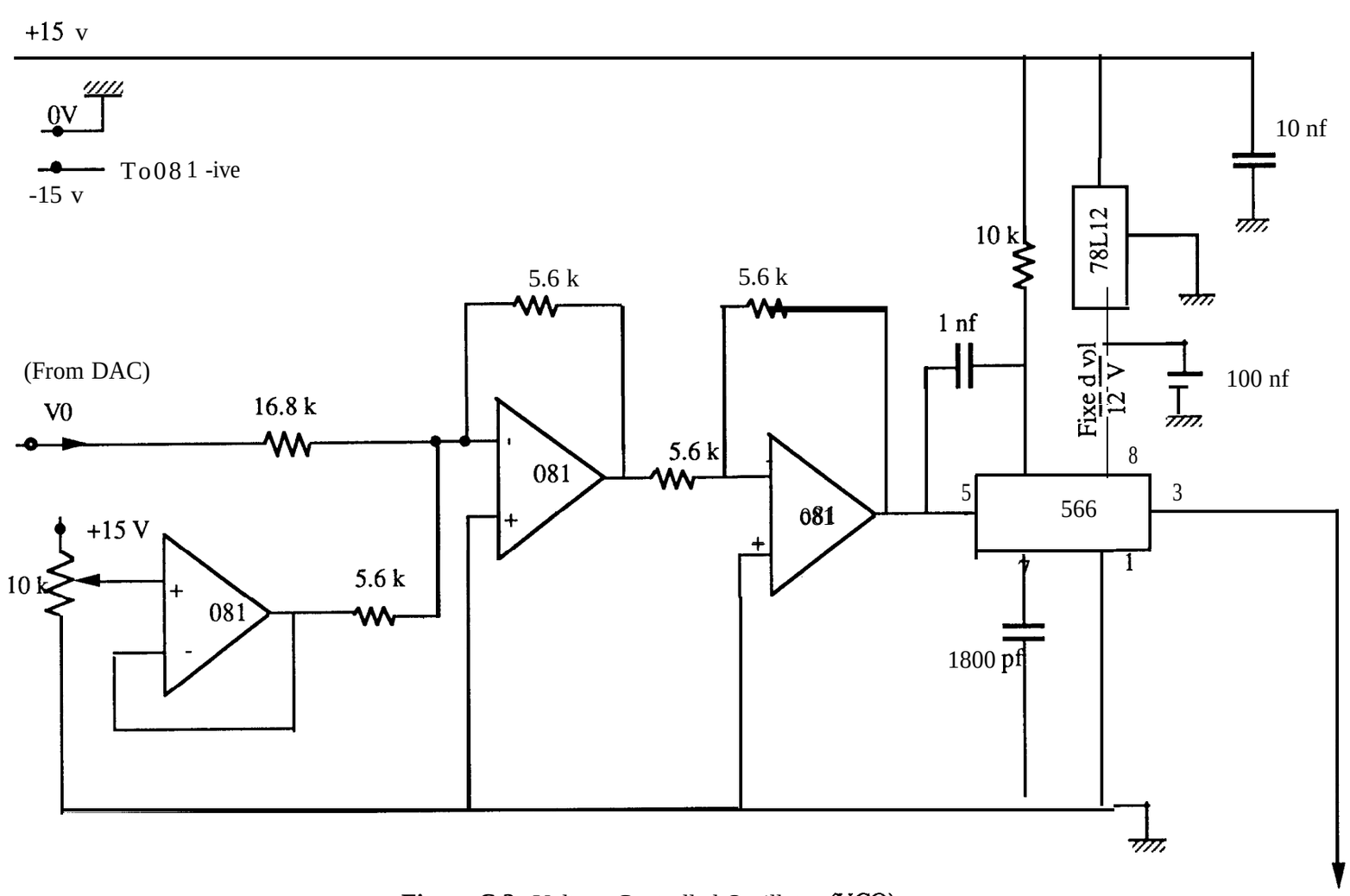

Figure C.3 Voltage Controlled Oscillator (VCO)

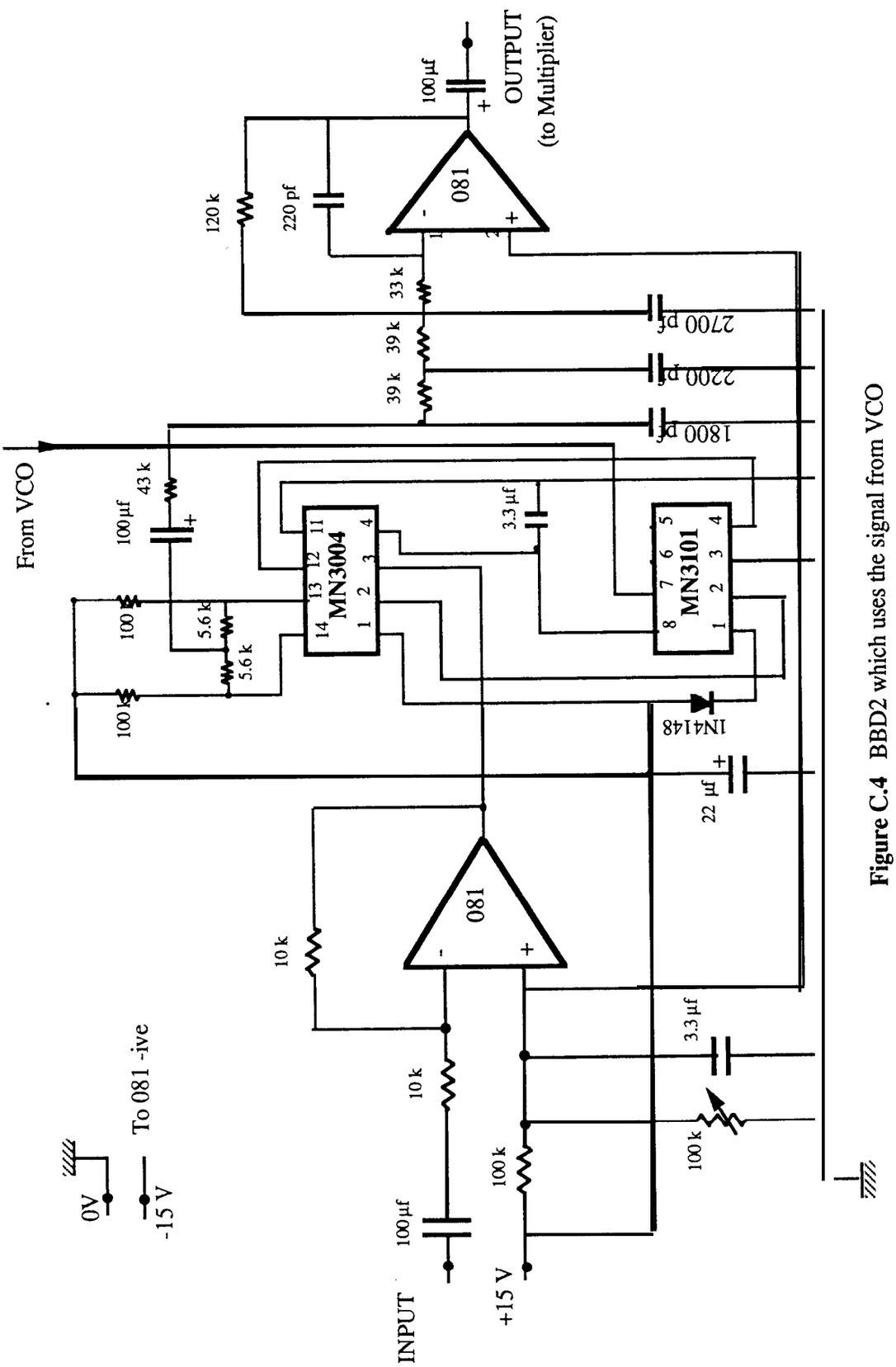

Figure C.4 BBD2 which uses the signal from VCO

C.1.3 Analogue Multiplier (M)

In order to make the ratio of two forces take the desired value, which is usually 1, the controller has to be able to change the magnitude of each signal to the shakers independently. A multiplier has been used in the path of each signal to the shaker as shown in figure C. 1. Each multiplier is controlled by a voltage coming from the DAC. The output voltage is one tenth of the product of the input voltage and controlling voltage, i.e. $Vout = \frac{V_{input} * V_{DAC}}{10}$.

C.2 Software for Controller

The program POLAR has been in use for many years in sine sweep tests and is quite popular. Its latest version, New-POLAR has been modified to make it suitable for two-excitation sine-sweep tests using the controller. This program is called 'POLAR_PHASH' .

In the sine-sweep test, at each frequency, the conditions of the simulation should be checked and if they are not in the acceptable range, they have to be changed using the controller. However, if they are acceptable, the measured values are recorded and the test will proceed for the next frequency.

The acceptable tolerance for the phase of the two forces has been chosen arbitrarily as $\pm 2^{o}$ and for their relative magnitude as $\pm$ 0.1. In section 4.5, it has been shown that with this amount of tolerance, the travelling wave component in the response is quite strong and acceptable for the simulation. These tolerances may also be examined if they are low enough to produce a smooth frequency response curve for analysis.

The controller has been programmed on the basis of trial and error, since the theoretical relationships between voltage input to the shakers and input forces to the disc for different

frequencies are very complicated. In the following, the procedure used is introduced and its flow-chart is presented in figure C.6.

C.2.1 Trial and error procedure for controller

Three parameters need to be changed in order to achieve the desired values of phase and the ratio of $(\frac{F_2}{F_1})$. These parameters are the magnitudes of and phase difference between the input voltages to shakers 1 and 2 which change with the voltages of the three channels of the DAC; V_0, V_1 and V_2 respectively. These three voltages, in turn, are changed with the input control words sent from the computer to the DAC which are called R20, R21 and R22 respectively. Each control word can be chosen independently in the range of 0 to 4095. Before the procedure of trial and error to be presented, the increments for the control words should be derived such that the required phase and relative force accuracy is achieved. In section C.2.3, the proper increments are introduced.

C.2.2 Initial values for DAC

At the beginning of each sweep, in order to start the trial and error procedure as close as possible to the target values of the phase, the initial value for the control word R20 is chosen by interpolation and using the appropriate lookup table. These tables are characteristics of the controller and the one for the case of ϕ_t=90° is shown in table C.l. This table shows the values of R20 which should be sent to the controller to have 90° phase angle in the output signals of the PHASH.

Table C.l Frequency vs control word for VCO when ϕ_t=90°

Freq.[Hz]	115	120	150	200	250	300	350	400	450	500	600
R20	4095	3930	3200	2175	1345	2820	2270	1720	1320	920	0

The amplitudes of forces F_1 and F_2 are controlled to some extent by the input voltages to the shakers. These voltages are proportional to the corresponding voltages from the DAC. The initial values for the corresponding control words are chosen as equal to their maximum value, i.e. 4095, which would produce 10v at the DAC outputs..

C.2.3 Tolerances and proper steps in the DAC

As mentioned earlier, a suitable accuracy or tolerance is chosen for data acquisition. In the program, the rate of the control word should be such that it satisfies these accuracies.

C.2.3.1 Increment of the word for force amplitudes

If V_g is the voltage of the signal from the generator, V_{f1}, the input voltage to the shaker 1 is equal to :

$$V_{f1}=\frac{V_g \cdot V_{DAC1}}{10}$$

Similarly for shaker 2 :

$$V_{f2}=\frac{V_g \cdot V_{DAC2}}{10}$$

The forces from the shakers are assumed to be proportional to the voltage inputs, thus :

$$\frac{F_2}{F_1}=\frac{V_{f2}}{V_{f1}}=\frac{V_{DAC2}}{V_{DAC1}} \qquad (C.1)$$

The output of the DAC has been set in the range of 0 - 10 volt. The input of the DAC is a number in the range of 0 to 4095. Hence, the slope will be 409.5 $\left(\frac{bits}{Volt}\right)$ for each channel. This means that the following relations can be written between R21 and V_{DAC1} and between R22 and V_{DAC2} respectively :

$$R21=409.5 \cdot V_{DAC1}$$

$$R22=409.5 \cdot V_{DAC2}$$

$$\frac{R22}{R21-\Delta_1} - \frac{R22}{R21} \leq 0.2$$

or : $$\Delta_1 \leq \frac{0.2\ (R21)^2}{R22\ +\ 0.2\ R21} \qquad (C.4)$$

b2) Assumed R21 is increased then we can have:

$$\frac{R22}{R21} - \frac{R22}{R21+\Delta_1} \leq 0.2$$

which leads to: $$\Delta_1 \leq \frac{0.2\ (R21)^2}{R22 -\ 0.2\ R21} \qquad (C.5)$$

Therefore, for changing R21 the increment should satisfy the relation (C.4), if R21 is decreasing and relation (C.5) if it is going to be increased.

C.3.2 The phase changing

Table C.2 shows the variation of phase angle against the control word R20 for different frequencies. It is seen that by increasing frequency and also with higher values of R20, the rate of change of the phase angle increases. The maximum rate should be taken into account in order to obtain the limitation or the minimum increment for R20 to produce the prescribed accuracy of the phase, (i.e. ±2°).

Table C.2 Phase angle against R20 for different frequency in PHASH

R20	100 Hz	150 Hz	200 Hz	300 Hz	400 Hz	500 Hz
0	125	-171	-107	+18	+144	-89
100	129	-166	-101	+28	+158	-72
500	143	-144	-72	72	-144	-0.4
1000	163	-114	-32	+132	-63	+100
1500	-173	-79	+14	-157	+29	-143
2000	-146	-38	+68	-77	+136	-9
2500	-114	+8	+131	+17	-97	+149
3000	-77	+64	-153	+130	+53	-23
3500	-32	+132 .	-63	-94	-125	-156
4000	+24	-144	+49	+73	+98	+123

This tolerance should be satisfied when the phase is around the spatial phase angle (90°). Figure C.5 shows the variation of the phase vs the control word R20 around 90° for 200 Hz. From this curve, the rate of 8.18 is deduced and hence, for the range of tolerance equal to 4° (i.e.from ±2°), the limit for the R20 increment becomes 32.72 bits. This means that in the trial and error procedure, the increment of R20 at 200Hz should be less than 32.75 in order that the acceptable tolerance for the phase angle to be achieved. The same procedure can be done for any desired frequencies to obtain the limit for the increment of the control word R20. In table C.3, maximum increments of R20 have been shown for some frequencies. In the experiments of chapter 4, the increment of 10 has been used for R20.

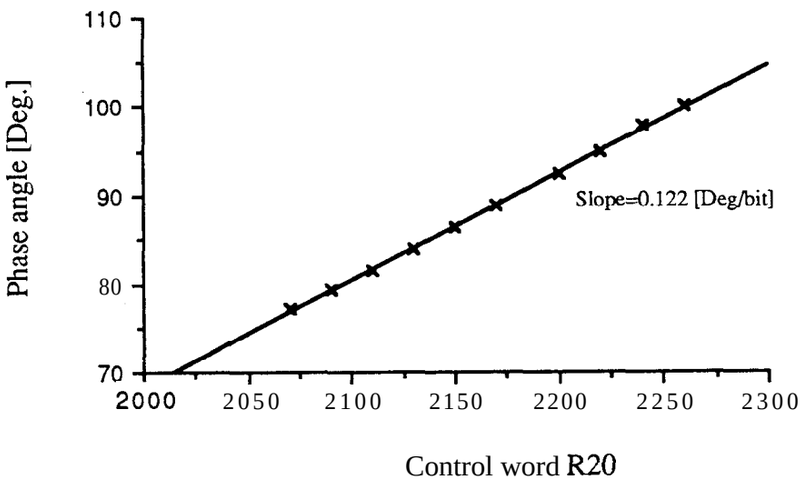

Figure C.5 Variation of the phase angle vs R20 around 90 at 200 Hz

Table C.3 Rate of R20 around 90° for different frequency

Freq.[Hz]	150	200	300 (1)	300 (2)	400 (1)	400 (2)
Slope [Bits/deg.]	7.49	8.18	8.58	4.45	4.61	2.89

Although the above recommendation is for ϕ_t=90°, it can also be applied with certainty in tests for which ϕ_t<90°. Since at any frequency, the slope for the lower phase angle is less than for the ϕ_t=90°.

C.4 LOGIC OF THE PROGRAM

Having chosen the initial values and considering the limitations in the control word increments, the procedure may be carried out by two approaches as shown in the flow-chart ; figure C.6. The first and shorter route considers the absolute error of A, and B_r which are called E_a and E_b respectively. A change is carried out to reduce the larger error. A, is the relative magnitude and B_r is the phase angle of the input forces. The second branch looks at the quality of the action and takes into account the last try. If it converges, i.e. goes in the proper direction, that action will be continued. Otherwise, the other parameter is changed. The string 'Convg$' is used to present this idea; if it is equal to "ON" then the action is converging, otherwise it is equal to "OFF".

There are three parameters to change : magnitudes of F_1 and F_2 and the relative phase between them. The corresponding parameters in the controller are V_0, V_1 and V_2 of the DAC. Each time one of these parameters is changed then a measurement is performed and the results are checked. Each parameter may be decreased or increased, therefore there are six types of change available which are labeled by 'Chgtypes' in program and 'Chgt' in the flow-chart. The string which represents the status of the procedure relevant to these changes is 'Chg$'. This string allocates different characters such as 'Chg_1_DN' which means the last action was reduction in channel 1 (on DAC).

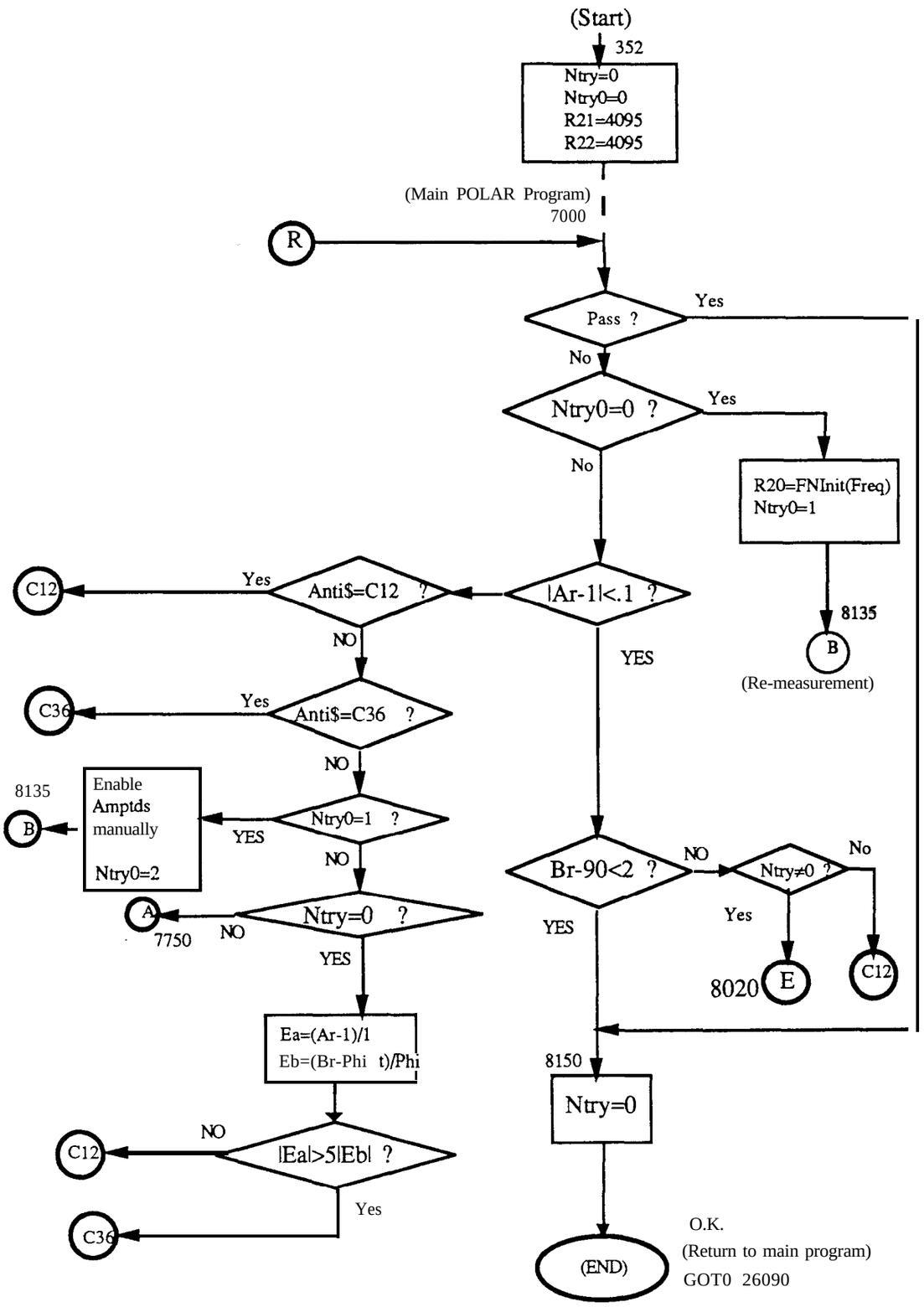

Figure C.6 Flow-chart of the sub-program for PHASH

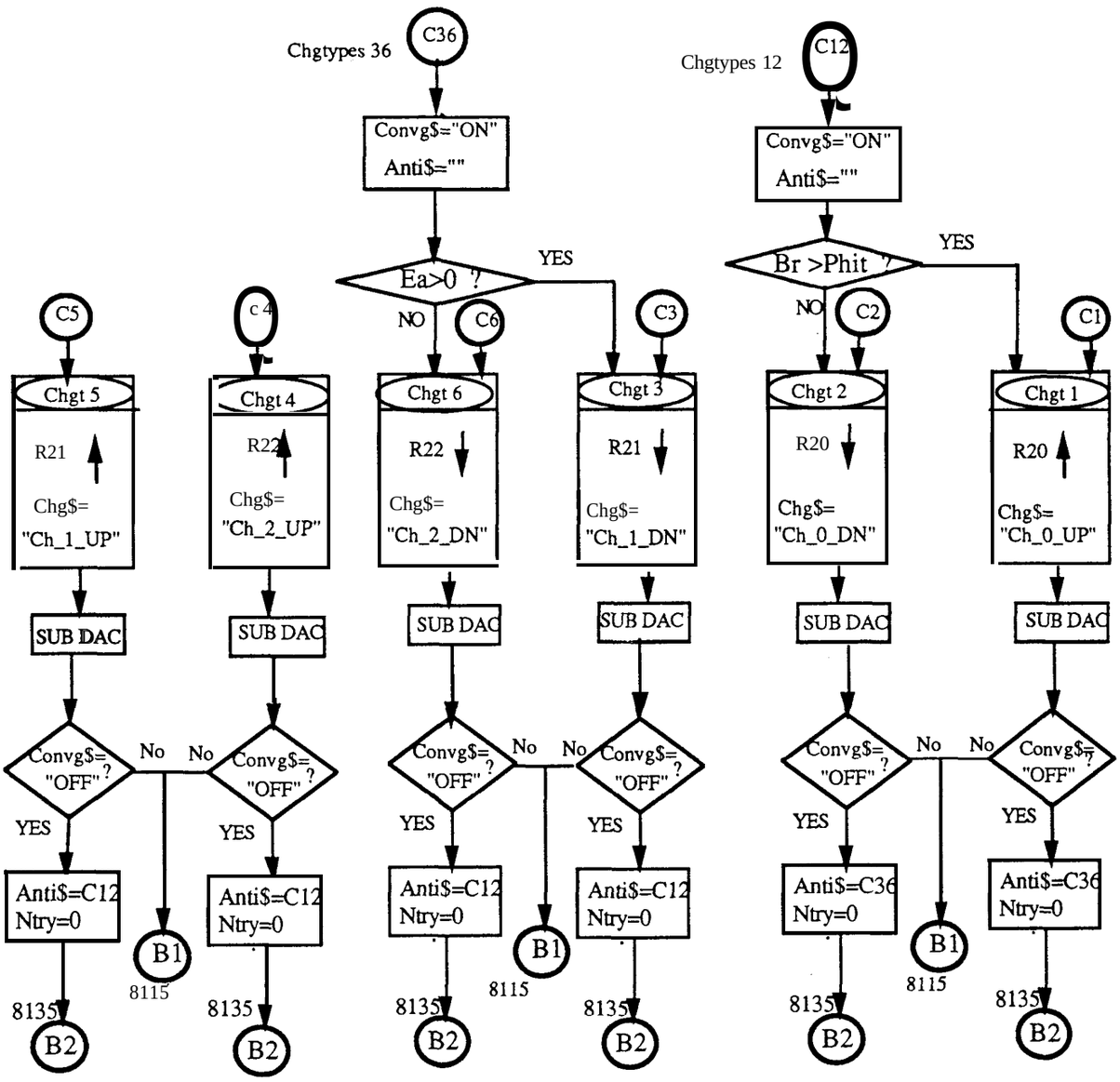

Figure C.6 *(Continued)*

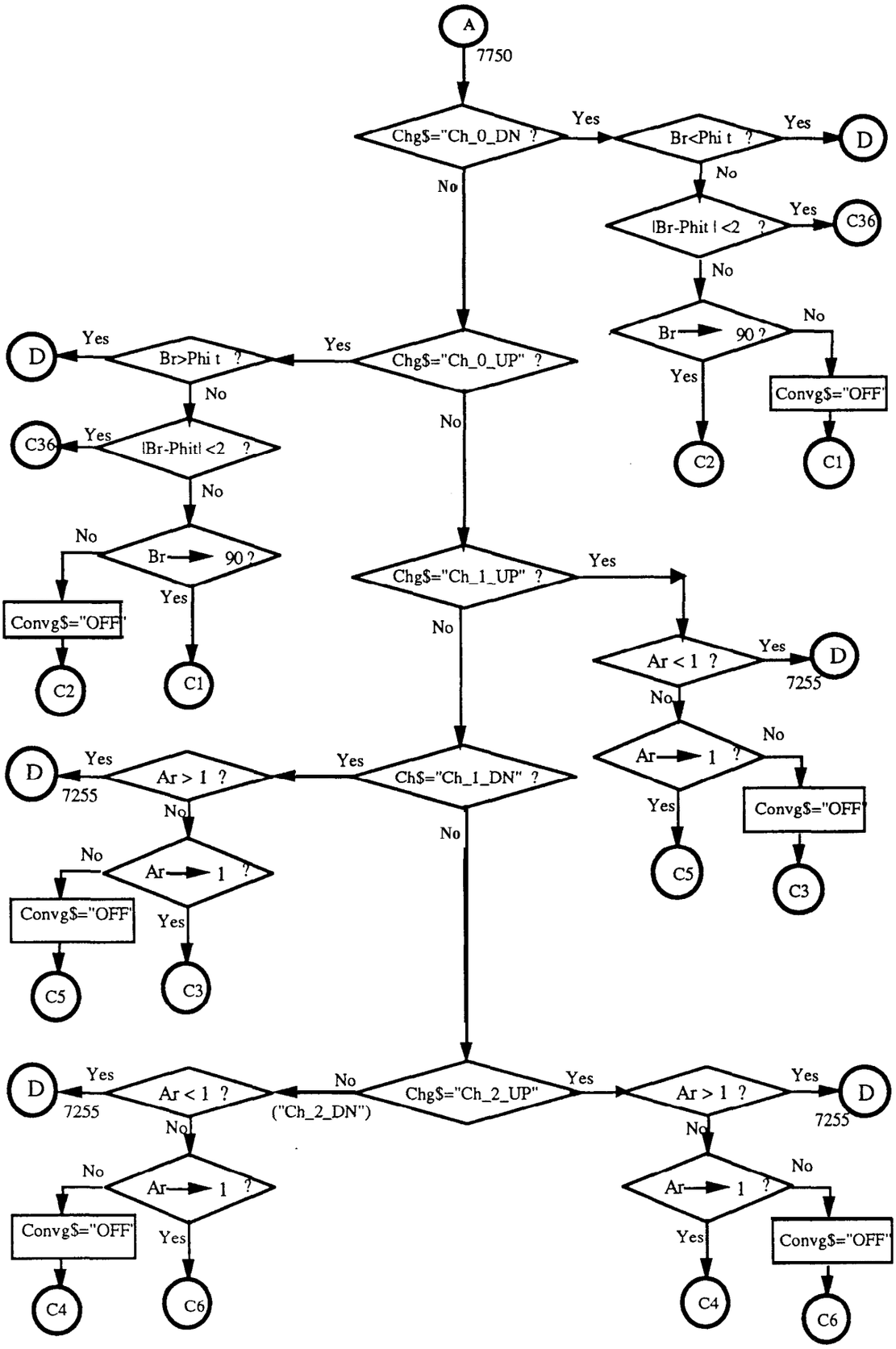

Figure C.6 (Continued)

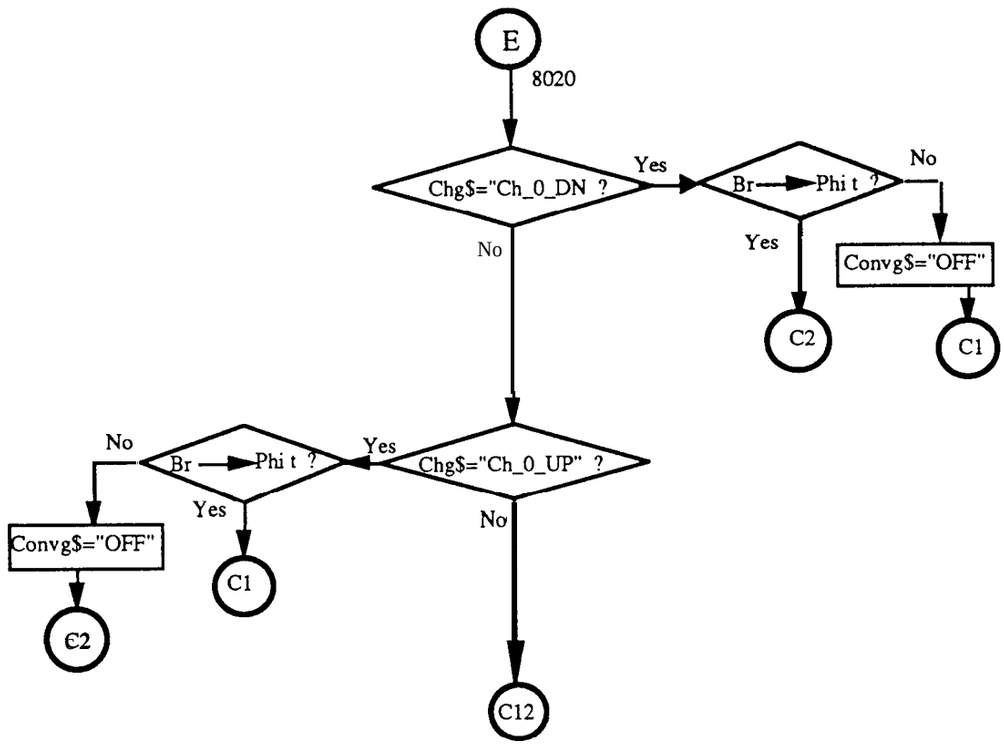

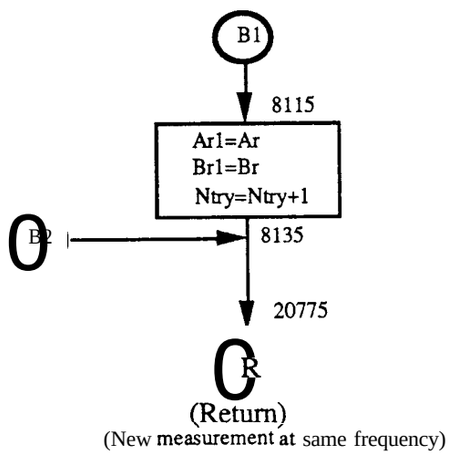

Figure C.6 *(Continued)*

APPENDIX ❑

INSTRUMENTS AND EQUIPMENT USED IN THE EXPERIMENTS

In two chapters 2 and 4, some experiments have been reported; the types of equipment and instruments used in those experiments are as follows:

Computers: There were two types of Hewlett Packard computers: HP 9816 and HP 300. Either could be used in the experiments and in the analyses with no significant difference. In chapter 5 computations were carried out with main frame CDC computer.

Analysers: FRA is a Solartron type 1254 (four channel), and was used in harmonic - single, double and 'dual controlled' - excitation tests.

FFT is a Bruel & Kjaer (B&K) dual channel signal analyser type 2034 and was used in hammer tests (in chapters 2 & 4) and in the spectrum measurement of the rotating disc in chapter 2.

Charge Amplifiers: A charge amplifier converts the charge generated in a transducer (piezo-electric) to an analogue voltage. Three different types of charge amplifiers could be used, B&K type 2626, B&K type 2635 (uses battery) and DJB type CA/04. There is also special charge amplifier in a packed instrumented hammer facilities, PCB piezotronics International Inc. type 4808 with sensitivities 2.04 mV/N and 10 mV/g which was used in hammer tests in chapter 2.

We should be careful when different types of charge amplifiers are used in a experiment, because there is possibility that different type of charge amplifier having different polarity (0° or 180°) relative to each other.

Force gauges: Different types of transducers could be chosen for measuring force. In chapter 4, B&K force gauge type 8200 has been used.

Accelerometers: Transducers B&K type 4344 in hammer test (in chapter 2), and DJB type A/02 in hammer test (in chapter 4) were used.

Proximity probe: The proximity probe was used in measurement of transverse displacement on the rotating disc (in chapter 2) was Bently Nevada made, model 2088501

VPI sensor: This is a non-contacting device made by OMETRON, using the laser Doppler phenomenon. It measures the velocity of the vibrating surface and is used to check the results from other devices measured the response of rotating disc.

Electra-magnetic shakers: In the single-, double- and dual controlled-excitation tests in chapter 4, Derritron shakers type VP 50 were used. In chapter 2 the non-contacting shaker was a nonstandard one and had been made with a C shape core and a coil.

Power amplifiers: A power amplifier is used to amplify the command signal before it is applied to a shaker. In chapter 2, the power amplifier - made by 'Ling Dynamic Systems Ltd.- type TPO300' was used. A Derritron type W25 WT was used in the experiments of chapter 4.

Phase shifter: In the dual controlled sine excitation method (chapter 4), the variable phase oscillator FEEDBACK type VPO 230 was used together with PHASH to control the two excitation forces.

REFERENCES

1 **BISHOP, R.E.D. and JOHNSON, D.C.**
"The Mechanics of Vibration"
Cambridge University Press, 1960.

2 **TIMOSHENKO, S. and YOUNG, D.H. and WEAVER, W.**
" Vibration Problems in Engineerings"
John Wiley & Sons, Inc., 4th Ed.(1974).

3 **EWINS, D.J.**
"Modal Testing: Theory and Practice"
Research Studies Press, 1984.

4 **CAMPBELL, W.**
"The Protection of Steam - turbine disk wheels from axial Vibration"
ASME Transaction,Vol. 46, 1924.

5 **ARMSTRONG, E.K.**
"An investigation into the coupling between turbine disk and blade Vibration"
PhD Thesis, Christ's College, Carnbrige (1955).

6 **TOBIAS, S.A. and ARNOLD, R.N.**
"The Influence of Dynamical Imperfection on the Vibration of Rotating Disks"
Institute of Mechanical Engineers Proceedings, V171, 1957.

7 **EWINS, D.J.**
"The Effects of Detuning upon the Forced Vibrations of Bladed Disks"
Journal of Sound and Vibration, 1969, 9(1), pp. 65-79.

8 EWINS, D.J.
"Vibration Characteristics of Bladed Disk Assemblies"
Journal of Mechanical Engineering Science, Vol 15, No. 3, 1973, pp. 65-79.

9 EWINS, D.J.
"Vibration Modes of Mistuned Bladed Disks"
Journal of Engineering for Power, ASME paper No. 75-GT-114.

10 SINGH, M.P. and EWINS, D.J.
"A Probabilistic analysis of Mistuned Bladed Turbine Disc"
Institute of Mechanical Engineers, 1988, C294/88.

11 AFOLABI, H.D.
"Vibration of Mistuned Bladed Disc Assemblies"
PhD Thesis, Imperial College, University of London, 1982.

12 EWINS, D. J. and SADASIVA RAO, Y.V.K.
"A Theoretical Study of the Damped Forced Vibration Response of Bladed Discs"
ASME winter annual meeting, Dec. 1976.

13 EWINS, D.J. and HAN, Z.S.
"Resonant Vibration Level of a Mistuned bladed Disk"
Journal of vibration, stress and Reliability in Design; Trans. of ASME, April 1984, Vol. 106, pp. 211-217.

14 SOUTHWELL, R.V.
"On the Free Transverse Vibrations of a Uniform Disc Clamped at its Centre and on the Effects of Rotation"
Proceedings of the Royal Society, London, 1922, Vol. 101, pp. 133-153.

15 KUSHNER, F.
"Disc Vibration - Rotating Blade and Stationary Vane Interaction"
Transaction of ASME, 79-DET-83, Journal of Mechanical Design, 1979.

16 FRENCH, R.F.
"Aircraft ***Gas Turbine Rotating Compressor Disk Vibration"***
An ASME Publication, 65-WA/GTP-11, Presented at the Winter annual Meeting, Chicago, Ill., November 7-l 1, 1965.

17 JAY, R.L. and McBAIN, J.C., AND BURNS, D.W.
"Structural Response due to Vane Interaction"
Transaction of ASME, Journal of Engineering for Gas turbines and Power, January 1984, Vol. 106, pp. 50-56.

18 IRRETIER, H.
"Experiments and Calculations on the Vibrations of Rotating Radial Impellers"
Transaction of ASME, Journal of Vibration, Acoustics, Stress, and Reliability in Design, April 1988, Vol. 110, pp. 137-142.

19 STANGE, W.A. and McBAIN, J.C.
"An Investigation of Dual Mode Phenomena in a Mistuned Bladed Disc"
Transaction of ASME, 81-DET-133, 1981.

20 SRINIVASAN, A.V.
"Vibration of Bladed Disk Assemblies - A Selected Survey"
Transaction of ASME, Journal of Vibration, Acoustics, Stress, and Reliability in Design, April 1984, Vol. 106, pp. 165-168.

21 BLEVINS, R.D.
"Formulas for Natural Frequency and Mode Shape"
Van Nostrand Reinhold Company, Litton Educational Publishing, Inc. (1979).

22 MACKE, H.J.
"Travelling Wave Vibration of Gas-Turbine Engine Shells"
Journal of Engineering for Power, April 1966.

23 STAPLES, B.C.
"Excitation of Travelling Wave Response in A&symmetric Structures"
Proceedings of the 15th Seminar on Modal Analysis, Leuven, Belgium, 19-21 Sep. 1990.

24 A F O L A B I , D .
"A note on the Rogue Failure of Turbine Blades"
Journal of Sound and Vibration, 122(3), 1988, pp.535-545.

25 EWINS, D.J.
"Further Studies of Bladed Disc Vibration: Effects of Packeting
I.Mech.E., 1980, pp.97-102.

26 PFEIFFER, R.
"Blade Vibrations of Continuously Coupled andPacketed Steam Turbine LP-Stages"
ASME Meeting, Vibration of Blades and Bladed Disk Assemblies, 1986.

27 COTTNEY, D.J. and EWINS, D.J.
"Towards the Efficient Vibration Analysis of Shrouded Bladed Disk Assemblies"
Transaction of the ASME, J. of Engineering for Industry, 1974, pp.1054-1059.

28 WHITEHEAD, D.S.
"Effect of Mistuning on Forced Vibration of Blade with Mechanical Coupling"
Journal of Mechanical Engineering Science, I.Mech.E. 1976, Vol. 18 No.6, pp.306-307.

30 YEH, L.
"Critical Speed Investigations of Turbo-Machines"
Proceedings of Institution of Mechanical Engineers, Applied Mechanics Convection 1960,Vol.180, part 31, pp. 23-37.

31 ROGERS, P.
"Genuine Modal Testing of Rotating Machinery"
Sound and Vibration, January 1985, pp. 36-42.

32 SINGH, M.P. and VARGO, J.J.
"Reliability Evaluation of Shrouded Blading Using the SAFE Interface Diagram"
Trans. of the ASME, J. of Engineering for Gas Turbines and Power, Oct. 1984, Vol. 111, pp.601-609.

33 EWINS, D.J.
"Modal Testing Techniques"
Vibration and Wear in High Speed Rotating Machinery, Kluwer Academic Publisher 1990, pp.299-309.

34 EWINS, D.J.
"Modal Testing of Machinery Components"
Vibration and Wear in High Speed Rotating Machinery, Kluwer Academic Publisher 1990, pp.323-337.

35 STROUD, R.C., and HAMMA, G.A., and LESTER, G., and JOCHEN, W.W.
"Digital Multiexciter Sine wave Vibration Control"
Proceedings of 60th Shock & Vibration Symposium, Virginia (U.S.A.), Nov. 14-16, 1989, Vol. 4, pp.181-197.

36 KENNEDY, C.C., and PANCU, C.D.P.
"Use *of Vectors in Vibration Measurement and Analysis"*
Journal of the Aeronatical Sciences, Vol.14, No.1 1, p.603, Nov.1947.

37 LEWIS, C.R., and WRISLEY, D.L.
"A System for the Excitation of Pure Modes of Complex Structures"
Journal of the Aeronatical Sciences, Vol. 17, No. 11, p.603, Nov. 1950.

38 ASHER, G.W.
"A Method of Normal Mode Excitation Utilizing Admittance Measurements"
Proc. National Specialists' Meeting on Dynamics and Aeroelasticity, Fort Worth, Inst. of Aeronatical Sciences, 1958, pp.69-76.

39 CRAIG, R.R.Jr., and SU, Y.W.T.
"On Multiple Shaker Resonance Testing"
AIAA Journal, Vol. 12, No.7, July 1974.

40 SLOANE, E., and MCKEEVER, B.
"Modal Survey Techniques and Theory"
Transaction of the Society of Automotive Engineer, Vo1.84, 1975, pp.2963-2988.

41 HALLAUER,W.L.Jr., and STAFFORD, J.
"On the Distribution of Shaker Forces in Multiple- Shaker Modal Testing"
The Shock and Vibration Bulletin, Bu11.48, Part 1, 1978, pp.49-63.

4 2 ALLEMANG R.J., and ROST, R.W., and BROWN, D.L.
"Dual Input Estimation of Frequency Response Functions For experimental Modal Analysis of Aircraft Structures"
1st IMAC, 1982, pp.333-340.

***4 3* HUNT, D.L., and WILLIAMS, R., and MATHEWS, J.**
"A State-of-the-Art Implementation of Multiple Input Sine Excitation"
5th IMAC, London 1987, pp.737-742.

44 **DEBLAUWE, F., and BROWN, D., and VOLD, H.**
"Some ***Concepts for Spatial Sine Testing Parameter Identification"***
IMAC7, 1989, pp.1 174-1178.

45 **SEVERYN, A.J., and BARNEY, P.S., and ROST, R.W., and BROWN, D.**
"Advances of a Spatial Sine Testing System"
IMAC7, 1989(?), pp.952-957.

46 GLADWELL, G.M.L.
"Vibrating Systems with Equal Natural frequencies"
Journal of Mechanical Engineering Science, Vol. 3, No. 2, 1961.

***47* MAHALINGAM, S. and BISHOP, R.E.D.**
"The Response of a System with Repeated Natural Frequencies to Forced and Displacement Excitation"
Journal of Sound and Vibration, 36(2), 1974.

***48* EWINS, D.J.**
"A Study of Resonance Coincidence in Bladed Discs"
Journal of Mechanical Engineering Science, Vol. 12, No. 5, 1970.

49 KIRSHENBOIM, J.
"Identification of the Wave Pattern of a Vibrating Disk"
Dynamics Section, Dept. of Mech. Eng., Imperial College, LONDON, Report No. 88003, 1988.

50 ROBB, D.A.
"BASIC Programs: POLAR, MODENT"
Dynamics Section, Dept. of Mech. Eng., Imperial College, LONDON, 1986.

51 TSE, F.S. and MORSE, I.E. and HINKLE, R.T.
"Mechanical Vibrations: Theory and Applications"
Allyn and Bacon, Inc., 1978.

52 COTTNEY, D. J.
"The Receptance Analysis of Disc, Blade and Shroud Vibration"
PhD Thesis, Imperial College, University of London, 1975.

53 STROUD, R.C.,.and HAMMA, G.A.
"Multiexciter and Multi-axis Vibration Exciter Control systems"
Sound and Vibration, April 1988.

54 BREITBACH, E.J.
"Recent Developments in Multiple Input Modal Analysis"
Trans. of the ASME, J. of Vibration, Acoustic, Stress, and Reliability in Design, Oct. 1988, Vol.llO,pp. 478-484.

55 LALANNE, M., and BERTHIER, P.,and HAGOPIAN, J.D.
"Mechanical Vibrations for Engineers"
John Willey & sons, 1983.

56 NEWLAND, D.E.
"Mechanical Vibration Analysis and Computation"
Longman Scientific & Technical, 1989.

57 THOMSON, W.T.
"Theory of Vibration with Applications"
Uniwin Hyman Ltd., 3rd ed., 1988.

58 OMETRON Limited (UK)
"VPI Sensor Vibration Measurement"

59 ROLLS ROYCE Limited
"The Jet Engine"
Rolls Royce, Derby Engine Division, England, 1981.

60 MEIROVITCH, L.
"Computational Methods in Structural Dynamics"
Sijthoff & Noordhoff, 1980.

61 EFSTATHIADES, G.J.
"A New Approach to the Large-Defection Vibrations of Imperfect Circular Disks Using Galerkin's Procedure"
Journal of Sound and Vibration, 16(2), 1971, pp. 231-253.

62 YU, R.C., and MOTE Jr, C.D.
"Vibration and Parametric Excitation in Asymmetric Circular Plates under Moving Load"
Journal of Sound and Vibration, 119(3), 1987, pp. 409-427.